DEVELOPMENT OF REMOTE OPTICAL INSTRUMENTATION FOR THE ENHANCED DETECTION OF AIRBORNE ENVIRONMENTAL TOXINS

by

Riley Mungo

A thesis

submitted in partial fulfillment

of the requirements for the degree of

Master of Science in Chemistry

Boise State University

August 2022

BOISE STATE UNIVERSITY GRADUATE COLLEGE

DEFENSE COMMITTEE AND FINAL READING APPROVALS

of the thesis submitted by

Riley Mungo

Thesis Title: Development of Remote Optical Instrumentation for the Enhanced Detection of Airborne Environmental Toxins

Date of Final Oral Examination: 26 May 2022

The following individuals read and discussed the thesis submitted by student Riley Mungo, and they evaluated the student's presentation and response to questions during the final oral examination. They found that the student passed the final oral examination.

Matthew King, Ph.D.	Chair, Supervisory Committee
Eric Brown, Ph.D.	Member, Supervisory Committee
Michael Callahan, Ph.D.	Member, Supervisory Committee

The final reading approval of the thesis was granted by Matthew King, Ph.D., Chair of the Supervisory Committee. The thesis was approved by the Graduate College.

DEDICATION

I dedicate my thesis work to my family and friends who have supported me throughout my education.

ACKNOWLEDGMENTS

I would like to thank my advisor, Dr. Matthew King, for allowing me to do research within his group and for starting this research project for me to begin and complete my thesis on. Also, I would like to thank my committee members, Dr. Eric Brown and Dr. Michael Callahan, for their support during this process.

The completion of my project could not have been accomplished without the help and support from the Department of Chemistry and Biochemistry and stockroom staff; Jeremy Daniels, Christina Mottishaw, and Thaeer Muhammed.

ABSTRACT

The severity of wildfires in the United States are increasing and in the amount of acreage burned due to climate change and a sustained drought in the western part of the country. As a greater number of wildfires burn in the west, the amount of smoke produced becomes a health concern to the public. Wildfires release airborne toxins and hazardous air pollutants that cause adverse health effects to the public in high concentrations but are of principle concern to health officials as they have differential impacts on infants and children. Some of the airborne toxins released are carbonyl compounds such as: formaldehyde, acetaldehyde, acetone, acrolein, and methacrolein. An air quality index (AQI) is the primary method of reporting air quality and the attributed health effects to the public. However, an AQI cannot quantify select pollutants or reliably quantify the airborne toxins *in situ*. The development of a mid-IR and nonlinear Raman detection instrumentation would allow for more dependable collection of wildfire smoke data and the quantification of select carbonyl compounds. Wildfire smoke was collected over the summer of 2021 around southwestern Idaho using EPA method TO-11A to determine the reliability of the method against optical detection methods. The initial development of a compact LED-based mid-IR instrument was constructed and limits of detection and quantitation were determined. Nonlinear Raman methods were explored using the optical output from photonic crystal fibers, for which output characterization and the sensitivity, selectivity, and limits of detection will be evaluated for the potential

development of a compact all fiber spectrometer with real time *in situ* capabilities in Idaho.

TABLE OF CONTENTS

LIST OF TABLES

LIST OF FIGURES

LIST OF ABBREVIATIONS

AQI:	Air Quality Index
ATSDR:	Agency for Toxic Substance and Disease Registry
$CaCl_2$:	Calcium chloride
CARS:	Coherent anti-Stokes Raman spectroscopy
CO_2:	Carbon dioxide
COPD:	Chronic obstructive pulmonary disease
DFT:	Density functional theory
DNPA:	2,4-dinitrophenylazide
DNPH:	2,4-dinitrophenylhydrazine
EPA:	Environmental Protection Agency
FSRS:	Femtosecond stimulated Raman spectroscopy
FT-IR:	Fourier transform infrared
HAP:	Hazardous air pollutant
HCPCF:	Hollow core photonic crystal fiber
HPLC:	High performance liquid chromatography
KBr:	Potassium bromide
KI:	Potassium iodide
N_2:	Nitrogen gas
NDIR:	Non-dispersive infrared
NL-PM:	Nonlinear polarization maintaining

NO_2:	Nitrogen dioxide
NOAA:	National Oceanic and Atmospheric Administration
ODS:	Octadecylsilyl
PAH:	Polyaromatic hydrocarbon
PCF:	Photonic crystal fiber
PM:	Particulate matter
PM_{10}:	Particulate matter smaller than 10 microns
$PM_{2.5}$:	Particulate matter smaller than 2.5 microns
SRS:	Stimulated Raman scattering/spectroscopy
TO:	Toxic organic
US:	United States
UV:	Ultraviolet
VOC:	Volatile organic compound

INTRODUCTION

Wildfire Statistics

Wildfire occurrence in the western United States (US) is increasing with the expectation of continued exacerbation from climate change.[1-5] The burning of biomass releases the most amount of particulate matter (PM) and volatile organic compounds (VOCs) globally.[6-8] Not only is the frequency of wildfires increasing, but the amount of acreage burned is increasing due to climate change and land management choices.[5,9] As the western US continues to dry out with decreased rainfall, the increase in wildfires is only expected to continue.[1,10,11] In June 2021, over 90% of the western US was in one of the five categories of a drought, with half of the region in an extreme to an exceptional drought; the two highest drought categories.[12] Not only was this the most expansive and intense drought experienced this century, multiple cities and states set records for widespread temperatures exceeding 100 ºF during the summer of 2021.

Over the past two decades, the US has averaged 70,600 wildfires that burn 7.0 million acres per year.[13] Wildfires occur as any unplanned fire caused by lightening, humans, or uncontrolled prescribed fires. Although variable, more wildfires are human caused than lightning with 89% of wildfires in 2021 being human caused.[12] In 2020, a total of 58,950 wildfires burned 10.1 million acres while in 2021, 58,895 wildfires burned 7.1 million acres. The number of fires and acreage burned that occur each year is

variable, but previous 30 year data indicates a general trend towards the amount of acreage burned has been increasing.[13] In addition, there are more fires that occur in the eastern and central US states, but more acreage burned in the west. In 2020, 33,000 fires burned 0.7 million acres in the eastern and central US states, while 26,000 wildfires burned 9.5 million acres in the west.

Some western US states are differentially impacted when it comes to wildfires. Of the fires that burned in 2020, almost 40% of the land burned was in California.[13] In California, half of all particulate matter is smaller than 2.5 microns ($PM_{2.5}$). Wildfires are expected to increase in frequency 20-100% through the year 2100 due to climate change in California.[14-16] In 2021, the largest fire in Californian history, the Dixie fire, burned over 960,000 acres.[12] Of the significant wildfires that burned over 40,000 acres in 2021, ten occurred in California, six in Washington, five in Oregon, four in Montana, four in Arizona, and three in Idaho.

Boise Region Geography

Boise, Idaho is a centrally located city that is within close proximity to areas with high western US summertime wildfire activity.[17] As Idaho borders Washington and Oregon to the west, winds carry wildfire smoke affected air from the west, northwest, and even southwest from California to settle into the valleys of Idaho. The United States Environmental Protection Agency (EPA) divides the US into differing ecoregions based upon similar environmental resources.[18] At the EPA's Level I ecoregions, the continental

US is separated into twelve regions in which Idaho is defined as being within two: Northwestern Forested Mountains and North American Deserts.[18]

Smoke Constituents

The combustion of biomass during wildfire season in the US releases many pollutants such as PM, VOCs, hazardous air pollutants (HAPs), and reactive nitrogen.[19-25] The release of $PM_{2.5}$ from transportation is the second greatest contributor of the pollutant after wildfire smoke.[26] In comparison to gas and diesel combustion, burning wood releases more semivolatile organic compounds and polyaromatic hydrocarbons (PAHs).[27,28] Other sources of air pollution is primarily produced from that of anthropogenic sources such as emissions from stationary fuel combustion sources, industrial and manufacturing processes, and non-road mobile sources.[29] Of the pollutants released during wildfires, those of concern are particulate matter smaller than 10 microns (PM_{10}), $PM_{2.5}$, carbon monoxide, ozone, and HAPs.

HAPs can be quantified under the $PM_{2.5}$ category as they are molecules much smaller than 2.5 microns. The EPA compiled a list of 188 HAPs as part of the Clean Air Act in 1990 as they are compounds that are known or suspected to be carcinogenic and lead to other severe health conditions.[30,31] Two of the most abundant VOCs emitted in wildfires, formaldehyde and acetaldehyde, are found on the EPA's list of HAPs.[6,21,32,33] However, the potential health risks of HAPs have not been quantified in nonoccupational settings such as ambient air exposure from summertime wildfire season.[34] VOCs such as formaldehyde, acetaldehyde, acrolein, acetone, and methacrolein are of principle concern

in respect to smoke emissions. These carbonyl containing compounds are formed by the oxidation of biogenic hydrocarbon sources, like biomass burning.[35] Not only is there the risk of exposure to these VOCs, the multitude of VOCs produced during wildfire episodes can interact with stable nitrogen compounds found in ambient air to generate ozone downwind of a fire and lead to coexposure.[36] Another compound that is found in wildfire smoke and is associated with human health risks is carbon monoxide. Carbon monoxide is formed by the incomplete combustion of biomass and has a lifetime of approximately 10 days in the summer.[37] The long lifetime of carbon monoxide leads to the risk of extended exposure to humans closer to the wildfire site as well as farther away as wind can transport the pollutant. Of the HAPs investigated, acetaldehyde, formaldehyde, and acetone have known half-lives, as well. Acetone has the longest half-life of 22 days while acetaldehyde has a half-life of 5 hours and formaldehyde's is much shorter at just hours.[38-40]

Since wildfires are the largest producers of PM emissions, understanding the chemical compositions of the biomass combustions would prove helpful in determining the human health impact of inhalation of those chemicals. There are chemical profiles of combustion of certain types of woods, plants, and animal materials available from under controlled conditions.[41-46] However, given the variable and uncontrolled nature of wildland forest fires, relatively few studies have been conducted on the concentrations of organic compounds released in wood smoke combustion during wildfire conditions.[47] Not only do wildfires release their own PM, the dispersed pollutants can interact and modify ambient PM.[48] The distinct vegetation types in different ecoregions provides changes in the types of fuel for wildfires as well as the way those particular pollutants are

found to interact with ambient $PM_{2.5}$ compositions.[49-53] In addition, environmental factors such as humidity, wind, and the combustion efficiency of the wildfire will impact the amount of fine PM released from wildfires; especially since drier conditions, higher winds, and the smoldering phase of fires release more particulate.[53-57]

Recent studies have researched and obtained data of specific VOC concentrations in smoke impacted areas during wildfire season. One study conducted in Boise, Idaho during the summer of 2018, found that the mixing rations of acrolein, acetaldehyde, and formaldehyde were found to be 238%, 103%, and 84% higher than average, respectively.[17] Also, during the summer of 2018, another study focused on collecting smoke over most of the western US to determine the composition of smoke as it aged.[24] It was found that the compounds formaldehyde and acetaldehyde were similar in their distribution in the air as the smoke aged while acrolein was not as concentrated in old smoke plumes, greater than three days old, than young smoke plumes, less than one day old.[24] This could be due to the half-life of each compounds or the type of biomass burning at each of the wildfire events.

Health Impact

The exposure of PM from wildfire smoke emissions to the public tends to be of greatest concern to health officials followed by carbon monoxide and ozone exposure. Particles larger than 10 micrometers generally do not reach the lungs and can irritate the nose and throat while PM_{10} can be inhaled into the lungs and affect the heart and blood vessels.[58] The smallest of particles, $PM_{2.5}$, can reach deeper into the lungs and enter the

bloodstream. Carbonyl compounds such as formaldehyde, acetaldehyde, acrolein, acetone, and methacrolein are especially dangerous $PM_{2.5}$ constituents as they are either known or suspected carcinogens to humans or irritants to the human body. While formaldehyde is a known carcinogen to humans and acetaldehyde is a possible human carcinogen, methacrolein and acetone are not listed as a possible, probable, or confirmed human carcinogen.[59-62] To date, acrolein has not been identified as a possible, probable, or confirmed human carcinogen, as well.[63] However, a 2021 study recently found acrolein to be carcinogenic in both mice and rats by inhalation; the first study conducted on acrolein through inhalation to yield it as a possible carcinogen to humans.[64] Carbon monoxide emission from wildfires is concentrated around the point of combustion and is of a larger concern for firefighters and at-risk populations with heart problems as it enters the bloodstream and reduces the amount of oxygen delivered to organs and tissues.[58] Ground-level ozone causes acute health effects with the lungs such as reduction of lung function, inflammation of airways, coughing, and wheezing.

Each of the carbonyls of interest are attributed with differing health impacts. Acute and chronic noncancer exposure to formaldehyde by inhalation can result in eye, nose, and throat irritation and respiratory symptoms.[65] It was found by the Agency for Toxic Substances and Disease Registry (ATSDR) the minimal risk level for chronic noncancer exposure to formaldehyde is 3 ppb. Due to the carcinogenic nature of formaldehyde, inhalation and exposure leads to an increased occurrence of lung and nasopharyngeal cancers. Acetaldehyde acute inhalation exposure leads to eye, skin, and respiratory irritation in humans, as well as, erythema, coughing, pulmonary edema, and necrosis at higher exposure levels.[66] An increase in the amount of nasal and laryngeal

tumors found in rats and hamsters by inhalation exposure to acetaldehyde lends it to its description as a probable human carcinogen. The acute health effects seen in humans by inhalation of acrolein are nose and throat irritation with a decrease in respiratory rate with a minimal reference level found by the ATSDR at 3 ppb.[67] As it is a strong dermal contact irritant, the chronic noncancer effects of acrolein are not as serious as other carbonyl compounds as respiratory congestion and eye, nose, and throat irritation are the primary symptoms. Methacrolein health effects are not at thoroughly researched and has a broader description of its potential exposure risk as acute toxicity by inhalation.[61] Acetone, although relatively safe to humans, is an acute irritant of the nose, throat, and lungs by inhalation but can cause pulmonary congestion, edema, and hemorrhage of the lungs at much higher concentrations, which was found in guinea pigs.[38]

During the summer 2018 research over the western US, it was found that the age of smoke impacted the health risks associated with aging smoke. Each of the observed HAPs were categorized based upon contributions to acute, chronic noncancer, and chronic cancer health outcomes for young smoke, medium smoke aged, one to three days, and old smoke, with the dominant contributors determined as acrolein and formaldehyde.[24] Acrolein was found to be the presiding contributor to acute health risk exposure in young smoke but quickly drops in medium and old smoke exposure risks. On the other hand, formaldehyde's acute health risk exposure persists across all ages of smoke. For chronic noncancer exposure from wildfire smoke, acrolein was, again, found to be the largest contributor in young smoke with its effects tapering in medium and old smoke. Formaldehyde was found to have a constant chronic cancer exposure health risk in each of the smoke age categories.

Unsurprisingly, wildland firefighters bear the brunt of the dangerous wildfire smoke pollutant and particulate exposure as they work to suppress the fires. Between prescribed fires and wildfires, wildland firefighters have a higher smoke exposure at prescribed fires as they are closer to the site to control the burn.[68] Wildland firefighters are exposed to high levels of formaldehyde and acrolein, sometimes as high as 600 ppb and 98 ppb, respectively.

The focus towards HAPs as opposed to carbon monoxide and ozone is due to their differential impact on infants and children compared to adults.[58] General air pollution in urban areas have been linked to reduced lung function during early childhood as the airways are maturing.[69-71] A study on infant rhesus macaque monkeys held outside during a heavy wildfire smoke impacted area was conducted in 2008 during the first three months of the monkeys lives.[72] Compared to the controls, the monkeys exposed to the $PM_{2.5}$ smoke impacted air had significant immune changes, respiratory changes, reduced inspiratory addition, and reduced total lung capacity. It was also found that the negative health impacts correlated to the exposure of wildfire smoke was dependent upon sex as males had a significantly lower expiratory reserve volume than females due to their larger mass. The reduced lung volumes on the rhesus macaque monkeys exposed to wildfire smoke in the study is consistent with human birth cohort studies exposed to general air pollution which also has observed associated lung growth deficits.[71-74] Nonetheless, little is known on the overall long-term effects of children due to the altered growth trajectory in the lungs from wildfire smoke.[69,70,73-76]

Along with the health impacts associated with the exposure to wildfire smoke, the economic impact is equally as substantial. The significant impact on the healthcare

system during smoke impacted areas comes from patients seeking medical care for respiratory symptoms.[76] In particular, patients seek care and are likely to visit an emergency room for respiratory issues such as asthma, bronchitis, dyspnea, and chronic obstructive pulmonary disease (COPD) symptoms.[77-84] Between 2008 and 2012 over the continental US, the estimated economic valuation from wildfire $PM_{2.5}$ smoke related health issues ranges from $11B to $20B for acute exposures and ranges from $76B to $130B for chronic exposures.[85] Although an exact number cannot be obtained, an estimated 1500 to 2500 premature deaths are attributed to acute smoke exposure and 8700 to 32,000 premature deaths are linked to chronic smoke exposure. However, a study on Canadian wildfires found the effects on life expectancy to be minimal at a loss of less than 0.05 years.[86]

Current Detection Methods

The presence of pollutants in wildfire smoke can currently be detected in many ways depending upon the origin of collection, either at ground level or suspended in the air. The EPA measures air quality using a colored index made available to the public to determine the level of health concern and groups affected by the air pollution.[87] The air quality index (AQI) measures carbon monoxide, ground-level ozone, $PM_{2.5}$, PM_{10}, sulfur dioxide, and nitrogen dioxide (NO_2). Each of these pollutants are monitored for a predetermined amount of time, ranging from one hour to one day, and a piecewise function is used to calculate the index value of the air quality to be presented to the public. The pollutant with the largest AQI is the value used to assess the level of public

health concern. In conjunction with the EPA, the National Oceanic and Atmospheric Administration (NOAA) helps provide air quality monitoring by equipping instruments on the ground for ground-level monitoring and satellites orbiting Earth for collection of qualitative and quantitative information of the particles and pollution suspended in the air.[88]

The EPA has established several methods for the determination of toxic organic (TO) compounds in ambient air. Each method differs based upon the detection method and the analyte of interest. EPA method Toxic Organic 11-A (TO-11A) is specific to the detection of formaldehyde and other carbonyl containing compounds found in ambient air by adsorption onto a 2,4-dinitrophenylhydrazine-silica (DNPH) cartridge followed by high performance liquid chromatography (HPLC).[89] The method is widely used for routine air quality monitoring of carbonyls along with other methods to detect air toxins. However, method TO-11A has drawbacks with the detection of select carbonyls and their DNPH-derivatives. One such problem is the interference of ozone that degrades the DNPH-silica cartridges and the DNPH-derivatives. The presence of ozone will yield products from the degradation reaction that absorb in the ultraviolet (UV) region, impeding on the detection of the DNPH-derivatives during HPLC-UV analysis.[90] The addition of an effective ozone scrubber using copper oxide or potassium iodide prevents such degradation. As well, issues with the detection of formaldehyde, acrolein, and acetaldehyde are well documented.[91] One of the difficulties with measuring the formaldehyde-DNPH derivative on the HPLC is the reaction of ambient NO_2 with DNPH to form 2,4-dinitrophenylazide (DNPA).[92] DNPA and the formaldehyde-DNPH derivative have similar chromatographic properties with DNPA's absorption maximum at

~300 nm and the latter's at ~360 nm.[93] Since the two compounds coelute, detection of the carbonyl-DNPH derivatives at 360 nm can yield a falsely high absorption of formaldehyde. This issue is worsened with the addition of an ozone scrubber that oxidizes nitrogen oxides to NO_2.[94] Detection difficulties of acrolein-DNPH derivatives has been so extensive that the compound has been removed from the list of applicable target analytes in method TO-11A.[95] The acrolein-DNPH derivative decomposes in the presence of excess acid and excess DNPH within the adsorption cartridge and results in a systematic negative bias towards the compound.[96] In addition, as acrolein is an unsaturated carbonyl, it can react multiple times with DNPH to form acrolein-polyderivatives named acrolein-(x) and acrolein-(y).[97] It was found that the summation of the acrolein-DNPH derivative and polyderivative peaks after only 5 hours of sample collection time will yield an acceptable estimate to acrolein concentration in a laboratory environment, but was not tested in real sample analysis. Acetaldehyde-DNPH derivative detection issues arise from collection efficiencies worsening with increased air sampling time.[98] The collection efficiency greatly increases with sampling times on the scale of a few minutes to few hours otherwise falsely low acetaldehyde concentrations are observed.

Optical detection methods of particulates have become more prevalent as the need for higher accuracy air pollution monitors grows. Raman lidars have been used to determine the amount of particulate in the air over a given region due to wildfires. A 2017 study used lidar detectors to find wildfire smoke present in the troposphere and lower stratosphere had traveled from western Canada to central Europe over a period of seven to ten days.[99,100] Although not able to determine the constituents of the wildfire

smoke, lidar detection methods can quantitatively obtain the amount of particulate suspended in the air. In addition, multiple optical interferometry techniques have been tested for VOC detection.[101] However, most of the techniques studied were single-point, targeting the molecules in a limited domain and the method would benefit from a multipoint detection of gas molecules in a real-life application.

Other common ways to detect wildfires and wildfire smoke use an aircraft or unmanned aerial vehicles with an airborne sensor platform equipped with various instruments.[102] Largely, this form of detection is used to determine the site of a wildfire, not the health impact from released pollutants. Nonetheless, heat, light, and smoke from a wildfire have been detected using the airborne sensor platforms. The heat produced from a wildfire can be detected using infrared in the mid-wave infrared (3 – 5 μm) region and the thermal infrared region but has disadvantages when using a single band detector and encounters issues with solar reflection. Light produced from a wildfire had mainly been detected by human observers until the use of near, short-wave infrared (0.75 – 3 μm) and visible light cameras with drawbacks attributed to daytime sunlight peaks in the visible and near infrared region and reflected glints of light in the mid-wave and short-wave infrared regions. Detection of smoke from wildfires is similar to that of the NOAA by employing satellites to calculate mixing ratios of constituents in smoke plumes. Moreover, ground-level and cost-effective wildfire smoke detection methods are lacking.

Gaps in Detection Methods

The presence of wildfires not only in the western US but across most of the globe will continue to become more prevalent as climate change progresses. Although there are several methods of detecting wildfire smoke pollutants and particulates, a gap still exists in obtaining data that is reliable in the qualitative and quantitative determination of smoke constituents. Ground-level observations of HAPs remain inadequate due to spatial and temporal limitations.[24] In addition, the ground-level EPA detection method TO-11A has many drawbacks and pitfalls that does not allow for a complete collection of airborne carbonyl HAP concentrations. To obtain a complete carbonyl HAP concentration profile, multiple EPA methods would need to be operated at the same time to yield desirable results. These limitations in ground-level observations proves difficult to assess the exposure to carbonyls during wildfire season. Overall, the need for future research in air quality monitoring from wildfire smoke events is needed as well as the ability to more reliably predict and report the toxins found in the air.[76]

Many types of local air quality monitoring systems are bulky, expensive, and inaccurate.[103] Currently, ultrafine particulate produced from wildfires is not thoroughly studied or reported by monitoring networks due to ultrafine particles being more difficult to measure.[76] Although limited in research, the mid-infrared spectral region and mid-infrared lasers show quality application promise in the field of gas component detection.[104-106] Utilizing a ground-level mid-infrared detection method could prove beneficial in the determination of the presence of some HAPs. Another potential ground-based gas sensing instrument with promise is a compact all fiber Raman spectrometer as

fiber optic based sensor systems have a prospective application in ambient air quality monitoring.[107] Raman spectroscopy, especially femtosecond stimulated Raman spectroscopy (FSRS), can effectively analyze the composition of complex gaseous samples. A photonic crystal fiber (PCF), more specifically a hollow core photonic crystal fiber (HCPCF) used in tandem with FSRS can help improve low signal intensities.[103] HCPCFs have axially aligned air cladding channels that confines light inside of the fiber, provides a photonic bandgap, and increases overlap with the analyte and laser resulting in enhanced sensitivity. A 2013 study demonstrated the near 4000-fold sensitivity increase in Raman signals from the utilization of a HCPCF. In addition, prior to the study, the multiplexing capabilities of a HCPCF had not been quantitatively shown and was found to show normal intensities of a gas mixture when also tested separately. Not only did the study find low detection limits of the tested gases, but it also concluded the multiplexing detection of the HCPCF to lend well to gas sensing in a complex environment. Optical fiber coupling enables multipoint sensing and locating the analyzer remotely from the measurement site to remove the potential of wildfire hazards.[107] However, a robust optical alignment is required for measurement accuracy and reproducibility of results given the variability in ambient air humidity, temperature, and wind can hinder optical gas sensors.

This thesis details the initial development of a mid-infrared (IR) and Raman spectrometer detection system for select carbonyl compounds present in wildfire smoke. EPA method TO-11A was utilized to determine its reliability in the collection of carbonyl concentrations of formaldehyde, acetaldehyde, and acetone, as well as to determine if unsaturated aldehydes such as acrolein and methacrolein can be detected. The effects of

elevation on the suspension of particulate was evaluated along with the impact of an urban location compared to a rural location for sample collection. The collected carbonyl concentrations using the EPA method was compared to daily AQI's to determine the reliability of method TO-11A. A constructed compact mid-IR device was evaluated using gas phase detection to determine the sensitivity, stability, and limits of detection of the instrument. Initial development of a compact coherent Raman spectrometer was completed by characterizing photonic crystal fiber outputs.

MATERIALS AND METHODS

Sampling Sites

Four sampling sites were chosen for biweekly to monthly collections of air samples between August 2 to November 1, 2021. The earlier samples collected were conducted during peak wildfire season in Idaho, defined as “wildfire season”, the latter served as a reference to the location’s ambient air during the off season, defined as “baseline”. Collection sites in Mountain Home, Idaho were completed monthly while air collection in Boise was completed every two weeks. The base of Bennett Mountain in Mountain Home (site 1) was located off Highway 20 at an elevation of 1195 m above sea level, while the top of Bennett Mountain (site 2) was located 8800 m south of Highway 20 at an elevation of 1650 m above sea level. Of the two sampling sites completed in Boise, one was conducted in the city to serve as a source of insight to urban air pollution mixed with wildfire smoke. The urban air collection site at the top of Brady Parking Garage on Boise State University’s campus (site 3) sits at an elevation of 830 m above sea level. The more remote Boise collection site location near the top of Bogus Basin Mountain Recreation Area (site 4) is approximately 26 km north of Boise at an elevation of 1900 m above sea level. Sites 1 and 2 served as rural sampling site locations whereas sites 3 and 4 served as urban sites. As well, the higher elevations of sites 2 and 4 were

used to determine the effects of elevation on wildfire smoke particulate suspension as compared to sites 1 and 3, respectively.

An additional sampling site (site 0) was used to determine the duration of sampling time, the number of cartridges used during sampling, and the number of elutions needed to collect adequate data on the HPLC. Site 0 was located in Challis, Idaho off Highway 21 at an elevation of 2000 m above sea level and was completed on July 13, 2021. The site was selected due to its proximity to an active wildfire in the area and the poor air quality on the day of collection due to prevalent wildfire smoke.

EPA Method TO-11A

The sampling and analysis of the collected air samples was followed closely to that of US EPA method TO-11A.[89] Ambient air carbonyl containing compounds were collected on DNPH-silica loaded cartridges (WAT037500, Waters) and connected to an air pump (TCS Electrical Motor Co. Ltd.) with tubing. The carbonyls react with the DNPH to form stable hydrazone derivatives to be later analyzed on HPLC, shown in Figure 1. The mini vacuum pumps had a rated voltage of 4.5V and an air flow rate that ranged from 1.2 to 1.6 L/min. Air sample collection was completed at site 0 to determine the duration of sampling by collecting samples at lengths of: 5 mins, 30 mins, and 1 hr. Two DNPH-silica cartridges were added in series to evaluate the efficiency of carbonyl collection in one cartridge versus two (Figure 2). A Luer lock syringe was added in front of the DNPH-silica cartridges with layers, bottom to top, of: glass wool (Supelco), calcium chloride ($CaCl_2$, Sigma Aldrich), glass wool, potassium iodide (KI, Sigma

Aldrich), glass wool. $CaCl_2$ was added to remove water from the air and KI was used to remove O_3. After sample collection, the cartridges were removed from the collection apparatus, capped, and sealed in an aluminum foil bag and stored in a refrigerator (<4 ºC) until analysis on HPLC. Two air samples collected on the DNPH-silica cartridges were obtained per each of the sampling sites.

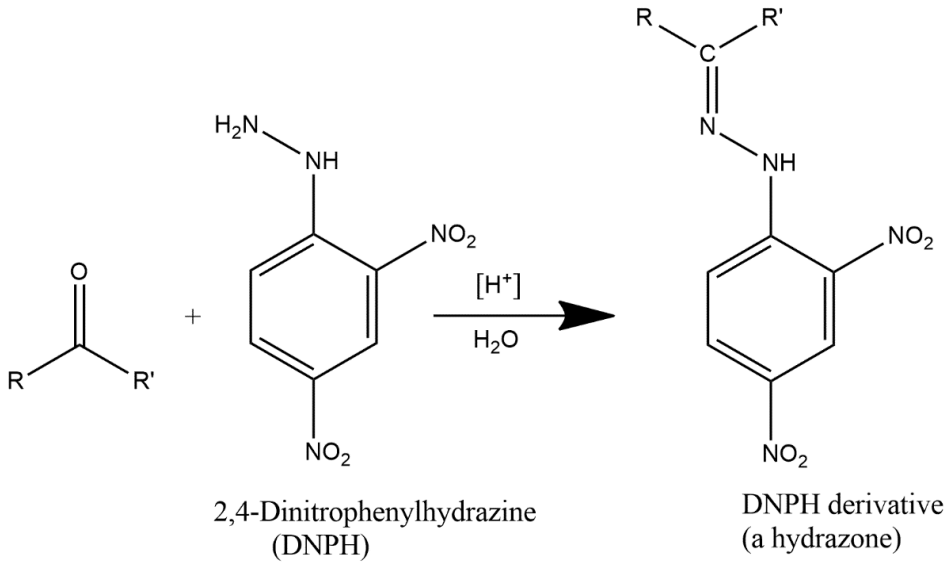

Figure 1 **Schematic of the reaction of a carbonyl with DNPH to form a stable hydrazone DNPH derivative.**

Figure 2 Ambient air collection apparatus. Two DNPH-silica cartridges are attached in series to a Luer lock syringe loaded with KI and CaCl2. The first DNPH-silica cartridge in series, A, is placed above the second, B.

The stable hydrazone derivatives were eluted with five mL of acetonitrile (HPLC grade, Sigma Aldrich) from the cartridges into a scintillation vial. The air samples collected at site 0 were eluted twice with five mL of acetonitrile to determine if several elutions were required to remove all hydrazone derivatives. Air samples collected at the remainder of the sites were eluted once with five mL of acetonitrile. The cartridge extracts were analyzed by HPLC (Agilent 1100 Series) with UV-Vis detection (Agilent 1100 Series G1315B DAD) at 360 nm. The carbonyls were separated on two Zorbax octadecylsilyl (ODS) reversed-phase columns (4.6 mm ID x 250 mm, 5 µm particle size, Agilent) in series at 30 ºC. The mobile phase was composed of acetonitrile and nanopure water with an elution gradient of: 0–30 min, 60% to 75% acetonitrile; 30–40 min, 75% to

90% acetonitrile; 40–41 min, 90% to 60% acetonitrile; 41–46 min, 60% acetonitrile. The flow rate was 1.000 mL/min and had an injection volume of 25 µL. A calibration standard of TO11/IP-6A aldehyde/ketone-DNPH mix derivatives (Sigma Aldrich) was diluted to 30, 75, 150, 300, and 600 ng/mL in acetonitrile and contained: formaldehyde, acetaldehyde, acrolein, acetone, propionaldehyde, crotonaldehyde, butyraldehyde, benzaldehyde, isovaleraldehyde, valeraldehyde, o-tolualdehyde, m-tolualdehyde, p-tolualdehyde, hexaldehyde, and 2,5-dimethylbenzaldehyde. An additional calibration standard of DNPH-derivative methacrolein (Chem Service) wad diluted in acetonitrile to 37.5, 75, 150, 300, and 600 ng/mL. The chromatograms of the DNPH-derivative standard mix and methacrolein standard at 600 ng/mL are shown in Figure 3. Concentrations of each of the carbonyls of interest during experimental air sampling collection was calculated following the EPA Method TO-11A. Table 1 provides details on the detection of the carbonyls from the DNPH-derivative standard mix and methacrolein standard. The limits of detection and quantitation were calculated as 3.3 times the signal-to-noise ratio and 10 times the signal-to-noise ratio, respectively.

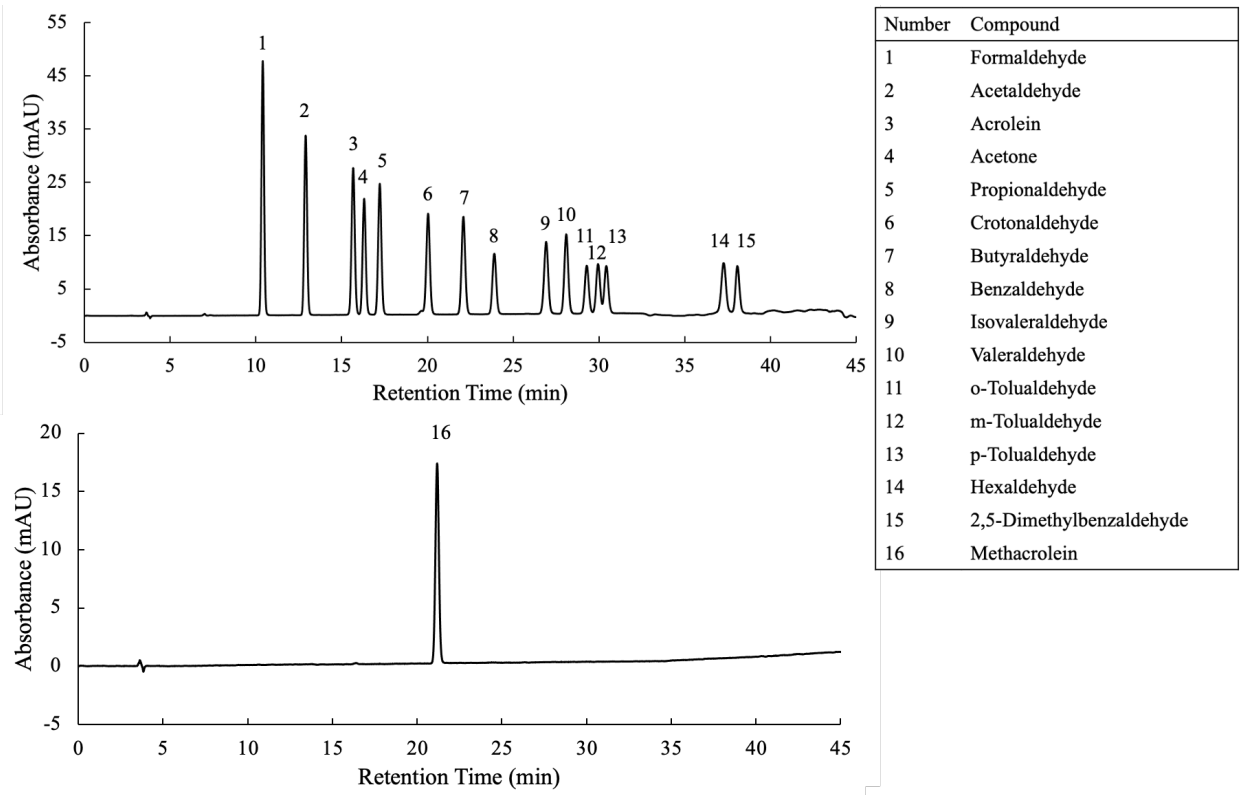

Number	Compound
1	Formaldehyde
2	Acetaldehyde
3	Acrolein
4	Acetone
5	Propionaldehyde
6	Crotonaldehyde
7	Butyraldehyde
8	Benzaldehyde
9	Isovaleraldehyde
10	Valeraldehyde
11	o-Tolualdehyde
12	m-Tolualdehyde
13	p-Tolualdehyde
14	Hexaldehyde
15	2,5-Dimethylbenzaldehyde
16	Methacrolein

Figure 3 Absorbance (mAU) vs. retention time (min) HPLC chromatogram of 600 ng/mL (top) DNPH-derivative standard mix, (bottom) DNPH-derivative methacrolein standard.

Table 1 Detection information of DNPH-derivative standard mix and methacrolein standard by HPLC-UV

Carbonyl	Retention time (min)	Correlation coefficient (R^2)	Detection limit (ppb)	Quantitation limit (ppb)
Formaldehyde	10.450	0.9997	14.59	44.22
Acetaldehyde	12.954	0.9998	13.75	41.66
Acrolein	15.726	0.9998	13.40	40.60
Acetone	16.366	0.9998	11.15	33.79
Propionaldehyde	17.886	0.9998	13.09	39.67
Crotonaldehyde	20.831	0.9999	11.34	34.36
Methacrolein	21.163	0.9995	24.39	73.92
Butyraldehyde	22.837	0.9997	15.68	47.52
Benzaldehyde	24.593	0.9997	16.40	49.69
Isovaleraldehyde	27.546	0.9997	17.06	51.70
Valeraldehyde	28.690	0.9997	15.73	47.65
o-Tolualdehyde	29.850	0.9995	21.12	63.99
m-Tolualdehyde	30.493	0.9995	20.16	61.10
p-Tolualdehyde	30.958	0.9996	18.41	55.78
Hexaldehyde	35.493	0.9998	12.26	37.15
2,5-Dimethylbenzaldehyde	36.235	0.9996	19.01	57.60

Mid-IR Detection

An integrated microcontroller circuit board (Analog Devices, EVAL-CN0338-ARDZ Shield) was used as the foundation for the construction of the mid-IR optical instrumentation. The apparatus was constructed for detection of carbon dioxide (CO_2) to gain proof-of-principle data collection at reduced material cost. The base board consists of a 24-bit data acquisition system with a sampling rate of 3.9k samples per second, multichannel analog-to-digital converters, a 32-bit ARM Cortex-M3 processor, and integrated USB ports for flash programming and serial port connection for data collection. A broadband IR filament lamp (International Light Technologies, MR3-1089) was used as the light source, and a dual-channel thermopile (Heimann Sensor, GmbH, HTS-E21-F3.91/F4.26) was used for non-dispersive infrared (NDIR) detection. The emission spectrum of the IR lamp is shown below in Figure 4. Optical filters allowed one detector thermopile channel to serve as a reference and the other channel to measure changes in IR intensity with gas concentration. The reference channel filter was a 3910 nm narrow-bandpass filter, and the CO_2 channel filter was a 4260 nm bandpass filter which spans the IR absorption of the CO_2 asymmetric stretching mode observed at ~2350 cm^{-1}. The ratio of voltages produced at each channel can be directly correlated to CO_2 concentrations. The light source fit to an aluminum parabolic reflector and the thermopile detector was placed at opposing ends of a 4-inch-long, 1-inch diameter PVC pipe as the gas cell.

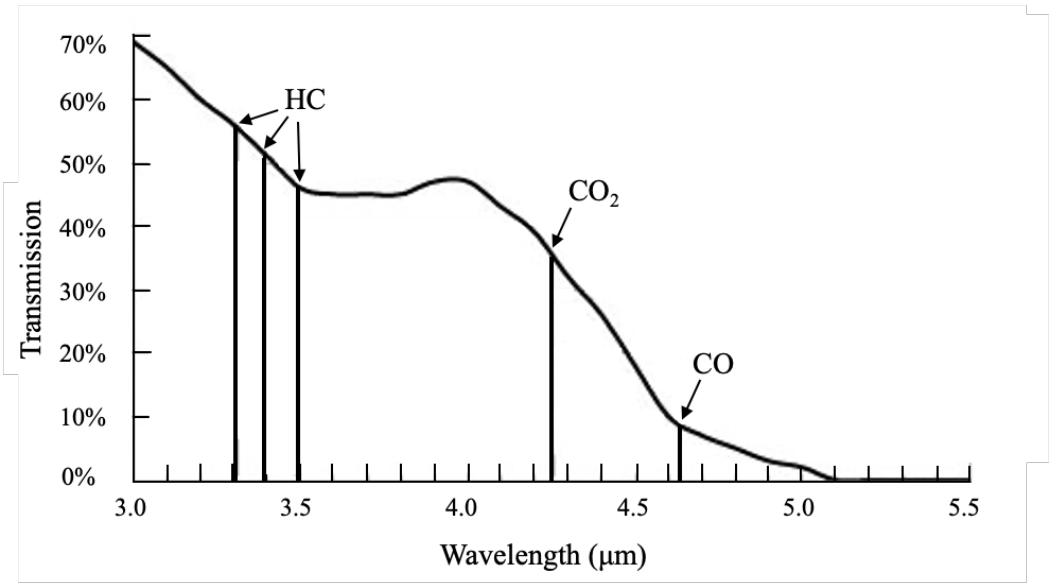

Figure 4 IR lamp emission spectrum.

An Arduino-compatible platform board (Analog Devices, EVAL-ADICUP360) was attached to the NDIR gas sensor circuit board with the electronics illustrated in Figure 5. The board was interfaced to a computer running a Linux Ubuntu 16.04 LTS operating system. The CrossCore Embedded Studio tool suite from Analog Devices was used to configure the hardware and firmware. A base ADuCM36x C++ project (ADuCM360_demo_cn0338) was configured to enable port configurations, ADC channel handling, data read/write functions, and NDIR calculations. The project also incorporated a command line interpreter to enable a user interface via an SSH client (PuTTY). Hardware parameters, data readouts, and storage were initiated and controlled through the PuTTY interface.

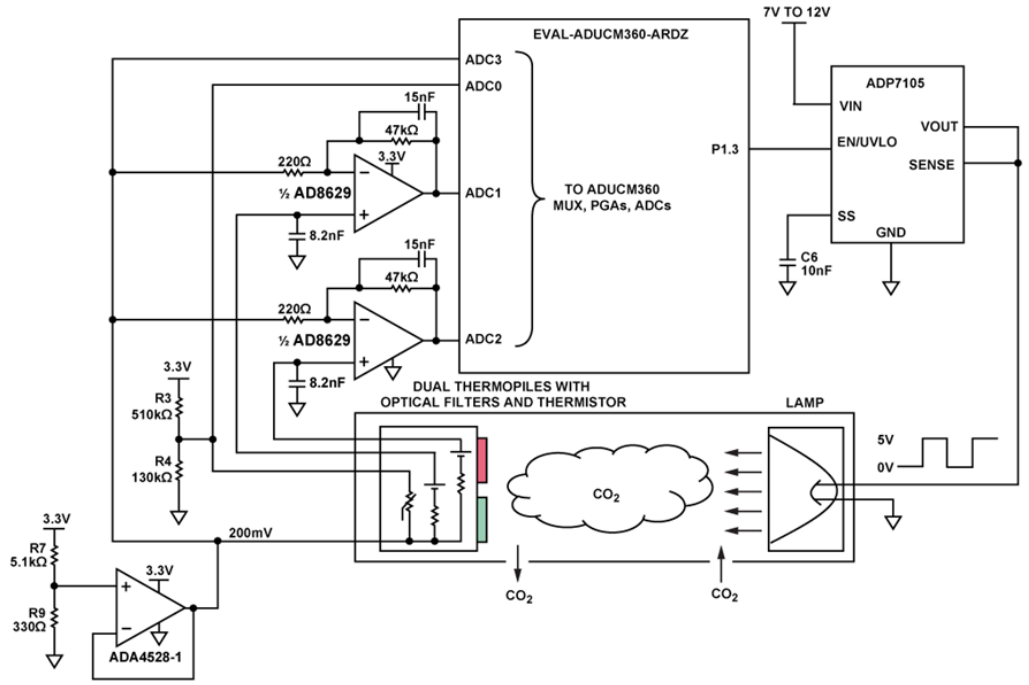

Figure 5 Schematic of CO2 gas sensor, EVAL-CN0338-ARDZ Shield, and Arduino-compatible platform board, EVAL-ADICUP360.

CO_2 gas sensing capabilities where then evaluated on the integrated sensor. The NDIR PVC pipe gas sensor was used with CO_2 gas to determine the response of the detector and electronics and provide limits of detection in a simple linear NDIR gas cell configuration. Inert nitrogen gas (N_2) was injected into the attached gas cell with known concentrations of CO_2 gas at: 50, 250, 500, 1000, and 2000 ppm. Calibrations were performed using Beer-Lambert Law and the Modified Beer-Lambert Law with inert N_2 gas and a calibration level of CO_2 gas at 5000 ppm. Two independent gas sensors and electronic platform boards were studied to discover a level of stability between the two instruments. The NDIR light source had a frequency of 0.25 Hz and 10 PuTTY fractional absorbance readouts of the asymmetric CO_2 were averaged for each of the injected CO_2 concentrations.

A brass cylinder (5.08 cm x 5.72 cm I.D.) was used to create an effective long-path gas cell. Holes were drilled to place the detector and NDIR light source used in the initial CO_2 gas cell and fit with a gas inlet and outlet adapter. A comparison of the newly constructed gas cell to the Analog Devices CO_2 gas sensor is shown in Figure 6. The gas cell was polished to allow for a high reflectivity. The cylindrical shape of the gas cell allows for a folded optical path of the NDIR beam that is approximately 30 m in length. Figure 7 illustrates the NDIR folded optical path in the new IR gas cell. N_2 gas was injected into the newly constructed brass gas cell with known CO_2 concentrations of: 5, 10, 25, 50, and 100 ppm. Calibrations were performed in the same manner as the PVC pipe gas sensor but with a calibration level of CO_2 gas at 2000 ppm. The NDIR light source had a frequency of 0.25 Hz and 10 PuTTY fractional absorbance readouts of the asymmetric CO_2 were averaged for each of the injected CO_2 concentrations.

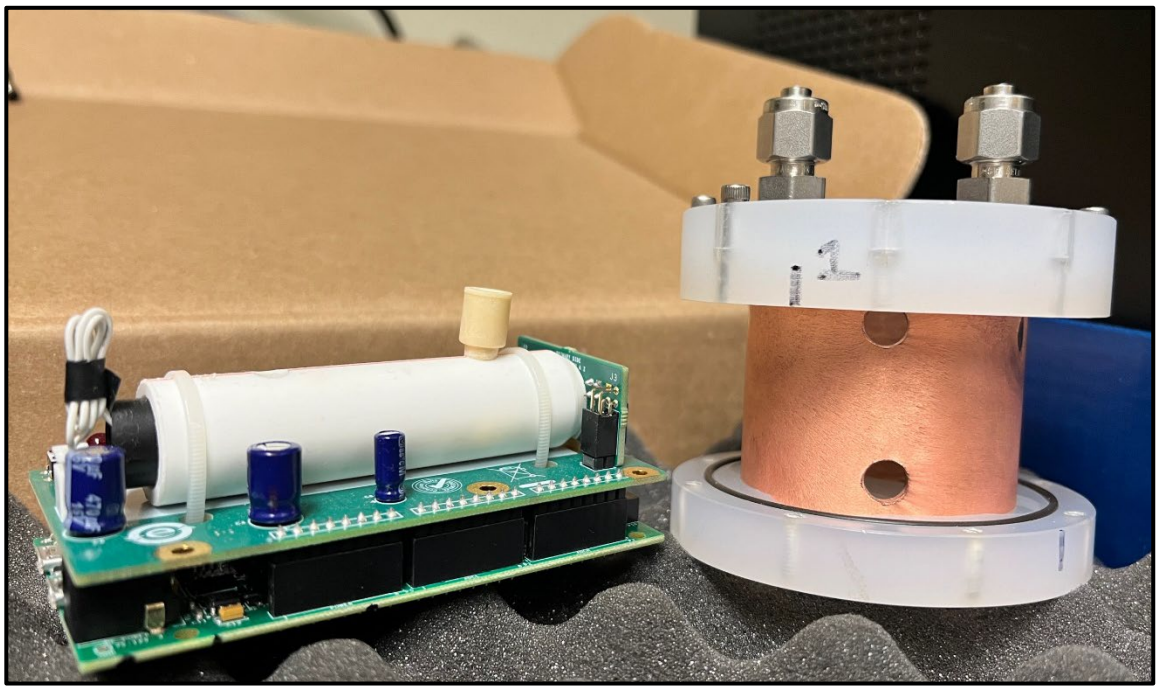

Figure 6 **Analog Devices PVC pipe gas sensor and electronics (left) compared to constructed brass gas cell (right).**

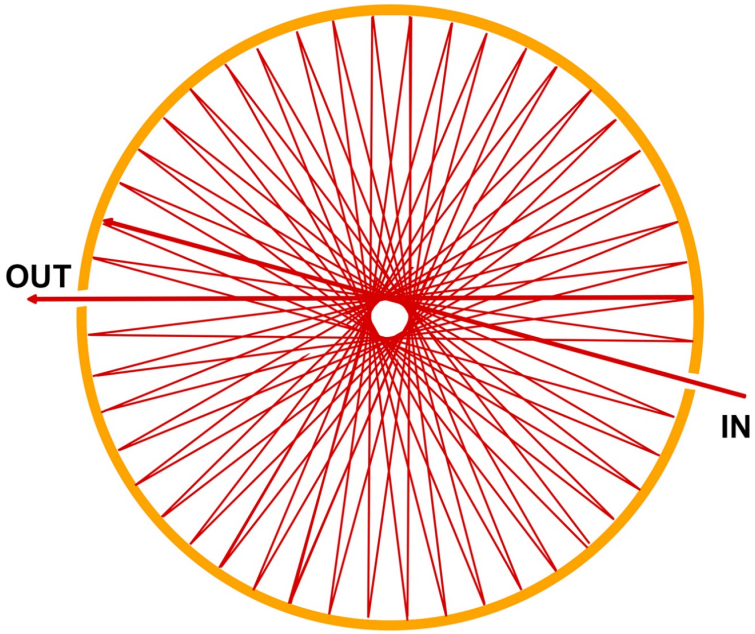

Figure 7 Schematic of the folded pathlength of the brass cylinder gas cell.

In addition to the data collected on the designed mid-IR optical instrument, IR data was obtained on an FT-IR spectrometer (PerkinElmer, Spectrum 100). Inert N_2 gas was injected into a short-path gas cell with potassium bromide (KBr) windows. Known concentrations of CO_2 were injected into the gas cell at about: 50, 100, 200, and 250 ppm. The background was taken with an empty gas cell and the IR spectra were collected with one scan.

Raman Detection

Several photonic crystal fibers (PCFs) were pumped with a passive mode-locked Ti:sapphire laser (Spectra Physics) pumped using a 5W frequency-doubled $NdYO_4$ CW laser. The laser system produces 100 fs pulses centered at 790 nm with a repetition rate of 87.2 MHz.

Four different fibers were used to characterize output and placed onto a polarization-maintaining fiber stage (ThorLabs) and output was measured with a fiber coupled spectrometer (Ocean Optics) and a liquid nitrogen cooled charge coupled device (CCD). One of the fibers (NKT Photonics, NL-PM-750) is a nonlinear polarization maintaining (NL-PM) fiber with a short zero-dispersion wavelength of 750 ± 15 nm. The pure silica fiber has a numerical aperture at 780 nm of 0.38 ± 0.05 and generates a broadband light to be used in coherent anti-Stokes Raman spectroscopy (CARS). One of the polarization maintaining PCF placed on the fiber stage is shown in Figure 8 with light coupled to the fiber. The three remaining PCF's outputs were characterized for stimulated Raman spectroscopy (SRS) and differed based upon their short zero-dispersion wavelength. Of the fibers, one had a short zero-dispersion wavelength at 615 nm (NKT Photonics, NL-PM-615), another at 760 nm (NKT Photonics, NL-PM-760), and the last at 590 nm (NKT Photonics, NL-1.5-590).

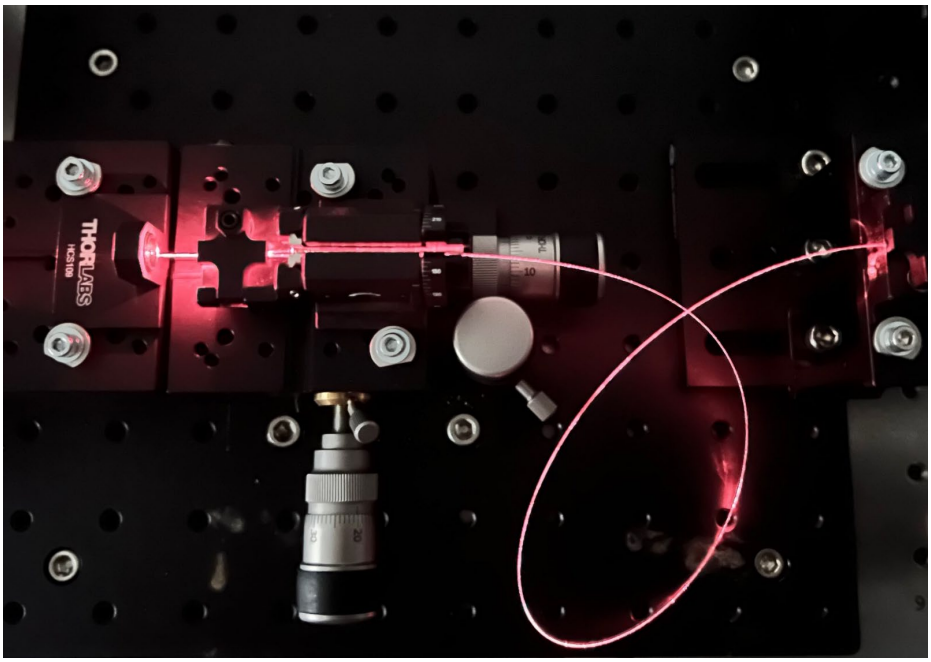

Figure 8 Hollow core photonic crystal fiber placed on polarization-maintaining stage.

RESULTS AND DISCUSSION

EPA Method TO-11A

Data collected from site 0 provided information on the duration of air sample collection, number of acetonitrile elutions of the DNPH-silica cartridges, and the number of cartridges needed to collect sufficient HAPs. It was determined from site 0 that one hour of air sample collection, one DNPH-silica cartridge, and one elution of the cartridge with acetonitrile was best suited for the method. Table A1 shows the varying concentrations of the selected carbonyls collected at 5 mins, 30 mins, and one hour, found in the appendix. Figure 9 illustrates some of the data collected at site 0. Figure 9a and 9c show the difference in HPLC chromatograms for one DNPH-silica cartridge attached to the air collection apparatus compared to two at one hour of sample collection. The first cartridge connected to the apparatus (Figure 9a), collected detectable amounts of formaldehyde, acetaldehyde, and acetone but did not detect the presence of acrolein and methacrolein. The second cartridge hooked up in series to the apparatus (Figure 9c) indicated the presence of only acetone and none of the other carbonyl compounds. It was also found, in Figures 16 – 22 in the appendix, that acetone was found in the seven cartridge blanks tested. The acetone present in the second DNPH-silica cartridge (Figure 9c) could be due to unforeseen acetone contamination during the sample extraction as the highest risk of contamination occurs then.[89] Sources of acetone contamination of the

DNPH-silica cartridges can be found in laboratory air, labeling inks, adhesives, and packaging containers and caps such as scintillation vials. Figure 9b and 9d compare one elution of the DNPH-silica cartridges on the collection apparatus compared to two elutions on the HPLC chromatogram at one hour of collection time. The amount of residual carbonyls present in the second elution of the first DNPH-silica cartridge on the apparatus (Figure 9b) compared to the second cartridge (Figure 9d) are comparable. As well, trace levels of formaldehyde, acetaldehyde, and acetone were able to be detected in the second elution (Figure 9b) and was determined that one acetonitrile elution was necessary to obtain sufficient data. Comparison of the chromatograms at five and 30 minutes of air sample collection time can be found in Figures 23 and 24 in the appendix.

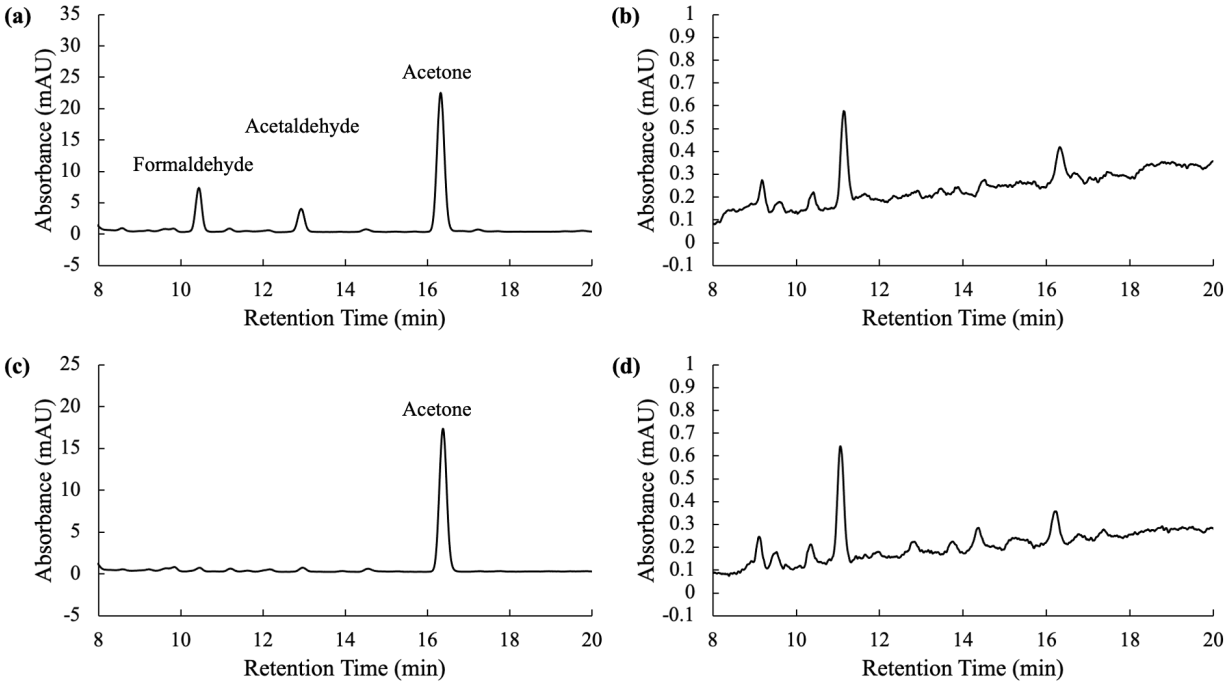

Figure 9 1 hour air collection at site 0 data (a), first cartridge on apparatus and first elution (b), first cartridge on apparatus and second elution (c), second cartridge on apparatus and first elution (d), second cartridge on apparatus and second elution.

In addition to the acetone contamination in each of the blank cartridges analyzed (Figures 16 – 22) an unknown contamination peak is found at 21.87 minutes. As the retention time for the unknown contamination is between the retention times for methacrolein and butyraldehyde, it can be presumed the compound is not one of the two compounds. As the contamination peaks in each of the blank cartridges is removed from the concentrations calculated in the experimental data, the acetone and unknown contamination peak may not interfere with the data. However, variations in the acetone contamination occur at 474.52 ± 156.72 ng per cartridge, lending to experimental data with unreliable acetone concentrations. The large variation in the acetone contamination concentration could be due to the unintentional contamination sources that vary based upon the exposure time to laboratory air, type of labeling ink, type of adhesive, and packaging container as some of the sources of contamination differed.

Baseline smoke days at sites 1 – 4 imparted a foundation for expected levels of the selected carbonyls on days without high levels of HAPs. Wildfire season smoke day carbonyl concentrations are listed along with baseline smoke carbonyl concentrations below in Table 2. Baseline days were selected after wildfire season had subsided to determine base level carbonyl concentrations at each of the collection sites. During the 2021 wildfire season, periods of high wind would blow out smoke that had settled in the Boise and Mountain Home areas to allow for some sampling days during the "wildfire season" collection interval to have a lower carbonyl concentration. It was found the outdoor ambient levels of the carbonyl HAPs vary based upon if the location is urban or rural. The carbonyl HAPs collected at each of the experimental sampling sites using EPA method TO-11A were formaldehyde, acetaldehyde, and acetone. Acrolein and

methacrolein were unable to be detected in each of the DNPH-silica cartridges at each of the sampling days. Formaldehyde has the widest range of ambient concentrations at 1.22 – 13.35 ppb as it is released from power plants, manufacturing facilities, incinerators, and automobile exhaust emissions.[65,108] Acetone ambient air levels range from 1 ppb in rural areas to 6.9 ppb in urban areas and outdoor concentrations of acetaldehyde in Canada were found to be between 1.33 and 4.00 ppb.[38,66]

Table 2 Sites 1 – 4 collected air sample carbonyl concentrations.

Smoke Intensity, Site	Date	AQI $PM_{2.5}$	Formaldehyde (ppbv)	Acetaldehyde (ppbv)	Acetone (ppbv)
Wildfire season, 1	8/2	40	2.50 ± 0.15	1.94 ± 0.62	9.25 ± 1.26
	9/1	79	2.61 ± 0.07	2.05 ± 0.23	6.83 ± 0.29
Baseline, 1	11/1	55	1.39 ± 0.21	0.65 ± 0.00	0.89 ± 0.03
Wildfire season, 2	8/2	40	1.80 ± 0.34	1.55 ± 0.19	9.20 ± 0.21
	9/1	79	2.46 ± 0.17	1.90 ± 0.22	6.95 ± 0.40
Baseline, 2	11/1	55	0.52 ± 0.50	0.27 ± 0.06	0.57 ± 0.10
Wildfire season, 3	8/3	58	4.18 ± 1.00	1.98 ± 0.34	8.77 ± 0.03
	8/16	144	5.83 ± 1.04	3.17 ± 0.31	10.82 ± 1.09
	8/27	75	1.69 ± 0.35	0.76 ± 0.05	5.26 ± 0.29
	9/9	103	10.56 ± 0.68	5.22 ± 0.01	12.38 ± 0.65
Baseline, 3	9/28	28	1.26 ± 0.11	1.20 ± 0.16	2.49 ± 0.17
Wildfire season, 4	8/3	58	1.99 ± 0.35	1.13 ± 0.01	8.90 ± 0.12
	8/18	77	1.51 ± 0.38	1.97 ± 0.41	8.43 ± 0.04
	8/25	33	1.97 ± 0.38	1.35 ± 0.08	7.95 ± 0.29
	9/8	135	3.30 ± 0.04	2.23 ± 0.45	8.60 ± 0.67
	9/23	24	1.34 ± 0.10	1.16 ± 0.08	1.97 ± 0.31
Baseline, 4	10/27	N/A	0.57 ± 0.14	0.81 ± 0.16	1.05 ± 0.32

ppbv = parts per billion volume

The remote location of site 2 had the lowest baseline concentrations of formaldehyde, acetaldehyde, and acetone on November 1 at 0.52, 0.27, and 0.57 parts per billion volume (ppbv), respectively. The highest wildfire season concentrations for formaldehyde, acetaldehyde, and acetone were found at site 3 on September 9 at 10.56, 5.22, and 12.38 ppbv respectively. Acetaldehyde was found to be above ambient levels during one of the sampling days, acetone was above ambient levels at several sampling days, while the highest concentration of formaldehyde collected was within the range of ambient levels. However, the above ambient level concentrations of acetaldehyde and acetone do not exceed the exposure limits to experience adverse health effects unless the obtained levels were sustained over a period of days to weeks. Chromatograms of the DNPH-silica cartridges at each of the sampling days can be found in Figures 25 – 41 in the appendix with the attributed data in Table 2.

AQI's for $PM_{2.5}$ on each of the sampling days was used to gauge the potential amount of smoke toxins present in the air for air sample collection.[109] However, the results varied based upon the sampling site and location, and the AQI $PM_{2.5}$ values compared to the collected carbonyl concentrations were found to be unreliable. As an AQI $PM_{2.5}$ value is indexed for all particulate matter smaller than 2.5 microns, compounds other than carbonyls will contribute to the value. As well, during periods of higher wildfire activity, particles of ash and soot will increase the AQI $PM_{2.5}$ value but may not increase the concentration of carbonyls by an equal amount. Moreover, on baseline sample collection days with higher AQI $PM_{2.5}$ values than wildfire season sampling days, it becomes evident that other particulates and compounds are increasing the AQI $PM_{2.5}$ value as carbonyl concentrations are decreased on those days. This was

observed at sites 1 and 2 on the baseline sampling day on November 1 when compared to the wildfire season sampling day on August 2. All concentrations of formaldehyde, acetaldehyde, and acetone were lower on November 1 than on August 2 despite a larger AQI $PM_{2.5}$ value.

Site 1 carbonyl concentrations peaked on August 2 for acetone at 9.25 ppbv, and peaked on September 1 for formaldehyde and acetaldehyde at 2.61 and 2.05 ppbv, respectively. Changes in the concentrations of formaldehyde and acetaldehyde between the two wildfire season sampling days at site 1 are minimal but a larger difference in concentration of acetone is observed. The higher concentration of acetone on August 2 could be attributed to a higher volume of vehicles on the highway near the collection site or higher emissions from industrial sources.[110] The decrease in acetone on September 1 is likely attributed to less outside sources of the carbonyl emissions while the increase in formaldehyde and acetaldehyde could be due to increased smoke as is evident by the increase in the AQI $PM_{2.5}$ value for total particulates. In addition, changes in wind can attribute to the variation in acetone concentration from August 2 to September 1 at both sites 1 and 2.

Wildfire season sampling day carbonyl concentrations at site 2 followed a similar pattern to site 1. The change in formaldehyde, acetaldehyde, and acetone concentrations at site 2 is similar to the change in concentrations observed at site 1. Overall, a general trend is observed between the two sites and carbonyl concentrations are lower at site 2 than site 1 with the exception of acetone levels on September 1. The changes in elevation from site 1 to site 2 can attribute to the lower carbonyl concentrations at site 2 as suspended particulates and compounds in the air will settle into the valleys of lower

elevations. The exception of acetone concentrations with this set of data could be due to changes in wind patterns and differing sources of acetone emissions as compared to formaldehyde and acetaldehyde, or could be due to the large variation in acetone contamination during the DNPH-silica cartridge elution.

The largest variation in carbonyl concentrations day-to-day was observed at site 3 during wildfire season sampling days due to periods of high winds both blowing out and blowing in smoke from nearby area wildfires. Site 3 witnessed a general trend of having higher concentrations of formaldehyde, acetaldehyde, and acetone on both wildfire season and baseline sampling days compared to the other sites. Some exceptions were observed on August 3 and August 27 due to days of high winds blowing out smoke from the valley and attributing to lower carbonyl concentrations. As site 3 had the highest carbonyl concentrations on baseline sampling days, higher carbonyl concentrations would be expected on wildfire season sampling days. This is due to the urban location of site 3 having higher emissions of carbonyls from transportation exhausts and other sources as compared to the rural locations of sites 1 and 2.

Site 4 experienced variations in carbonyl concentrations on wildfire season sampling days similar to that of site 3. Formaldehyde and acetaldehyde concentrations peaked on September 8 at 3.30 and 2.23 ppbv respectively, while acetone levels peaked on August 3 at 8.90 ppbv. Acetone concentrations were above ambient levels on five of the sampled wildfire season days. Again, these levels are not expected to be dangerous unless sustained for days to weeks. However, the higher acetone concentrations could be attributed to transportation exhausts as Bogus Basin is a recreational mountain relatively high levels of vehicle traffic during the summer months. In general, carbonyl

concentrations were lower at site 4 than site 3 and can be associated with the substantial elevation change between Boise and Bogus Basin Mountain at approximately 1070 m. Although not a widespread observation of lower carbonyl concentrations at site 4, though, it can be concluded that some particulates and compounds will, again, settle into the lower elevation valley of site 3 and not be suspended in the air at higher elevations.

Mid-IR Detection

Mid-IR detection from the PVC pipe gas sensor, newly constructed brass gas cell, and FT-IR short-path gas cell were collected and plotted against the injected CO_2 concentrations. The calibration curves for each of the gas cells is shown below in Figure 10 with the extrapolated data found in Table 3. Overall, it was found that there was an improvement in the limit of detection and limit of quantitation with the PVC pipe gas cell and the newly constructed brass gas cell as compared to the short-path gas cell used with the FT-IR.

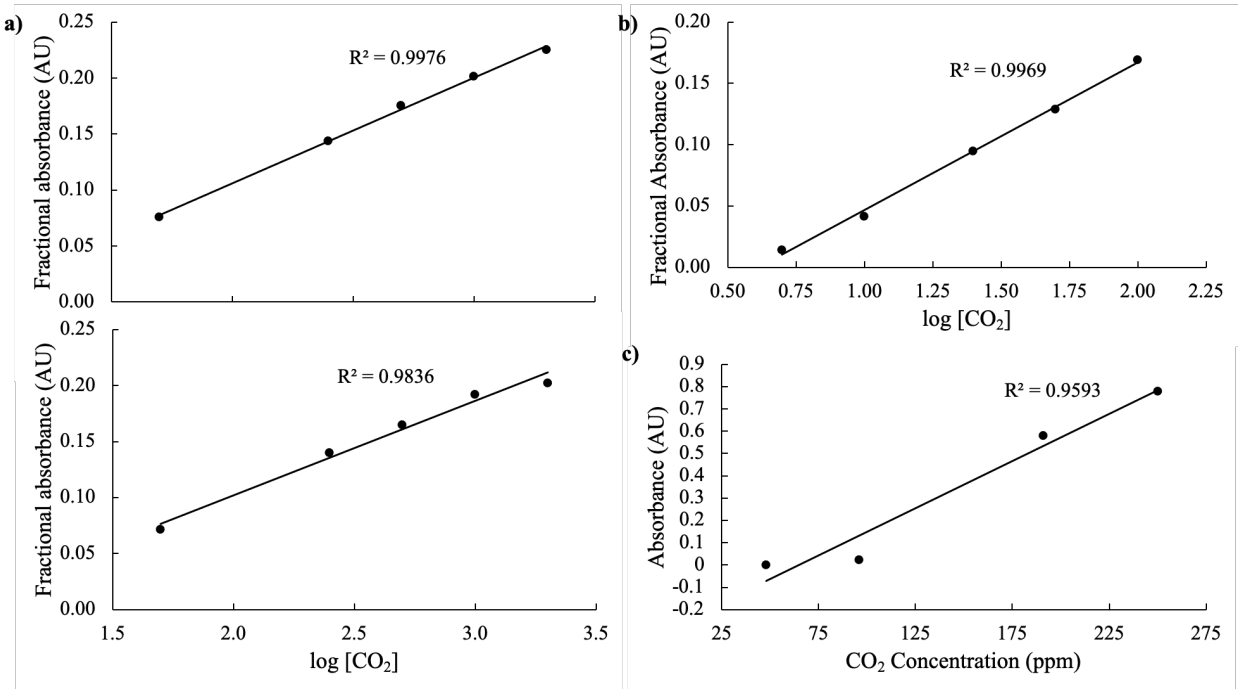

Figure 10 Calibration curves of the tested gas cells (a) Analog Devices PVC pipe thermopile-based gas sensor (EVAL-CN0338-ARDZ Shield) calibration curve (b), constructed brass gas cell (c), FT-IR short-path gas cell.

Data output from the PVC pipe and brass gas cell was obtained from the readout through PuTTY. The average of the 10 fractional absorbance values of the asymmetric CO_2 stretch was plotted against the injected CO_2 concentrations. The detection of CO_2 with the original PVC pipe gas sensor, Figure 10a, showed a logarithmic response, illustrating it followed Beer-Lambert Law and experienced some nonlinear effects at higher CO_2 concentrations. The data was linearized by taking the log of the CO_2 concentrations. The average limit of detection of the two gas sensors was found to be 1.66 ppm and the average limit of quantitation was 5.24 ppm, and was calculated from the linearized data. The limit of detection and limit of quantitation was calculated as 3.3 times the signal-to-noise ration and 10 times the signal-to-noise ratio, respectively. Data obtained from one gas sensor (Figure 10a, top) was found to be more linear than the other

(Figure 10a, bottom) and exhibited a greater R^2 value, attributing to the standard deviation of the obtained limit of detection and limit of quantitation.

Much like the PVC pipe gas cells, the data for the brass gas cell in Figure 10b, was obtained in the same matter and was also found to have a logarithmic response to the increasing CO_2 concentrations. As the data followed Beer-Lambert Law and exhibited nonlinear effects with higher CO_2 concentrations, the data was linearized, again. The limit of detection and limit of quantitation were found to be 1.29 and 2.16 ppm, respectively. The data obtained for the brass gas cell (Figure 10b) was found to have a slightly lower R^2 value than one of the PVC pipe gas sensors (Figure 10a, top). Despite the lower R^2 value, the brass gas cell was found to have a slightly lower limit of detection and limit of quantitation compared to the PVC pipe gas sensors.

Data obtained from the FT-IR short-path gas cell was in the form of a mid-IR absorption spectrum. The percent transmittance of the asymmetric CO_2 stretch at ~2350 cm^{-1} was converted into the absorbance and was plotted against the injected CO_2 concentrations to obtain a Beer-Lambert curve (Figure 10c). The data did not exhibit a logarithmic response by the detector but did experience a slightly linear response to the CO_2. The short-path gas cell used with the FT-IR was found to have a worsened limit of detection at 75.89 ppm and worsened limit of quantitation at 229.97 ppm. Difficulty obtaining data was experienced at concentrations of CO_2 gas below 150 ppm.

Table 3 Limits of detection and limits of quantitation from each of the tested gas cells.

Gas cell type	Limit of detection (ppm)	Limit of quantitation (ppm)
PVC pipe	1.66 ± 0.50	5.24 ± 4.25
Brass	1.29	2.16
Short-path	75.89	229.97

Comparison of the data between the PVC pipe gas sensors and the brass gas cell through Table 3 and Figure 10a and 10b proves to be comparable. The limit of detection and limit of quantitation of the brass gas cell was slightly improved upon from the two PVC pipe gas cells. This could be attributed to the differing CO_2 gas concentrations used during the initial calibration of the instruments. The PVC pipe gas cells were calibrated with 5000 ppm CO_2 gas in inert N_2 gas; the brass gas cell was calibrated with a concentration of CO_2 gas at 2000 ppm. During the experimental set-up, CO_2 gas concentrations were able to reach as low as 5 ppm in the brass gas cell before obtaining negative fractional absorbances by the PuTTY interface and were only able to reach concentration lows of 50 ppm in the PVC pipe gas cell. This could be attributed to the change in the calibration CO_2 gas levels as a calibration with a lower concentration could allow for more trace detection. However, the change in the limit of detection and limit of quantitation of the brass gas cell was expected to be better enhanced due to the longer effective path length obtained by the polished cylindrical gas cell shape.

Raman Detection

Initial fiber output characterization of fiber NL-PM-760 can be found below in Figure 11 and was used for SRS. The pump wavelength into the fiber was centered around 800 nm and had a bandwidth of 50 nm. New light was generated within the PCF in the form of a soliton, or probe, that originated at an output wavelength around 850 nm at a 10 mW pump power. As the pump power was increased into the fiber, the soliton frequency and wavelength was shifted. When increased to a power of 25 mW, the soliton wavelength shifted to about 900 nm and as the pump power was increased to 50 and 65 mW, the soliton was subsequentially shifted to about 1075 and 1125 nm, respectively. The shift in the soliton frequency and wavelength allows for tuning to resonant stretching modes of compounds. SRS was completed on a drop of oil with the fiber and the soliton output was tuned to the C-H stretch of the compound. The drop of oil was placed on a moveable stage and as the position of the oil droplet from the fiber output was moved the intensity of the SRS changed (Figure 11, bottom left). It was found the intensity of the SRS was greater at distances closer to the fiber output than farther away (>95 μm).

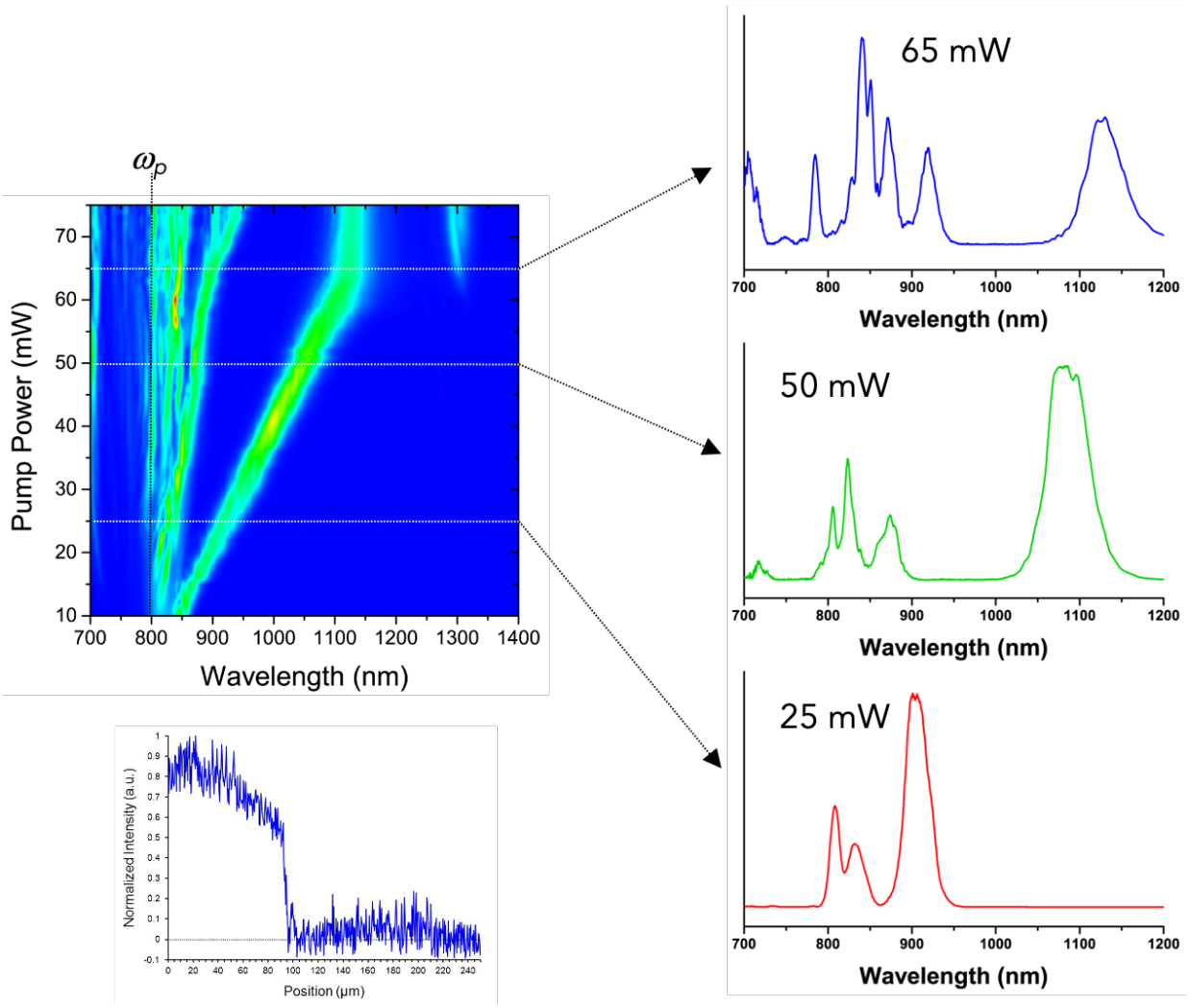

Figure 11 Fiber (NL-PM-760) output at a 50 nm pump bandwidth.

The same fiber (NL-PM-760) was measured with a changed in the pump bandwidth to determine if there was a change in the soliton generation. Figure 12 compares the pump bandwidth of the fiber at 50 nm and 90 nm. The 50 nm pump bandwidth (Figures 11 and 12a) was investigated above and generated a soliton, or probe, to be tuned to resonant compound stretches. As the pump bandwidth increases to 90 nm (Figure 12b), higher peak intensity of the soliton is observed. A longer pump bandwidth is associated with shorter laser pulse durations and increased peak intensities. Higher soliton intensities could allow for stronger SRS intensities when tuned to compound

stretches at the soliton peak. However, as the fiber output is not as neat at a pump bandwidth of 90 nm (Figure 12b) as compared to the fiber output at a pump bandwidth of 50 nm (Figure 12a), this specific fiber would be more well suited to operate at the 50 nm pump bandwidth for SRS.

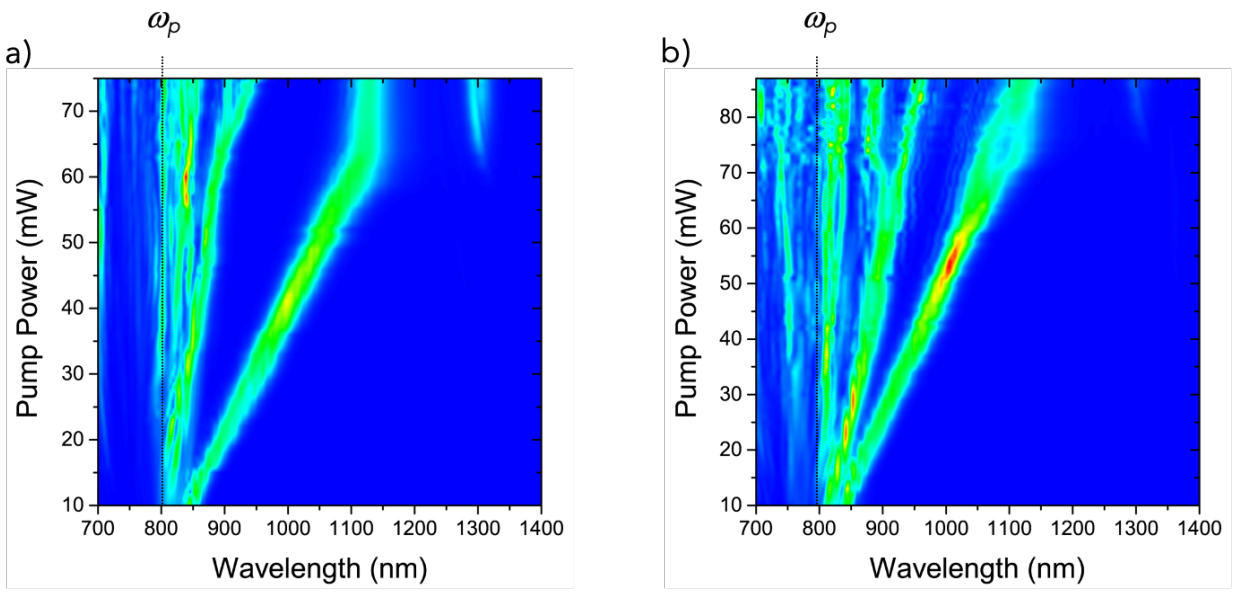

Figure 12 Fiber (NL-PM-760) output at a pump bandwidth of (a) 50 nm, (b) 90 nm.

Fiber output data collected for fiber NL-1.5-590 is found in Figure 13 below. The pump wavelength was centered around 800 nm and soliton generation was initially observed at a pump power of 10 mW at about 875 nm. As coupling efficiency of the pump and fiber was increased, it was observed that there was no increase in the soliton power. As well, the behavior of the soliton maintained the same as coupling efficiency increased. The pump bandwidth was increased to observe the behavior of the soliton and it was found there was, again, no increase in the soliton power. However, there was an increase in the bandwidth of the soliton. An increase in the soliton bandwidth would allow for overlap of different compound stretching modes when tuning around the pump.

The generation of a single resonant stretching mode would prove difficult when using this fiber. However, example SRS on a drop of oil was not completed to determine the fiber's efficiency.

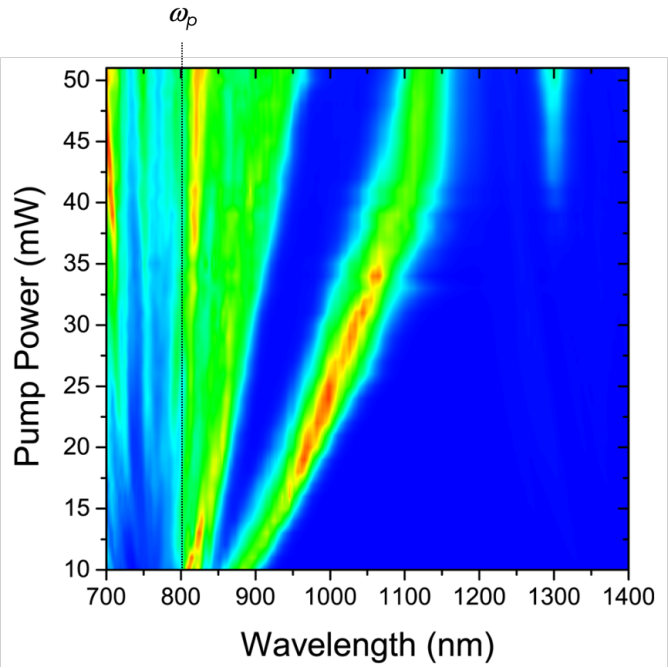

Figure 13 Fiber NL-1.5-590 output and soliton generation.

Inconclusive fiber output data for fiber NL-PM-615 was obtained and illustrated in Figure 14. The pump wavelength is centered around 800 nm and similar to the other fibers, a soliton is initially generated within the fiber. However, as the pump power is increased, the produced soliton disappears. At the initial pump power of 10 mW, the soliton is observed around 850 nm. Once the pump power is increased to 25 mW, the soliton is observed at about 940 nm but begins to disappear above this power. It is weakly generated and has low peak intensities found at pump powers of 35, 45, and 50 mW (Figure 14, right). As the soliton disappeared, example SRS could not be conducted, and the fiber was determined to be incapable of tuning to resonant compound stretches.

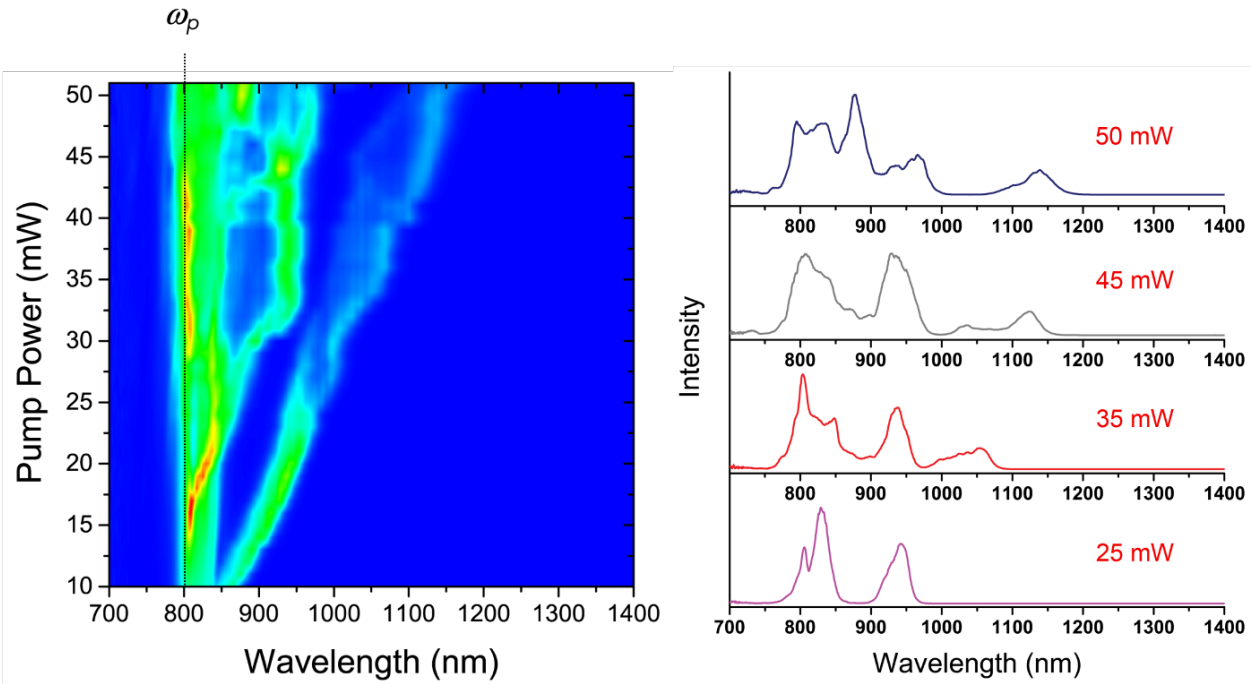

Figure 14 Fiber (NL-PM-615) output.

The final fiber evaluated, NL-PM-750 found in Figure 15, generated supercontinuum light with an input pump wavelength centered around 790 nm. As light enters the fiber, the 790 nm wavelength is diffracted against the fiber cladding to generate a broadband light source at the fiber's terminal output. The broadband of light generated can be used for CARS as it requires multiple wavelengths of light to generate a spectrum. However, the fiber did not exhibit a strong supercontinuum generation and would benefit from increased coupling efficiency. As the coupling efficiency is increased for a supercontinuum generating fiber, the intensity and bandwidth of light created is greater. The present spectrum obtained of the fiber output has peak intensities centered around the input pump wavelength and decreases sharply at wavelengths larger than the input pump and more slowly at shorter wavelengths.

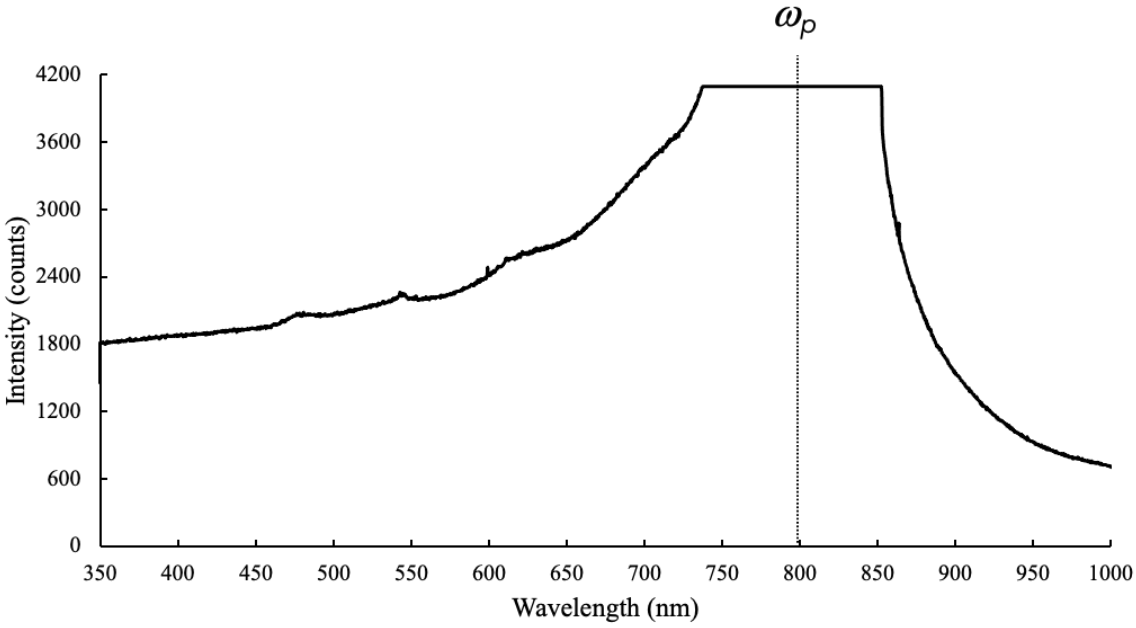

Figure 15 Fiber (NL-PM-750) output supercontinuum generation.

CONCLUSION

Wildfires will continue to be an increased issue in the US with climate change and the prolonged and extensive drought experienced in the western half of the country. The regulated detection methods of VOCs and HAPs released from wildfires are limited in their capabilities of a complete overview of toxins in ambient air and the timeliness of data collection. EPA method TO-11A proved effective in determining concentrations of select carbonyls, formaldehyde, acetaldehyde, and acetone, in ambient air. As was previously observed in research labs and reported by the EPA, unsaturated carbonyls, such as acrolein and methacrolein, cannot be determined using the method and must be detected by other means. Acetone had significant contamination issues and the collected concentrations may not accurately reflect the levels that were present at each of the collection sites. A general trend towards higher elevation collection sites having lower levels of carbonyls was found as the toxins settle into the valleys. As well, urban locations were found to have higher ambient concentrations of carbonyls compared to the rural location sites as there is a greater amount of carbonyl emission sources. Using multiple EPA methods in tandem would provide a complete profile of the toxins in the air but could yield inaccurate data in some of the collected toxins and variation in the concentrations detected as well as become ineffective in the cost and time needed for data collection. Other detection methods of wildfire HAPs would prove beneficial in reporting

a health outlook to the public as formaldehyde, acetaldehyde, acrolein, and methacrolein have substantial health effects on the public.

As has been reported by multiple research labs, optical detection methods of ultrafine particulate matter is effective but is limited in real applications. The compact LED-based mid-IR instrument that was constructed allowed for a slight improvement in the limits of detection of CO_2 compared to the PVC pipe gas sensors. The short-path gas cell used with the FT-IR proved to be the most ineffective detection method of the three tested. However, the brass gas cell limit of detection and limit of quantitation were not as improved upon as was expected. Although it does not provide the limits of detection and quantitation for each of the carbonyls tested using the EPA method, the more sensitive detection and quantitation limit of CO_2 in the brass gas cell proves promising for trace gas detection of other compounds.

Initial development of the compact coherent Raman instrument provided insight into the PCFs that would be most beneficial to use in component detection. Fiber __ proved to be unable to tune to a single compound stretch around the pump as the soliton bandwidth increased with an increased pump bandwidth. As well, fiber's NL-PM-615 soliton generation disappeared with increasing pump power and would be unable to be utilized for SRS. Fiber NL-PM-760 had successful completion of SRS on a drop of oil at a pump bandwidth of 50 nm and will be best suited for soliton tuning to the carbonyl compound stretches tested in the EPA method. Lastly, the supercontinuum generation fiber, NL-PM-750, was not fully capable of generating a broadband light source and would benefit from increased coupling efficiency to complete CARS on formaldehyde, acetaldehyde, acetone, acrolein, and methacrolein.

The construction of compact optical instrumentation for gas component detection and ambient air quality monitoring would provide rapid data to the public for air quality hazards. The EPA methods are beneficial in detection of select compounds, but multiple methods would need to be utilized at the same time to provide a complete chemical profile of the air. The initial construction of the compact LED-based mid-IR instrument and compact coherent Raman spectrometer could provide data on air quality year-round. These instruments could be placed at remote locations to allow for the user to remove themselves from any wildfire hazards present during wildfire season. As the detection methods of the constructed instrumentation becomes more selective and sensitive, the use of new air quality monitoring systems would become instrumental in the reporting of air quality hazards.

FUTURE DIRECTIONS

Future directions of the project would further explore the capabilities of the constructed optical detection instruments. The brass gas cell will be fit with a four-channel broadband detector and optical filters to isolate different IR active modes of the airborne toxins. One channel will serve as a reference while the remaining three will observe the intensities of selected IR active modes. Each of the selected carbonyls would be tested with the new detector and limits of detection and limits of quantitation will be obtained to ensure trace detection is achieved. However, as overlap of the IR stretching modes of the selected carbonyls will occur when detected simultaneously and separation is unable to be achieved, a total carbonyl concentration may be the reported data values for *in situ* use. Further alignment of the IR lamp and detector will allow for higher sensitivity of the instrument. Modifications of the IR lamp and cylindrical gas cell may need to be completed for enhanced detection.

Further development of the compact coherent Raman spectrometer would benefit from testing several other PCFs. Once the optimal PCFs are selected for SRS and CARS, the nonlinear Raman instrument would collect spontaneous, stimulated, and coherent anti-Stokes Raman spectra of formaldehyde, acetaldehyde, acetone, acrolein, and methacrolein and other atmospheric components. Limits of detection and limits of quantitation will be calculated and compared to the compact mid-IR instrumentation. In the end, the project hopes for the development of a compact all fiber spectrometer with

real time *in situ* capabilities in Idaho of ambient air quality monitoring and wildfire season hazard reporting.

REFERENCES

(1) Abatzoglou, J. T.; Williams, A. P. Impact of anthropogenic climate change on wildfire across western US forests. *Proc. Natl. Acad. Sci. U. S. A.* **2016**, *113* (42), 11770-11775. DOI: 10.1073/pnas.1607171113.

(2) Brey, S. J.; Barnes, E. A.; Pierce, J. R.; Swann, A. L. S.; Fischer, E. V. Past Variance and Future Projections of the Environmental Conditions Driving Western U.S. Summertime Wildfire Burn Area. *Earths Future* **2020**, *9* (2), e2020EF001645. DOI: 10.1029/2020EF001645.

(3) Ford, B.; Val Martin, M.; Zelasky, S. E.; Fischer, E. V.; Anenberg, S. C.; Heald, C. L.; Pierce, J. R. Future Fire Impacts on Smoke Concentrations, Visibility, and Health in the Contiguous United States. *Geohealth* **2018**, *2* (8), 229-247. DOI: 10.1029/2018GH000144.

(4) Harvey, B. J. Human-caused climate change is now a key driver of forest fire activity in the western United States. *Proc. Natl. Acad. Sci. U. S. A.* **2016**, *113* (42), 11649-11650. DOI: 10.1073/pnas.1612926113.

(5) Yue, X.; Mickley, L. J.; Logan, J. A.; Kaplan, J. O. Ensemble projections of wildfire activity and carbonaceous aerosol concentrations over the western United States in the mid-21st century. *Atmos. Environ.* **2013**, *77*, 767-780. DOI: 10.1016/j.atmosenv.2013.06.003.

(6) Akagi, S. K.; Yokelson, R. J.; Wiedinmyer, C.; Alvarado, M. J.; Reid, J. S.; Karl, T.; Crounse, J. D.; Wennberg, P. O. Emission factors for open and domestic biomass burning for use in atmospheric models. *Atmos. Chem. Phys.* **2011**, *11* (9), 4039-4072. DOI: 10.5194/acp-11-4039-2011.

(7) Crutzen, P. J.; Andreae, M. O. Biomass burning in the tropics: impact on atmospheric chemistry and biogeochemical cycles. *Science (Washington, D. C., 1883-)* **1990**, *250* (4988), 1669. DOI: 10.1126/science.250.4988.1669.

(8) Yokelson, R. J.; Christian, T. J.; Karl, T. G.; Guenther, A. The tropical forest and fire emissions experiment: laboratory fire measurements and synthesis of campaign data. *Atmos. Chem. Phys.* **2008**, *8* (13), 3509-3527. DOI: 10.5194/acp-8-3509-2008.

(9) Spracklen, D. V.; Mickley, L. J.; Logan, J. A.; Hudman, R. C.; Yevich, R.; Flannigan, M. D.; Westerling, A. L. Impacts of climate change from 2000 to 2050 on wildfire activity and carbonaceous aerosol concentrations in the western United States. *J. Geophys. Res., [Atmos.]* **2009**, *114* (D20), D20301/20301. DOI: 10.1029/2008jd010966.

(10) Lozano, O. M.; Salis, M.; Ager, A. A.; Arca, B.; Alcasena, F. J.; Monteiro, A. T.; Finney, M. A.; Del Giudice, L.; Scoccimarro, E.; Spano, D. Assessing Climate Change Impacts on Wildfire Exposure in Mediterranean Areas. *Risk Anal* **2017**, *37* (10), 1898-1916. DOI: 10.1111/risa.12739.

(11) Pugh, B.; Sanchez-Lugo, A. *West U.S. Drought Monitor*. National Drought Mitigation Center, University of Nebraska-Lincoln, 2022. (accessed 2022 1 March).

(12) Center, N. I. F. *National Interagency Coordination Center Wildland Fire Summary and Statistics Annual Report 2021*. 2021. (accessed 2022 25 February).

(13) Hoover, K.; Hanson, L. A. *Wildfire Statistics*. Congressional Research Service, (accessed 2022 28 February).

(14) Pinkerton, K. E.; Rom, W. N.; Akpinar-Elci, M.; Balmes, J. R.; Bayram, H.; Brandli, O.; Hollingsworth, J. W.; Kinney, P. L.; Margolis, H. G.; Martin, W. J.; et al. An official American Thoracic Society workshop report: Climate change and human health. *Proc Am Thorac Soc* **2012**, *9* (1), 3-8. DOI: 10.1513/pats.201201-015ST.

(15) Rice, M. B.; Thurston, G. D.; Balmes, J. R.; Pinkerton, K. E. Climate change. A global threat to cardiopulmonary health. *Am J Respir Crit Care Med* **2014**, *189* (5), 512-519. DOI: 10.1164/rccm.201310-1924PP.

(16) Hurteau, M. D.; Westerling, A. L.; Wiedinmyer, C.; Bryant, B. P. Projected Effects of Climate and Development on California Wildfire Emissions through 2100. *Environ. Sci. Technol.* **2014**, *48* (4), 2298-2304. DOI: 10.1021/es4050133.

(17) Lill, E.; Lindaas, J.; Juncosa Calahorrano, J. F.; Campos, T.; Flocke, F.; Apel, E. C.; Hornbrook, R. S.; Hills, A.; Jarnot, A.; Blake, N.; et al. Wildfire-driven changes in the abundance of gas-phase pollutants in the city of Boise, ID during summer 2018. *Atmos. Pollut. Res.* **2022**, *13* (1), 101269. DOI: 10.1016/j.apr.2021.101269.

(18) EPA, U. *Ecoregions*. United States Environmental Protection Agency, 2021. https://www.epa.gov/eco-research/ecoregions (accessed 2022 1 March).

(19) Wiedinmyer, C.; Quayle, B.; Geron, C.; Belote, A.; McKenzie, D.; Zhang, X.; O'Neill, S.; Wynne, K. K. Estimating emissions from fires in North America for air quality modeling. *Atmos. Environ.* **2006**, *40* (19), 3419-3432. DOI: 10.1016/j.atmosenv.2006.02.010.

(20) Garofalo, L. A.; Pothier, M. A.; Levin, E. J. T.; Campos, T.; Kreidenweis, S. M.; Farmer, D. K. Emission and Evolution of Submicron Organic Aerosol in Smoke from Wildfires in the Western United States. *ACS Earth Space Chem.* **2019**, *3* (7), 1237-1247. DOI: 10.1021/acsearthspacechem.9b00125.

(21) Liu, X.; Huey, L. G.; Yokelson, R. J.; Selimovic, V.; Simpson, I. J.; Mueller, M.; Jimenez, J. L.; Campuzano-Jost, P.; Beyersdorf, A. J.; Blake, D. R.; et al. Airborne measurements of western U.S. wildfire emissions: Comparison with prescribed burning and air quality implications. *J. Geophys. Res.: Atmos.* **2017**, *122* (11), 6108-6129. DOI: 10.1002/2016jd026315.

(22) Palm, B. B.; Peng, Q.; Fredrickson, C. D.; Lee, B. H.; Garofalo, L. A.; Pothier, M. A.; Kreidenweis, S. M.; Farmer, D. K.; Pokhrel, R. P.; Shen, Y.; et al. Quantification of organic aerosol and brown carbon evolution in fresh wildfire plumes. *Proc. Natl. Acad. Sci. U. S. A.* **2020**, *117* (47), 29469-29477. DOI: 10.1073/pnas.2012218117.

(23) Permar, W.; Wang, Q.; Selimovic, V.; Wielgasz, C.; Yokelson, R. J.; Hornbrook, R. S.; Hills, A. J.; Apel, E. C.; Ku, I. T.; Zhou, Y.; et al. Emissions of Trace Organic Gases From Western U.S. Wildfires Based on WE-CAN Aircraft Measurements. *J. Geophys. Res.: Atmos.* **2021**, *126* (11), e2020JD033838. DOI: 10.1029/2020jd033838.

(24) O'Dell, K.; Hornbrook, R. S.; Permar, W.; Levin, E. J. T.; Garofalo, L. A.; Apel, E. C.; Blake, N. J.; Jarnot, A.; Pothier, M. A.; Farmer, D. K.; et al. Hazardous air pollutants in fresh and aged western US wildfire smoke and implications for long-term exposure. *Environ. Sci. Technol.* **2020**, *54* (19), 11838-11847, 10.1021/acs.est.0c04497. DOI: 10.1021/acs.est.0c04497.

(25) Lindaas, J.; Pollack, I. B.; Garofalo, L. A.; Pothier, M. A.; Farmer, D. K.; Kreidenweis, S. M.; Campos, T. L.; Flocke, F.; Weinheimer, A. J.; Montzka, D. D.; et al. Emissions of Reactive Nitrogen From Western U.S. Wildfires During Summer 2018. *J. Geophys. Res.: Atmos.* **2021**, *126* (2), e2020JD032657. DOI: 10.1029/2020jd032657.

(26) Meng, J.; Martin, R. V.; Li, C.; van Donkelaar, A.; Tzompa-Sosa, Z. A.; Yue, X.; Xu, J.-W.; Weagle, C. L.; Burnett, R. T. Source Contributions to Ambient Fine Particulate Matter for Canada. *Environ. Sci. Technol.* **2019**, *53* (17), 10269-10278. DOI: 10.1021/acs.est.9b02461.

(27) Mauderly, J. L.; Barrett, E. G.; Day, K. C.; Gigliotti, A. P.; McDonald, J. D.; Harrod, K. S.; Lund, A. K.; Reed, M. D.; Seagrave, J. C.; Campen, M. J.; et al. The National Environmental Respiratory Center (NERC) experiment in multi-pollutant air quality health research: II. Comparison of responses to diesel and gasoline engine exhausts, hardwood smoke and simulated downwind coal emissions. *Inhalation Toxicol.* **2014**, *26* (11), 651-667. DOI: 10.3109/08958378.2014.925523.

(28) Totlandsdal, A. I.; Oevrevik, J.; Cochran, R. E.; Herseth, J.-I.; Boelling, A. K.; Laag, M.; Schwarze, P.; Lilleaas, E.; Holme, J. A.; Kubatova, A. The occurrence of polycyclic aromatic hydrocarbons and their derivatives and the proinflammatory potential of fractionated extracts of diesel exhaust and wood smoke particles. *J. Environ. Sci. Health, Part A: Toxic/Hazard. Subst. Environ. Eng.* **2014**, *49* (4), 383-396. DOI: 10.1080/10934529.2014.854586.

(29) EPA, U. *Our Nation's Air Trends Through 2020*. United States Environmental Protection Agency, 2021. https://gispub.epa.gov/air/trendsreport/2021/#home (accessed 2022 3 March).

(30) EPA, U. *Hazardous Air Pollutants*. United State Environmental Protection Agency, 2022. https://www.epa.gov/haps (accessed 2022 3 March).

(31) EPA, U. *Initial List of Hazardous Air Pollutants with Modifications*. United States Environmental Protection Agency, 2022. https://www.epa.gov/haps/initial-list-hazardous-air-pollutants-modifications (accessed 2022 3 March).

(32) Stockwell, C. E.; Yokelson, R. J.; Kreidenweis, S. M.; Robinson, A. L.; DeMott, P. J.; Sullivan, R. C.; Reardon, J.; Ryan, K. C.; Griffith, D. W. T.; Stevens, L. Trace gas emissions from combustion of peat, crop residue, domestic biofuels, grasses, and other fuels: configuration and Fourier transform infrared (FTIR) component of the fourth Fire Lab at Missoula Experiment (FLAME-4). *Atmos. Chem. Phys.* **2014**, *14* (18), 9727. DOI: 10.5194/acp-14-9727-2014.

(33) Stockwell, C. E.; Veres, P. R.; Williams, J.; Yokelson, R. J. Characterization of biomass burning emissions from cooking fires, peat, crop residue, and other fuels with high-resolution proton-transfer-reaction time-of-flight mass spectrometry. *Atmos. Chem. Phys.* **2015**, *15* (2), 845. DOI: 10.5194/acp-15-845-2015.

(34) Reid, C. E.; Brauer, M.; Johnston, F. H.; Jerrett, M.; Balmes, J. R.; Elliott, C. T. Critical Review of Health Impacts of Wildfire Smoke Exposure. *Environ Health Perspect* **2016**, *124* (9), 1334-1343. DOI: 10.1289/ehp.1409277.

(35) Zhu, B.; Han, Y.; Wang, C.; Huang, X.; Xia, S.; Niu, Y.; Yin, Z.; He, L. Understanding primary and secondary sources of ambient oxygenated volatile organic compounds in Shenzhen utilizing photochemical age-based parameterization method. *J Environ Sci (China)* **2019**, *75*, 105-114. DOI: 10.1016/j.jes.2018.03.008.

(36) Jaffe, D. A.; Wigder, N. L. Ozone production from wildfires: A critical review. *Atmos. Environ.* **2012**, *51*, 1-10. DOI: 10.1016/j.atmosenv.2011.11.063.

(37) Holloway, T.; Levy, H., II; Kasibhatla, P. Global distribution of carbon monoxide. *J. Geophys. Res., [Atmos.]* **2000**, *105* (D10), 12123-12147.

(38) ATSDR. *Toxicological Profile for Acetone*. U.S. Department of Health and Human Services Agency for Toxic Substances and Disease Registry, 2021. (accessed 2022 14 March).

(39) Atkinson, R.; Baulch, D. L.; Cox, R. A.; Crowley, J. N.; Hampson, R. F.; Hynes, R. G.; Jenkin, M. E.; Rossi, M. J.; Troe, J. Evaluated kinetic and photochemical data for atmospheric chemistry: Volume II - gas phase reactions of organic species. *Atmos. Chem. Phys.* **2006**, *6* (11), 3625-4055. DOI: 10.5194/acp-6-3625-2006.

(40) Pope, F. D.; Smith, C. A.; Davis, P. R.; Shallcross, D. E.; Ashfold, M. N. R.; Orr-Ewing, A. J. Photochemistry of formaldehyde under tropospheric conditions. *Faraday Discuss.* **2005**, *130*, 59-72. DOI: 10.1039/b419227c.

(41) Fine, P. M.; Cass, G. R.; Simoneit, B. R. T. Chemical Characterization of Fine Particle Emissions from Fireplace Combustion of Woods Grown in the Northeastern United States. *Environ. Sci. Technol.* **2001**, *35* (13), 2665-2675. DOI: 10.1021/es001466k.

(42) Fine, P. M.; Cass, G. R.; Simoneit, B. R. T. Chemical Characterization of Fine Particle Emissions from the Fireplace Combustion of Woods Grown in the Southern United States. *Environ. Sci. Technol.* **2002**, *36* (7), 1442-1451. DOI: 10.1021/es0108988.

(43) Fine, P. M.; Cass, G. R.; Simoneit, B. R. T. Chemical Characterization of Fine Particle Emissions from the Fireplace Combustion of Wood Types Grown in the Midwestern and Western United States. *Environ. Eng. Sci.* **2004**, *21* (3), 387-409. DOI: 10.1089/109287504323067021.

(44) Hays, M. D.; Geron, C. D.; Linna, K. J.; Smith, N. D.; Schauer, J. J. Speciation of Gas-Phase and Fine Particle Emissions from Burning of Foliar Fuels. *Environ. Sci. Technol.* **2002**, *36* (11), 2281-2295. DOI: 10.1021/es0111683.

(45) Sheesley, R. J.; Schauer, J. J.; Chowdhury, Z.; Cass, G. R.; Simoneit, B. R. T. Characterization of organic aerosols emitted from the combustion of biomass indigenous to south Asia. *J. Geophys. Res., [Atmos.]* **2003**, *108* (D9), AAC. DOI: 10.1029/2002jd002981.

(46) Lee, S.; Baumann, K.; Schauer, J. J.; Sheesley, R. J.; Naeher, L. P.; Meinardi, S.; Blake, D. R.; Edgerton, E. S.; Russell, A. G.; Clements, M. Gaseous and Particulate Emissions from Prescribed Burning in Georgia. *Environ. Sci. Technol.* **2005**, *39* (23), 9049-9056. DOI: 10.1021/es051583l.

(47) Ward, T. J.; Hamilton, R. F.; Dixon, R. W.; Paulsen, M.; Simpson, C. D. Characterization and evaluation of smoke tracers in PM: results from the 2003 Montana wildfire season. *Atmos. Environ.* **2006**, *40* (36), 7005-7017. DOI: 10.1016/j.atmosenv.2006.06.034.

(48) Liu, J. C.; Peng, R. D. The impact of wildfire smoke on compositions of fine particulate matter by ecoregion in the Western US. *J. Exposure Sci. Environ. Epidemiol.* **2019**, *29* (6), 765-776. DOI: 10.1038/s41370-018-0064-7.

(49) Alves, C.; Vicente, A.; Nunes, T.; Goncalves, C.; Fernandes, A. P.; Mirante, F.; Tarelho, L.; Sanchez de la Campa, A. M.; Querol, X.; Caseiro, A.; et al. Summer 2009 wildfires in Portugal: Emission of trace gases and aerosol composition. *Atmos. Environ.* **2011**, *45* (3), 641-649. DOI: 10.1016/j.atmosenv.2010.10.031.

(50) Littell, J. S.; McKenzie, D.; Peterson, D. L.; Westerling, A. L. Climate and wildfire area burned in western U.S. ecoprovinces, 1916-2003. *Ecol Appl* **2009**, *19* (4), 1003-1021. DOI: 10.1890/07-1183.1.

(51) Urbanski, S. P.; Hao, W. M.; Baker, S. Chemical composition of wildland fire emissions. *Dev. Environ. Sci.* **2009**, *8*, 79-107. DOI: 10.1016/s1474-8177(08)00004-1.

(52) Gyawali, M.; Arnott, W. P.; Lewis, K.; Moosmuller, H. In situ aerosol optics in Reno, NV, USA during and after the summer 2008 California wildfires and the influence of absorbing and non-absorbing organic coatings on spectral light absorption. *Atmos. Chem. Phys.* **2009**, *9* (20), 8007-8015. DOI: 10.5194/acp-9-8007-2009.

(53) Zhang, Y.; Obrist, D.; Zielinska, B.; Gertler, A. Particulate emissions from different types of biomass burning. *Atmos. Environ.* **2013**, *72*, 27-35. DOI: 10.1016/j.atmosenv.2013.02.026.

(54) Calvo, A. I.; Alves, C.; Castro, A.; Pont, V.; Vicente, A. M.; Fraile, R. Research on aerosol sources and chemical composition: Past, current and emerging issues. *Atmos. Res.* **2013**, *120-121*, 1-28. DOI: 10.1016/j.atmosres.2012.09.021.

(55) Ito, A.; Penner, J. E. Global estimates of biomass burning emissions based on satellite imagery for the year 2000. *J. Geophys. Res., [Atmos.]* **2004**, *109* (D14), D14S05/11. DOI: 10.1029/2003jd004423.

(56) Tian, D.; Wang, Y.; Bergin, M.; Hu, Y.; Liu, Y.; Russell, A. G. Air Quality Impacts from Prescribed Forest Fires under Different Management Practices. *Environ. Sci. Technol.* **2008**, *42* (8), 2767-2772. DOI: 10.1021/es0711213.

(57) Urbanski, S. P. Combustion efficiency and emission factors for wildfire-season fires in mixed conifer forests of the Northern Rocky Mountains, US. *Atmos. Chem. Phys.* **2013**, *13* (14), 7241. DOI: 10.5194/acp-13-7241-2013.

(58) Stone, S. L.; Anderko, L.; Berger, M.; Butler, C. R.; Cascio, W. E.; Clune, A.; Damon, S.; Garbe, P.; Hauptman, M.; Haskell, W. E.; et al. *Wildfire Smoke: A Guide for Public Health Officials*. 2021. (accessed 2021.

(59) Sigma-Aldrich. *Safety Data Sheet: Formaldehyde*. Sigma-Aldrich Co LLC, 2021. (accessed 2022 14 March).

(60) Sigma-Aldrich. *Safety Data Sheet: Acetaldehyde*. Sigma-Aldrich Co LLC, 2021. (accessed 2022 14 March).

(61) Sigma-Aldrich. *Safety Data Sheet: Methacrolein*. 2021. (accessed 2022 14 March).

(62) Sigma-Aldrich. *Safety Data Sheet: Acetone*. Sigma-Aldrich Co LLC, 2021. (accessed 2022 14 March).

(63) Sigma-Aldrich. *Safety Data Sheet: Acrolein*. Sigma-Aldrich Co LLC, 2021. (accessed 2022 14 March).

(64) Matsumoto, M.; Yamano, S.; Senoh, H.; Umeda, Y.; Hirai, S.; Saito, A.; Kasai, T.; Aiso, S. Carcinogenicity and chronic toxicity of acrolein in rats and mice by two-year inhalation study. *Regul. Toxicol. Pharmacol.* **2021**, *121*, 104863, 10.1016/j.yrtph.2021.104863. DOI: 10.1016/j.yrtph.2021.104863.

(65) EPA, U. *Formaldehyde*. U.S. Environmental Protection Agency, 2000. https://www.epa.gov/sites/default/files/2016-09/documents/formaldehyde.pdf (accessed 2022 14 March).

(66) EPA, U. *Acetaldehyde*. U.S. Environmental Protection Agency, 2000. https://www.epa.gov/sites/default/files/2016-09/documents/acetaldehyde.pdf (accessed 2022 14 March).

(67) EPA, U. *Acrolein*. U.S. Environmental Protection Agency, 2009. https://www.epa.gov/sites/default/files/2016-08/documents/acrolein.pdf (accessed 2022 14 March).

(68) Reinhardt, T.; Ottmar, R. Baseline Measurements of Smoke Exposure Among Wildland Firefighters. *J. Occup. Environ. Hyg.* **2004**, *1* (9), 593-606. DOI: 10.1080/15459620490490101.

(69) Gauderman, W. J.; Avol, E.; Gilliland, F.; Vora, H.; Thomas, D.; Berhane, K.; McConnell, R.; Kuenzli, N.; Lurmann, F.; Rappaport, E.; et al. The effect of air pollution on lung development from 10 to 18 years of age. *N. Engl. J. Med.* **2004**, *351* (11), 1057-1067. DOI: 10.1056/nejmoa040610.

(70) Gehring, U.; Gruzieva, O.; Agius, R. M.; Beelen, R.; Custovic, A.; Cyrys, J.; Eeftens, M.; Flexeder, C.; Fuertes, E.; Heinrich, J.; et al. Air pollution exposure and lung function in children: the ESCAPE project. *Environ Health Perspect* **2013**, *121* (11-12), 1357-1364. DOI: 10.1289/ehp.1306770.

(71) Urman, R.; McConnell, R.; Islam, T.; Avol, E. L.; Lurmann, F. W.; Vora, H.; Linn, W. S.; Rappaport, E. B.; Gilliland, F. D.; Gauderman, W. J. Associations of children's lung function with ambient air pollution: joint effects of regional and near-roadway pollutants. *Thorax* **2014**, *69* (6), 540-547. DOI: 10.1136/thoraxjnl-2012-203159.

(72) Black, C.; Gerriets, J. E.; Fontaine, J. H.; Harper, R. W.; Kenyon, N. J.; Tablin, F.; Schelegle, E. S.; Miller, L. A. Early life wildfire smoke exposure is associated with immune dysregulation and lung function decrements in adolescence. *Am. J. Respir. Cell Mol. Biol.* **2017**, *56* (5), 657-666. DOI: 10.1165/rcmb.2016-0380oc.

(73) Gauderman, W. J.; Gilliland, G. F.; Vora, H.; Avol, E.; Stram, D.; McConnell, R.; Thomas, D.; Lurmann, F.; Margolis, H. G.; Rappaport, E. B.; et al. Association between air pollution and lung function growth in southern California children: results from a second cohort. *Am J Respir Crit Care Med* **2002**, *166* (1), 76-84. DOI: 10.1164/rccm.2111021.

(74) Schultz, E. S.; Gruzieva, O.; Bellander, T.; Bottai, M.; Hallberg, J.; Kull, I.; Svartengren, M.; Melén, E.; Pershagen, G. Traffic-related air pollution and lung function in children at 8 years of age: a birth cohort study. *Am J Respir Crit Care Med* **2012**, *186* (12), 1286-1291. DOI: 10.1164/rccm.201206-1045OC.

(75) Oftedal, B.; Brunekreef, B.; Nystad, W.; Madsen, C.; Walker, S.-E.; Nafstad, P. Residential outdoor air pollution and lung function in schoolchildren. *Epidemiology* **2008**, *19* (1), 129-137. DOI: 10.1097/EDE.0b013e31815c0827.

(76) Black, C.; Tesfaigzi, Y.; Bassein, J. A.; Miller, L. A. Wildfire smoke exposure and human health: Significant gaps in research for a growing public health issue. *Environ. Toxicol. Pharmacol.* **2017**, *55*, 186-195. DOI: 10.1016/j.etap.2017.08.022.

(77) Chew, F. T.; Ooi, B. C.; Hui, J. K.; Saharom, R.; Goh, D. Y.; Lee, B. W. Singapore's haze and acute asthma in children. *Lancet* **1995**, *346* (8987), 1427. DOI: 10.1016/s0140-6736(95)92443-4.

(78) Delfino, R. J.; Brummel, S.; Wu, J.; Stern, H.; Ostro, B.; Lipsett, M.; Winer, A.; Street, D. H.; Zhang, L.; Tjoa, T.; et al. The relationship of respiratory and cardiovascular hospital admissions to the southern California wildfires of 2003. *Occup Environ Med* **2009**, *66* (3), 189-197. DOI: 10.1136/oem.2008.041376.

(79) Dennekamp, M.; Abramson, M. J. The effects of bushfire smoke on respiratory health. *Respirology* **2011**, *16* (2), 198-209. DOI: 10.1111/j.1440-1843.2010.01868.x.

(80) Dohrenwend, P. B.; Le, M. V.; Bush, J. A.; Thomas, C. F. The impact on emergency department visits for respiratory illness during the southern california wildfires. *West J Emerg Med* **2013**, *14* (2), 79-84. DOI: 10.5811/westjem.2012.10.6917.

(81) Johnston, F. H.; Kavanagh, A. M.; Bowman, D. M. J. S.; Scott, R. K. Exposure to bushfire smoke and asthma: an ecological study. *Med J Aust* **2002**, *176* (11), 535-538. DOI: 10.5694/j.1326-5377.2002.tb04551.x.

(82) Rappold, A. G.; Cascio, W. E.; Kilaru, V. J.; Stone, S. L.; Neas, L. M.; Devlin, R. B.; Diaz-Sanchez, D. Cardio-respiratory outcomes associated with exposure to wildfire smoke are modified by measures of community health. *Environ Health* **2012**, *11*, 71. DOI: 10.1186/1476-069X-11-71.

(83) Schranz, C. I.; Castillo, E. M.; Vilke, G. M. The 2007 San Diego Wildfire impact on the Emergency Department of the University of California, San Diego Hospital System. *Prehosp Disaster Med* **2010**, *25* (5), 472-476. DOI: 10.1017/s1049023x0000858x.

(84) Viswanathan, S.; Eria, L.; Diunugala, N.; Johnson, J.; McClean, C. An analysis of effects of San Diego wildfire on ambient air quality. *J. Air Waste Manage. Assoc.* **2006**, *56* (1), 56-67. DOI: 10.1080/10473289.2006.10464439.

(85) Fann, N.; Alman, B.; Broome, R. A.; Morgan, G. G.; Johnston, F. H.; Pouliot, G.; Rappold, A. G. The health impacts and economic value of wildland fire episodes in the U.S.: 2008-2012. *Sci. Total Environ.* **2018**, *610-611*, 802-809. DOI: 10.1016/j.scitotenv.2017.08.024.

(86) Matz, C. J.; Egyed, M.; Xi, G.; Racine, J.; Pavlovic, R.; Rittmaster, R.; Henderson, S. B.; Stieb, D. M. Health impact analysis of PM2.5 from wildfire smoke in Canada (2013-2015, 2017-2018). *Sci. Total Environ.* **2020**, *725*, 138506. DOI: 10.1016/j.scitotenv.2020.138506.

(87) AirNow. *Air Quality Index (AQI) Basics*. https://www.airnow.gov/aqi/aqi-basics/ (accessed 2021).

(88) NOAA. *How is Air Quality Measured?* National Oceanic and Atmospheric Administration, 2022. https://scijinks.gov/air-quality/ (accessed 2022).

(89) EPA, U. *Compendium Method TO-11A, Determination of Formaldehyde in Ambient Air Using Adsorbent Cartridge Followed by High Performance Liquid Chromatography (HPLC)*. 1999. (accessed 2021).

(90) Pal, R.; Kim, K.-H. Experimental choices for the determination of carbonyl compounds in air. *J. Sep. Sci.* **2007**, *30* (16), 2708-2718. DOI: 10.1002/jssc.200700206.

(91) Herrington, J. S.; Hays, M. D. Concerns regarding 24-h sampling for formaldehyde, acetaldehyde, and acrolein using 2,4-dinitrophenylhydrazine (DNPH)-coated solid sorbents. *Atmos. Environ.* **2012**, *55*, 179-184. DOI: 10.1016/j.atmosenv.2012.02.088.

(92) Karst, U.; Binding, N.; Cammann, K.; Witting, U. Interferences of nitrogen dioxide in the determination of aldehydes and ketones by sampling on 2,4-dinitrophenylhydrazine-coated solid sorbent. *Fresenius' J. Anal. Chem.* **1993**, *345* (1), 48-52. DOI: 10.1007/bf00323325.

(93) Poetter, W.; Karst, U. Identification of Chemical Interferences in Aldehyde and Ketone Determination Using Dual-Wavelength Detection. *Anal. Chem.* **1996**, *68* (19), 3354-3358. DOI: 10.1021/ac960319v.

(94) Tang, S.; Graham, L.; Shen, L.; Zhou, X.; Lanni, T. Simultaneous Determination of Carbonyls and NO2 in Exhausts of Heavy-Duty Diesel Trucks and Transit Buses by HPLC following 2,4-Dinitrophenylhydrazine Cartridge Collection. *Environ. Sci. Technol.* **2004**, *38* (22), 5968-5976. DOI: 10.1021/es0353356.

(95) EPA, U. *Compendium of Methods for the Determination of Toxic Organic Compounds in Ambient Air*. 2000.

(96) Goelen, E.; Lambrechts, M.; Geyskens, F. Sampling intercomparisons for aldehydes in simulated workplace air. *Analyst (Cambridge, U. K.)* **1997**, *122* (5), 411-419. DOI: 10.1039/a607047g.

(97) Schulte-Ladbeck, R.; Lindahl, R.; Levin, J.-O.; Karst, U. Characterization of chemical interferences in the determination of unsaturated aldehydes using aromatic hydrazine reagents and liquid chromatography. *J. Environ. Monit.* **2001**, *3* (3), 306-310. DOI: 10.1039/b101354h.

(98) Herrington, J. S.; Fan, Z.-H.; Lioy, P. J.; Zhang, J. Low Acetaldehyde Collection Efficiencies for 24-Hour Sampling with 2,4-Dinitrophenylhydrazine (DNPH)-Coated Solid Sorbents. *Environ. Sci. Technol.* **2007**, *41* (2), 580-585. DOI: 10.1021/es061247k.

(99) Haarig, M.; Ansmann, A.; Baars, H.; Jimenez, C.; Veselovskii, I.; Engelmann, R.; Althausen, D. Depolarization and lidar ratios at 355, 532, and 1064 nm and microphysical properties of aged tropospheric and stratospheric canadian wildfire smoke. *Atmos. Chem. Phys.* **2018**, *18* (16), 11847-11861. DOI: 10.5194/acp-18-11847-2018.

(100) Ansmann, A.; Baars, H.; Chudnovsky, A.; Mattis, I.; Veselovskii, I.; Haarig, M.; Seifert, P.; Engelmann, R.; Wandinger, U. Extreme levels of Canadian wildfire smoke in the stratosphere over central Europe on 21-22 August 2017. *Atmos. Chem. Phys.* **2018**, *18* (16), 11831-11845. DOI: 10.5194/acp-18-11831-2018.

(101) Khan, S.; Le Calve, S.; Newport, D. A review of optical interferometry techniques for VOC detection. *Sens. Actuators, A* **2020**, *302*, 111782. DOI: 10.1016/j.sna.2019.111782.

(102) Allison, R. S.; Johnston, J. M.; Craig, G.; Jennings, S. Airborne Optical and Thermal Remote Sensing for Wildfire Detection and Monitoring. *Sensors (Basel)* **2016**, *16* (8). DOI: 10.3390/s16081310.

(103) Yang, X.; Chang, A. S. P.; Chen, B.; Gu, C.; Bond, T. C. High sensitivity gas sensing by Raman spectroscopy in photonic crystal fiber. *Sens. Actuators, B* **2013**, *176*, 64-68. DOI: 10.1016/j.snb.2012.09.004.

(104) Gong, Y.; Bu, L.; Yang, B.; Mustafa, F. High repetition rate mid-infrared differential absorption lidar for atmospheric pollution detection. *Sensors* **2020**, *20* (8), 2211, 10.3390/s20082211. DOI: 10.3390/s20082211.

(105) Saito, Y.; Weibring, P.; Edner, H.; Svanberg, S. Possibility of hard-target lidar detection of a biogenic volatile organic compound, α-pinene gas, over forest areas. *Appl. Opt.* **2001**, *40* (21), 3572-3574. DOI: 10.1364/ao.40.003572.

(106) Mirov, S. B.; Fedorov, V. V.; Martyshkin, D.; Moskalev, I. S.; Mirov, M.; Vasilyev, S. Progress in mid-IR lasers based on Cr and Fe-doped II-VI chalcogenides. *IEEE J. Sel. Top. Quantum Electron.* **2015**, *21* (1), 1601719/1601711. DOI: 10.1109/jstqe.2014.2346512.

(107) Tütüncü, E.; Kokoric, V.; Wilk, A.; Seichter, F.; Schmid, M.; Hunt, W. E.; Manuel, A. M.; Mirkarimi, P.; Alameda, J. B.; Carter, J. C.; et al. Fiber-Coupled Substrate-Integrated Hollow Waveguides: An Innovative Approach to Mid-infrared Remote Gas Sensors. *ACS Sensors* **2017**, *2* (9), 1287-1293. DOI: 10.1021/acssensors.7b00253.

(108) Kaden, D. A.; Mandin, C.; Nielsen, G. D.; Wolkoff, P. Formaldehyde. *WHO Guidelines for Indoor Air Quality: Selected Pollutants* **2010**, *World Health Organization* (3).

(109) *Air Quality Historical Data Platform*. Institution and University Registration, 2022. https://aqicn.org/data-platform/register/.

(110) Government, A. *Acetone*. Department of Agriculture, Water and the Environment, 2021. http://www.npi.gov.au/resource/acetone.

APPENDIX: SUPPLEMENTAL TABLES AND FIGURES

Table 4 Concentrations of formaldehyde, acetaldehyde, acrolein, and acetone at site 0 to compare air sample collection times.

Collection Time	Carbonyl	Concentration (ppbv)
5 minutes	Formaldehyde	21.46
	Acetaldehyde	13.33
	Acetone	176.00
30 minutes	Formaldehyde	9.80
	Acetaldehyde	3.77
	Acetone	36.03
1 hour	Formaldehyde	6.48
	Acetaldehyde	2.88
	Acetone	19.40

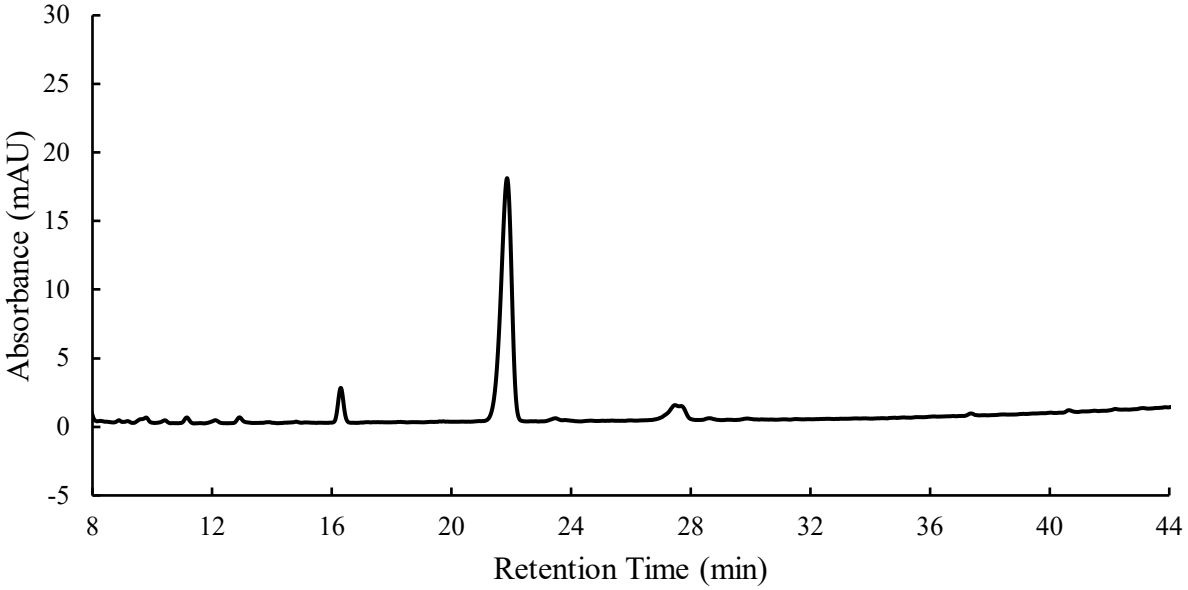

Figure 16 Absorbance (mAU) vs. retention time (min) HPLC graph of blank silica-DNPH cartridge 1.

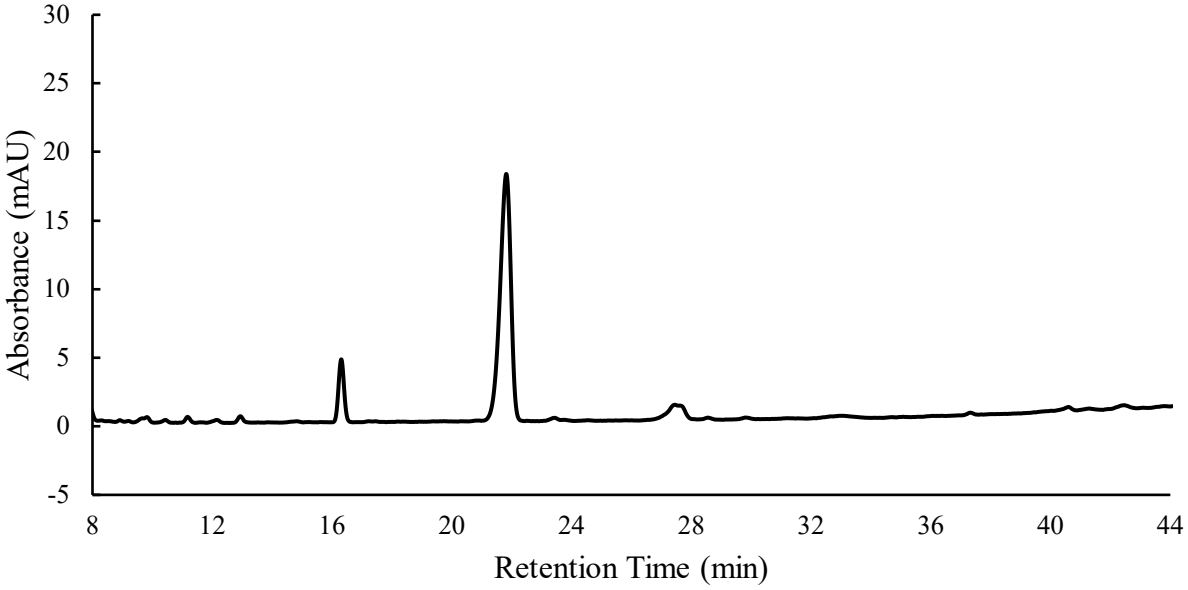

Figure 17 Absorbance (mAU) vs. retention time (min) HPLC graph of blank silica-DNPH cartridge 2.

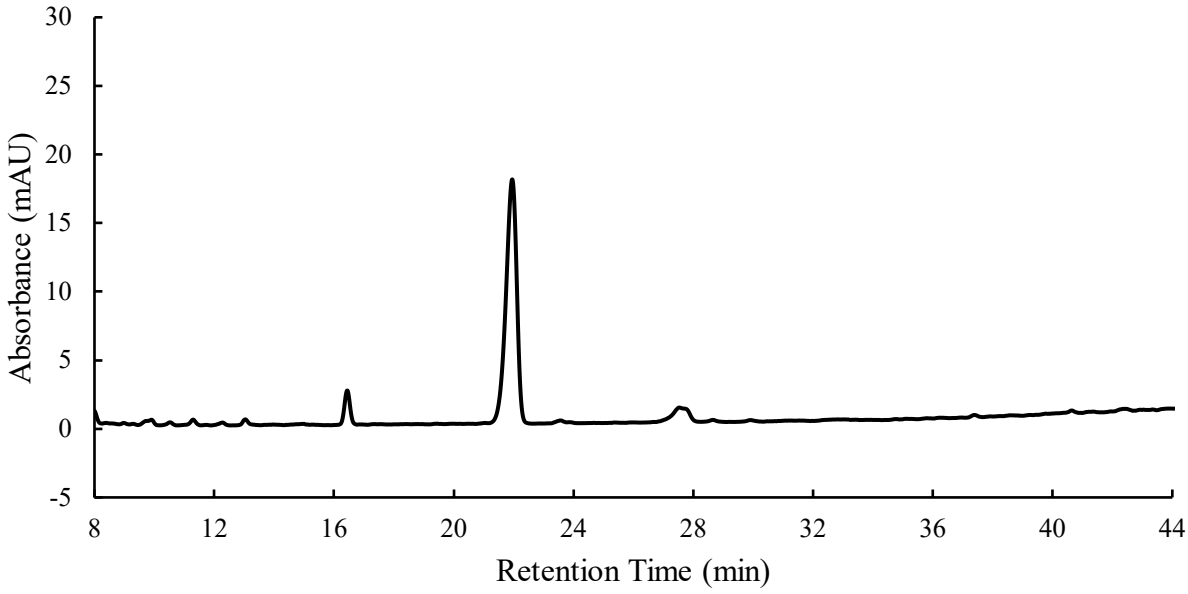

Figure 18 Absorbance (mAU) vs. retention time (min) HPLC graph of blank silica-DNPH cartridge 3.

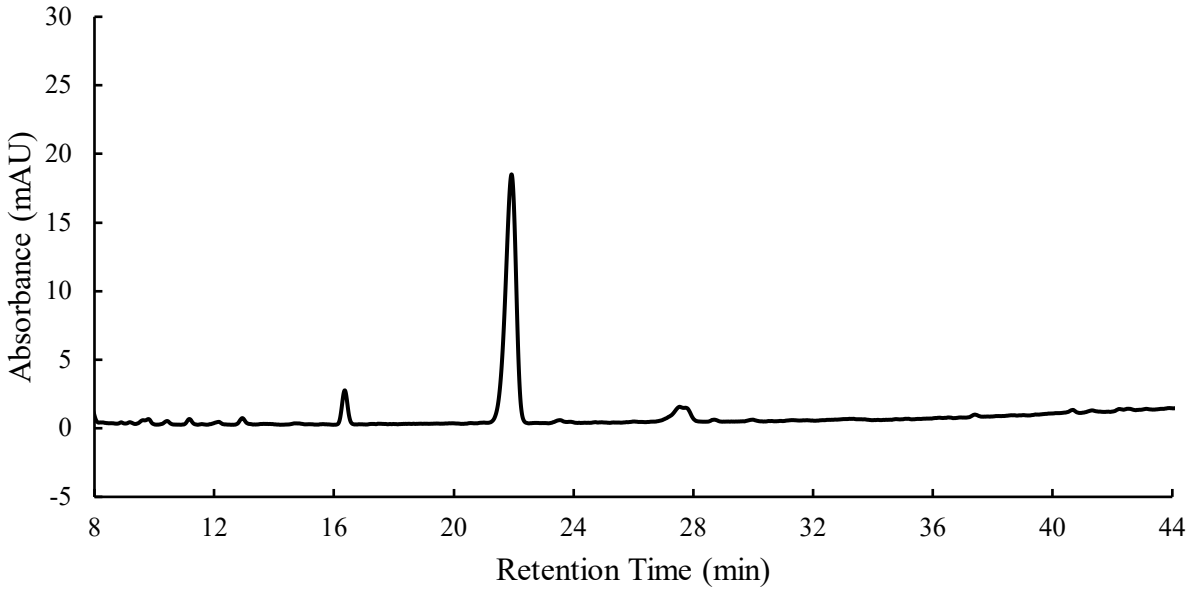

Figure 19 Absorbance (mAU) vs. retention time (min) HPLC graph of blank silica-DNPH cartridge 4.

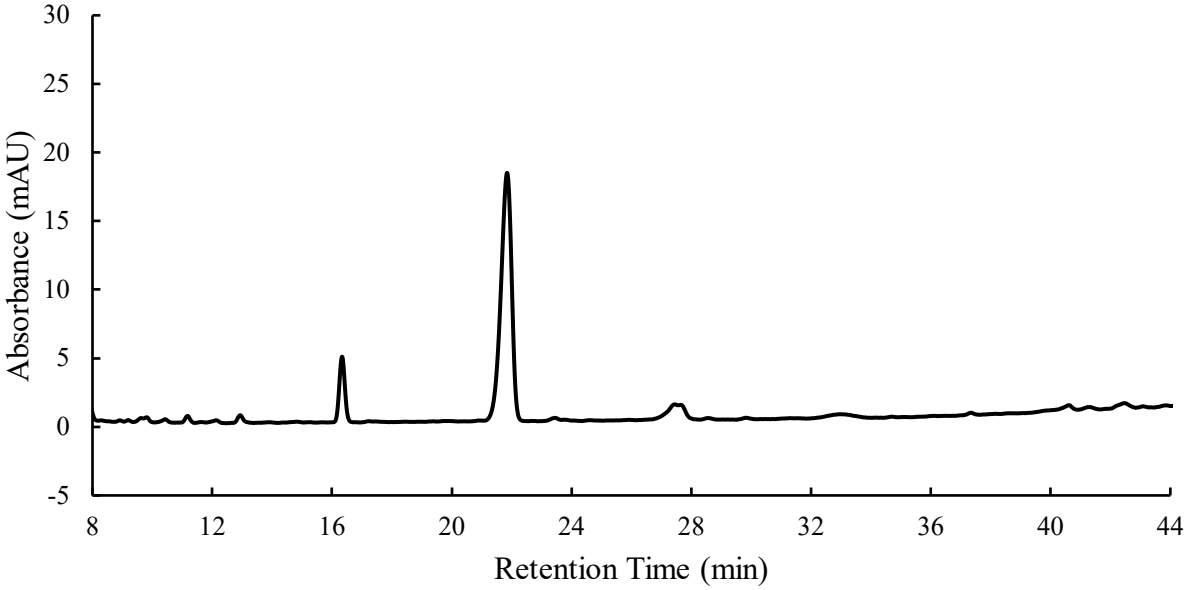

Figure 20 Absorbance (mAU) vs. retention time (min) HPLC graph of blank silica-DNPH cartridge 5.

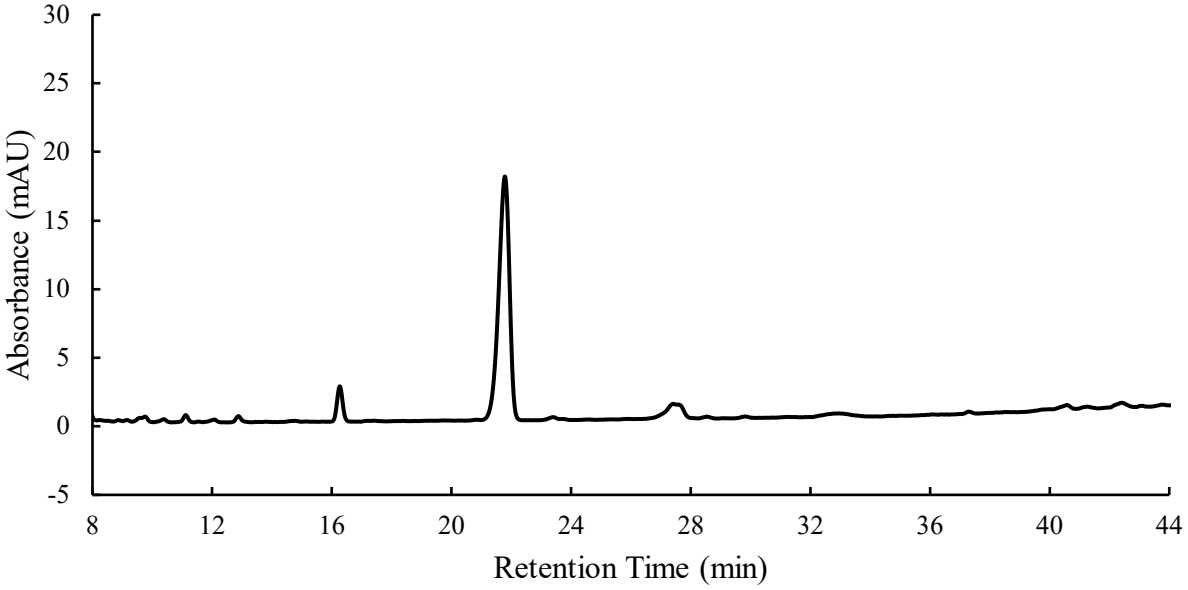

Figure 21 Absorbance (mAU) vs. retention time (min) HPLC graph of blank silica-DNPH cartridge 6.

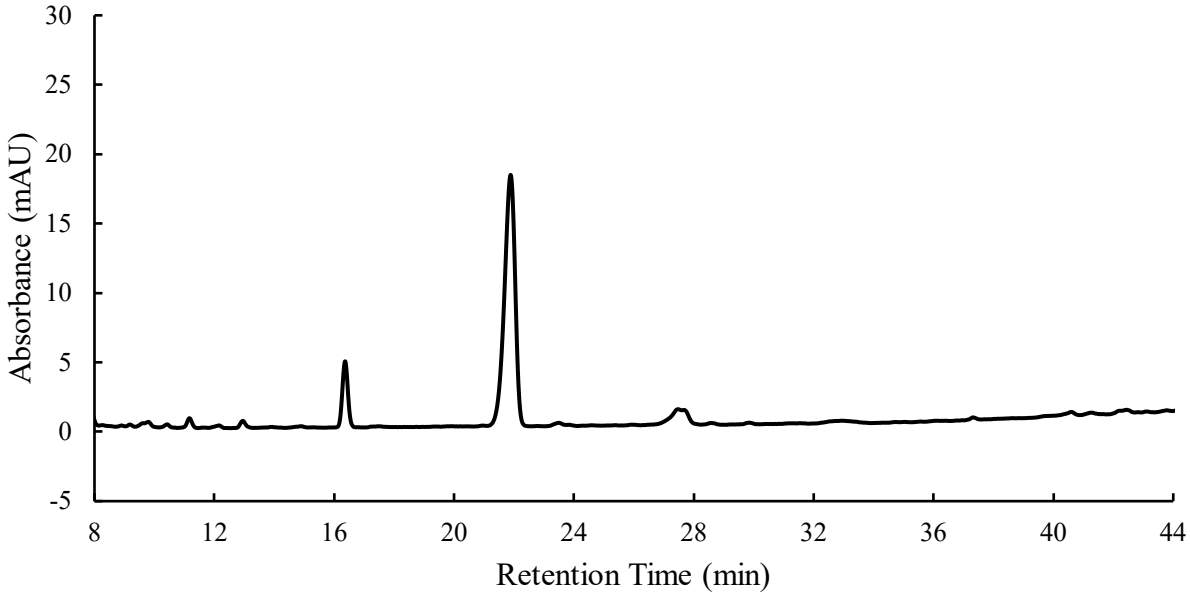

Figure 22 Absorbance (mAU) vs. retention time (min) HPLC graph of blank silica-DNPH cartridge 7.

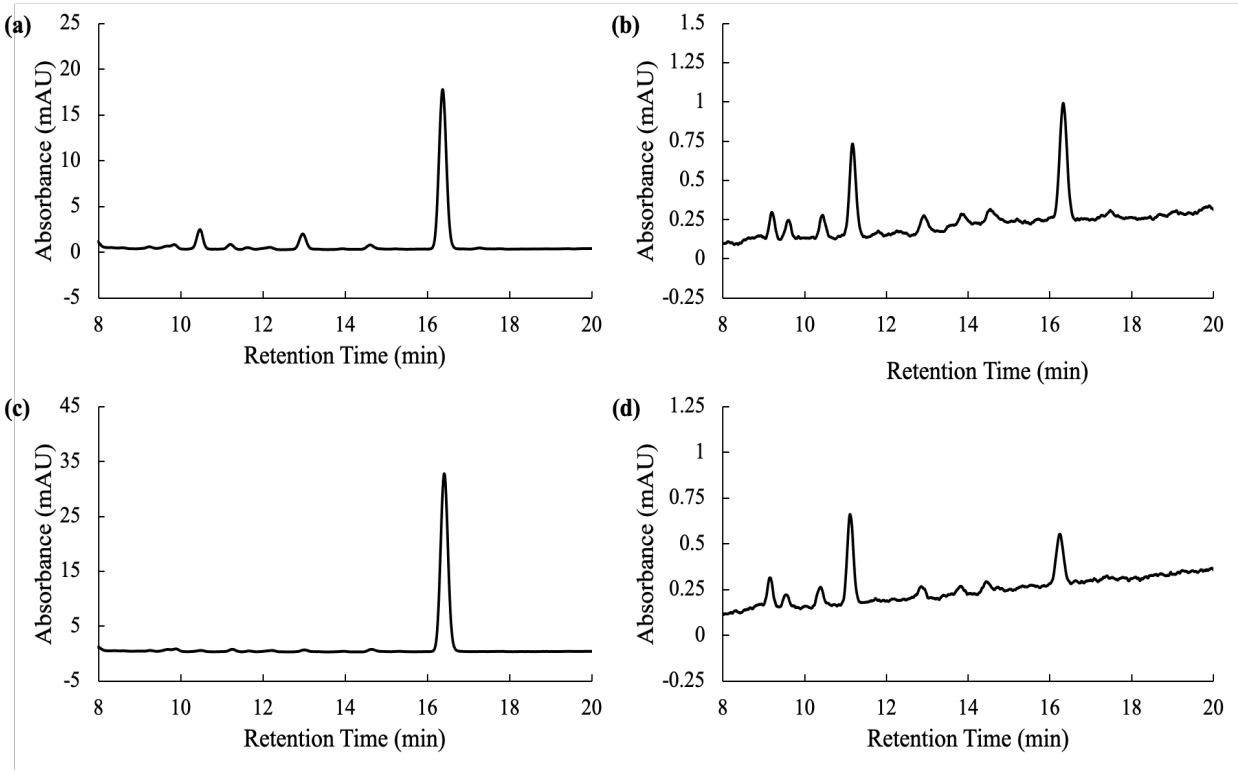

Figure 23 5 minutes air collection at site 0 data (a), first cartridge on apparatus and first elution (b), first cartridge on apparatus and second elution (c), second cartridge on apparatus and first elution (d), second cartridge on apparatus and second elution.

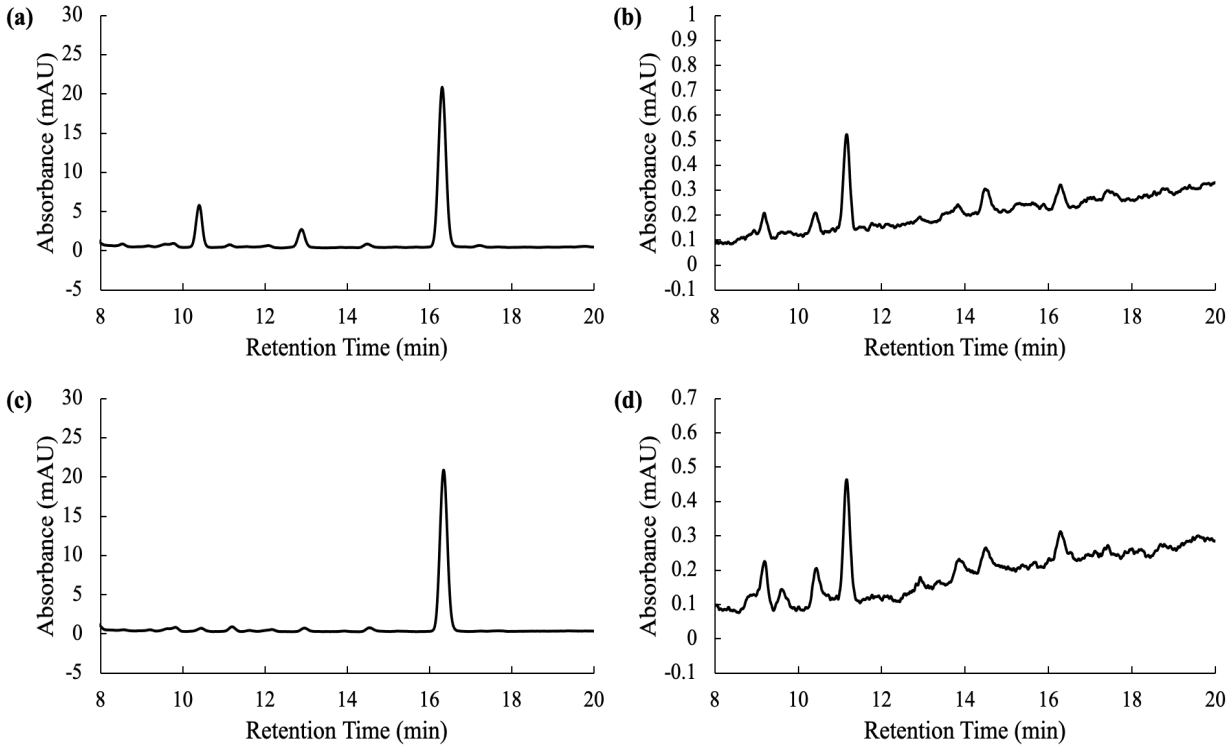

Figure 24 30 minutes air collection at site 0 data (a), first cartridge on apparatus and first elution (b), first cartridge on apparatus and second elution (c), second cartridge on apparatus and first elution (d), second cartridge on apparatus and second elution.

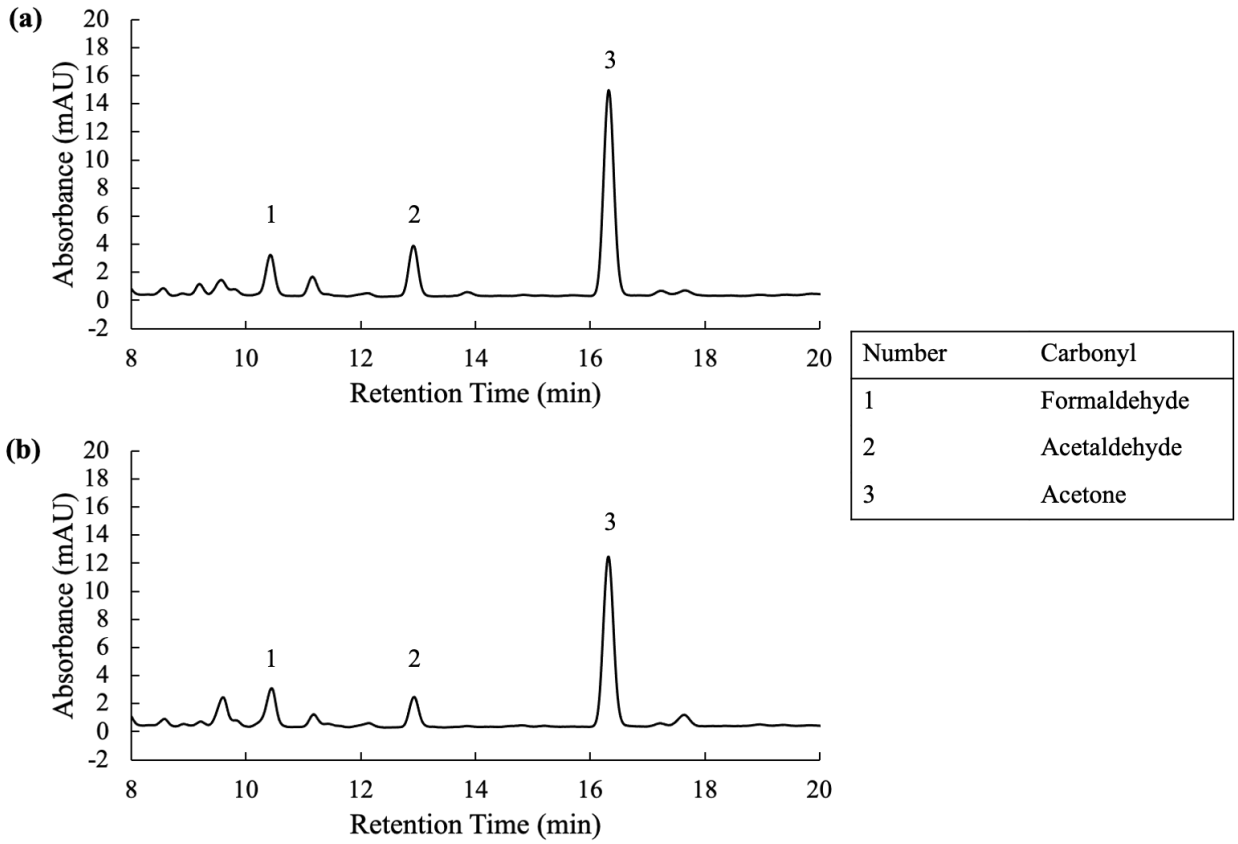

Number	Carbonyl
1	Formaldehyde
2	Acetaldehyde
3	Acetone

Figure 25 Absorbance (mAU) vs. retention time (min) HPLC graph of silica-DNPH cartridge from site 1 on August 2, 2021 (a), pump 1 (b), pump 2.

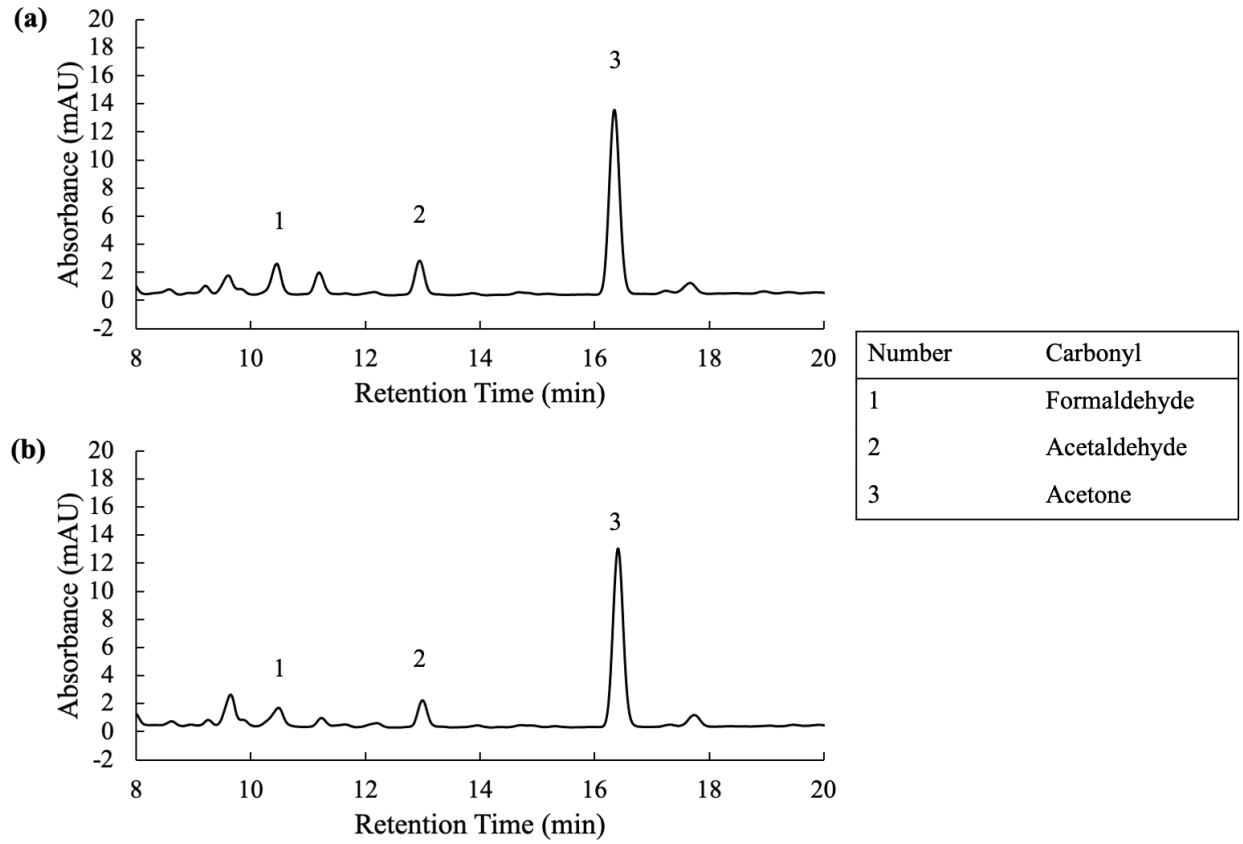

Number	Carbonyl
1	Formaldehyde
2	Acetaldehyde
3	Acetone

Figure 26 Absorbance (mAU) vs. retention time (min) HPLC graph of silica-DNPH cartridge from site 2 on August 2, 2021 (a), pump 1 (b), pump 2.

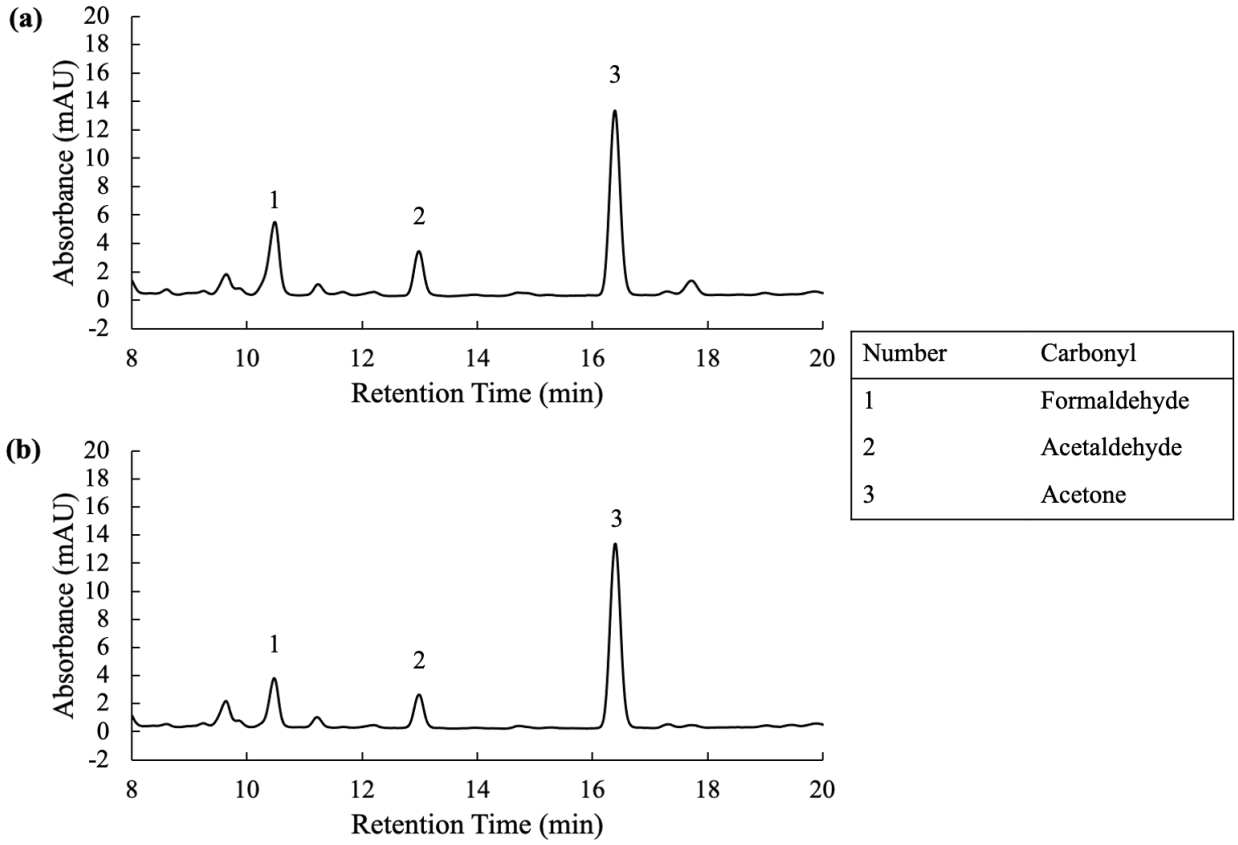

Number	Carbonyl
1	Formaldehyde
2	Acetaldehyde
3	Acetone

Figure 27 Absorbance (mAU) vs. retention time (min) HPLC graph of silica-DNPH cartridge from site 3 on August 3, 2021 (a), pump 1 (b), pump 2.

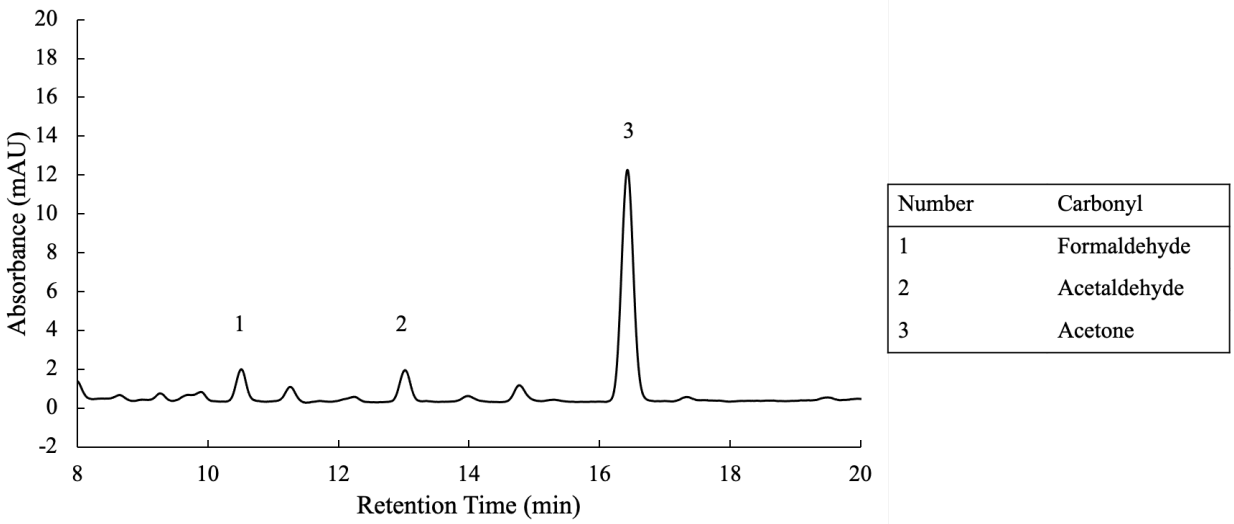

Figure 28 Absorbance (mAU) vs. retention time (min) HPLC graph of silica-DNPH cartridge using pump 2 from site 4 on August 3, 2021.

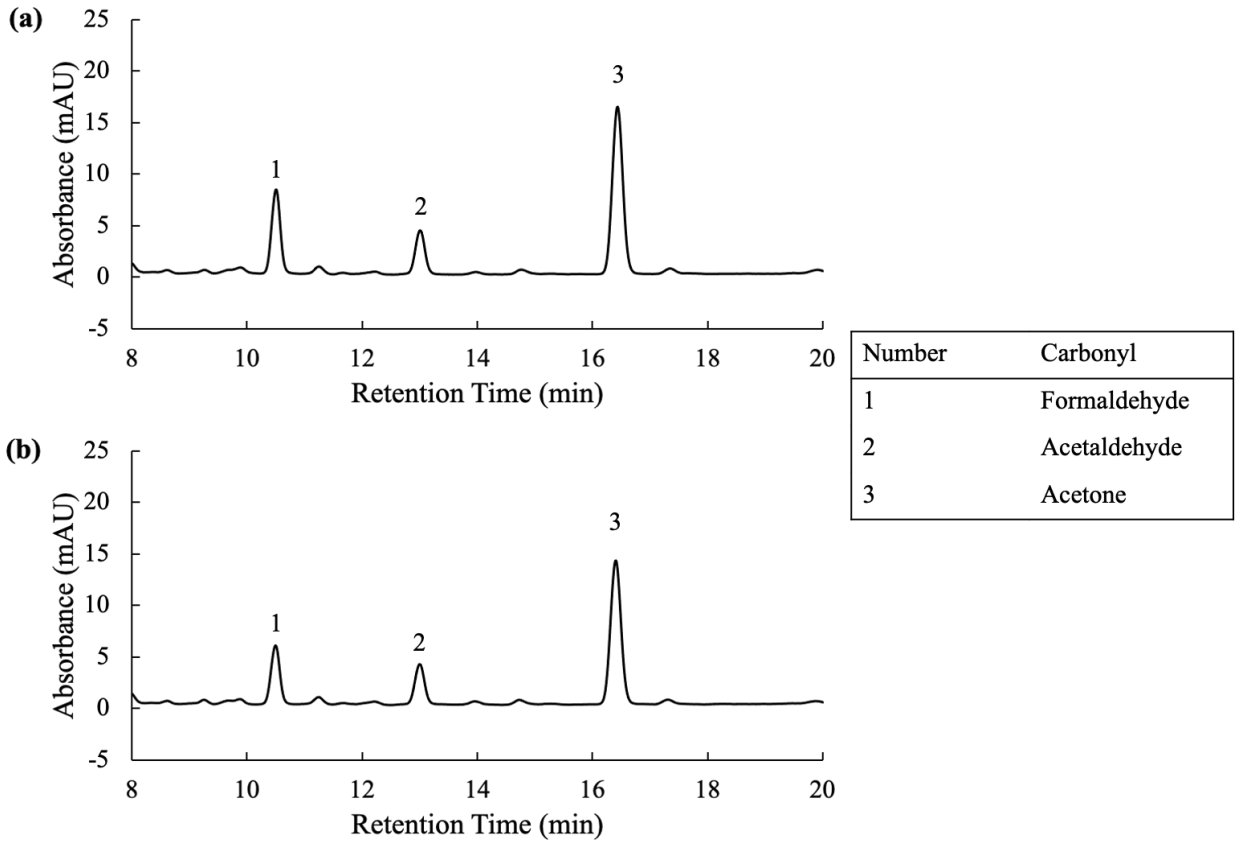

Figure 29 Absorbance (mAU) vs. retention time (min) HPLC graph of silica-DNPH cartridge from site 3 on August 16, 2021 (a), pump 1 (b), pump 2.

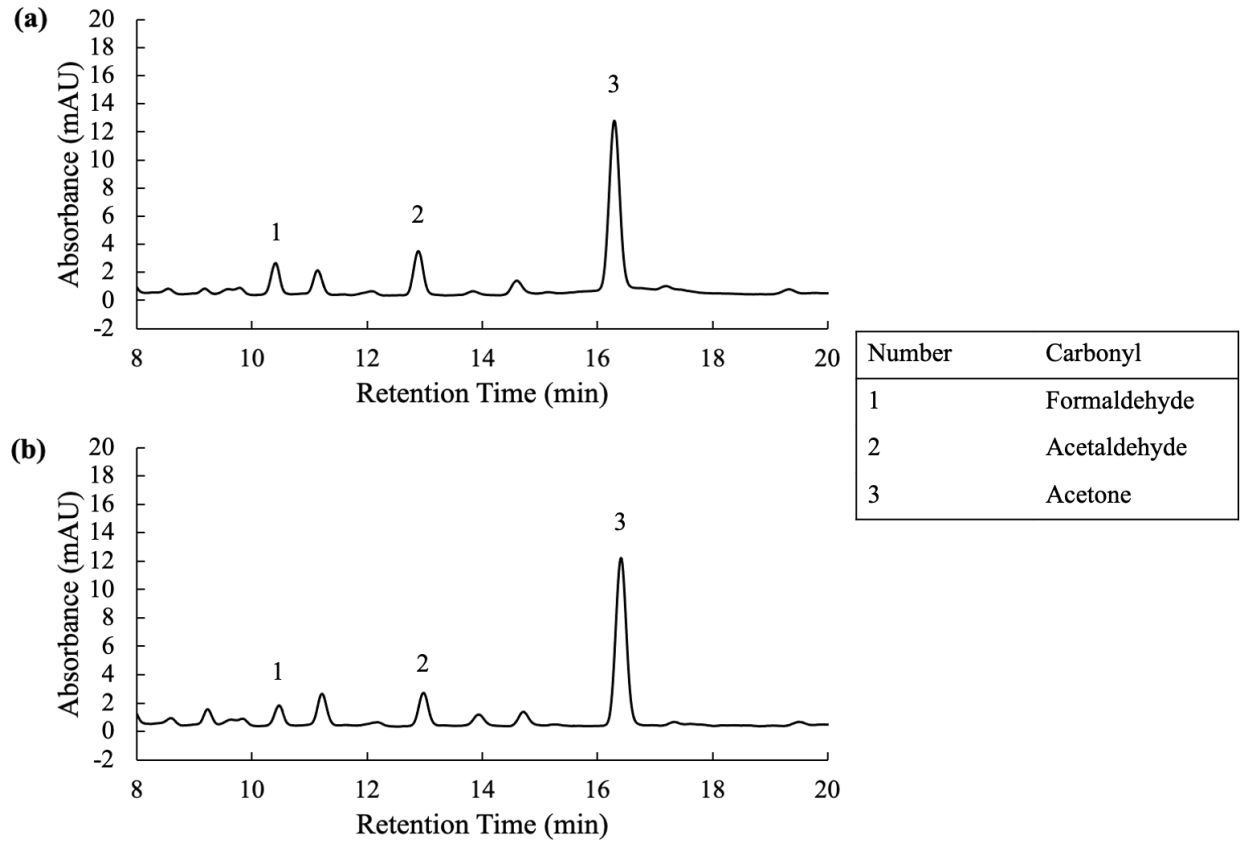

Figure 30 Absorbance (mAU) vs. retention time (min) HPLC graph of silica-DNPH cartridge from site 4 on August 18, 2021 (a), pump 1 (b), pump 2.

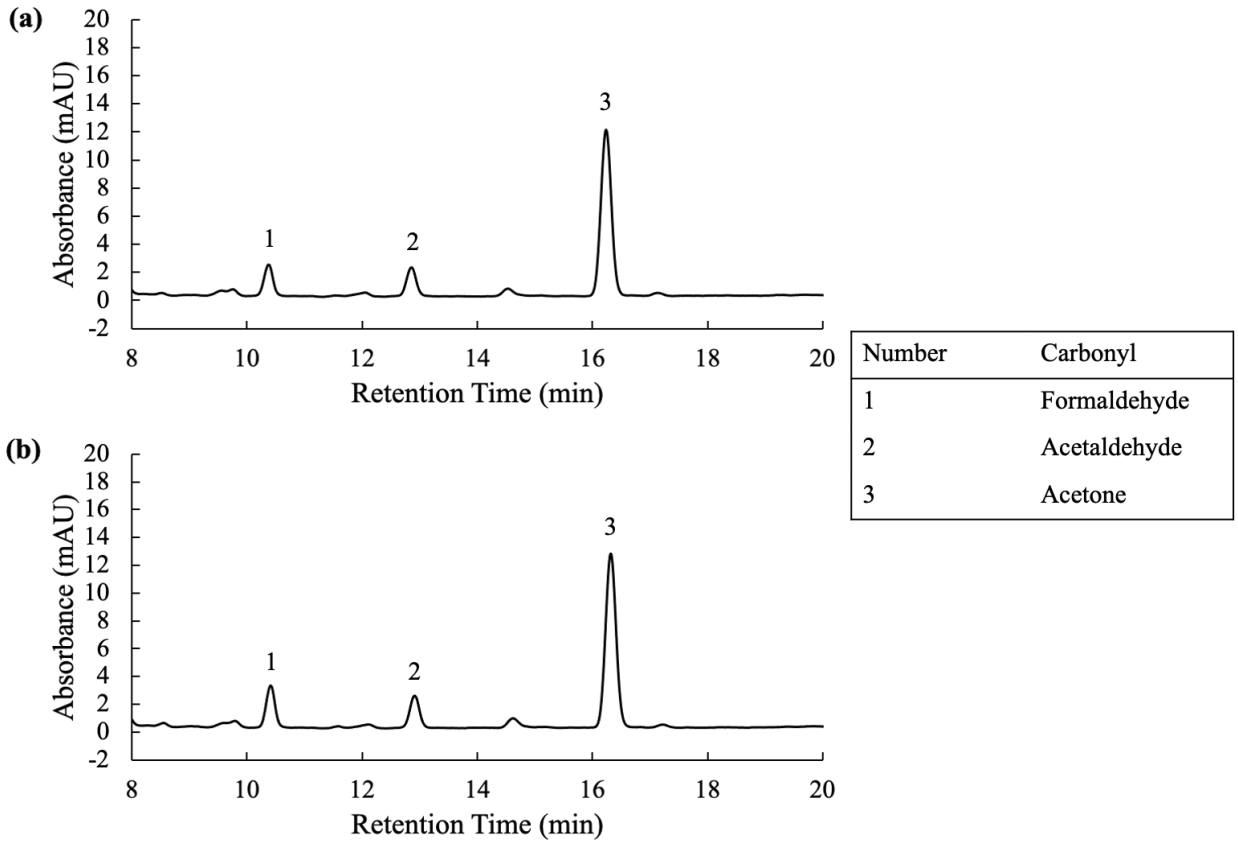

Figure 31 Absorbance (mAU) vs. retention time (min) HPLC graph of silica-DNPH cartridge from site 4 on August 25, 2021 (a), pump 1 (b), pump 2.

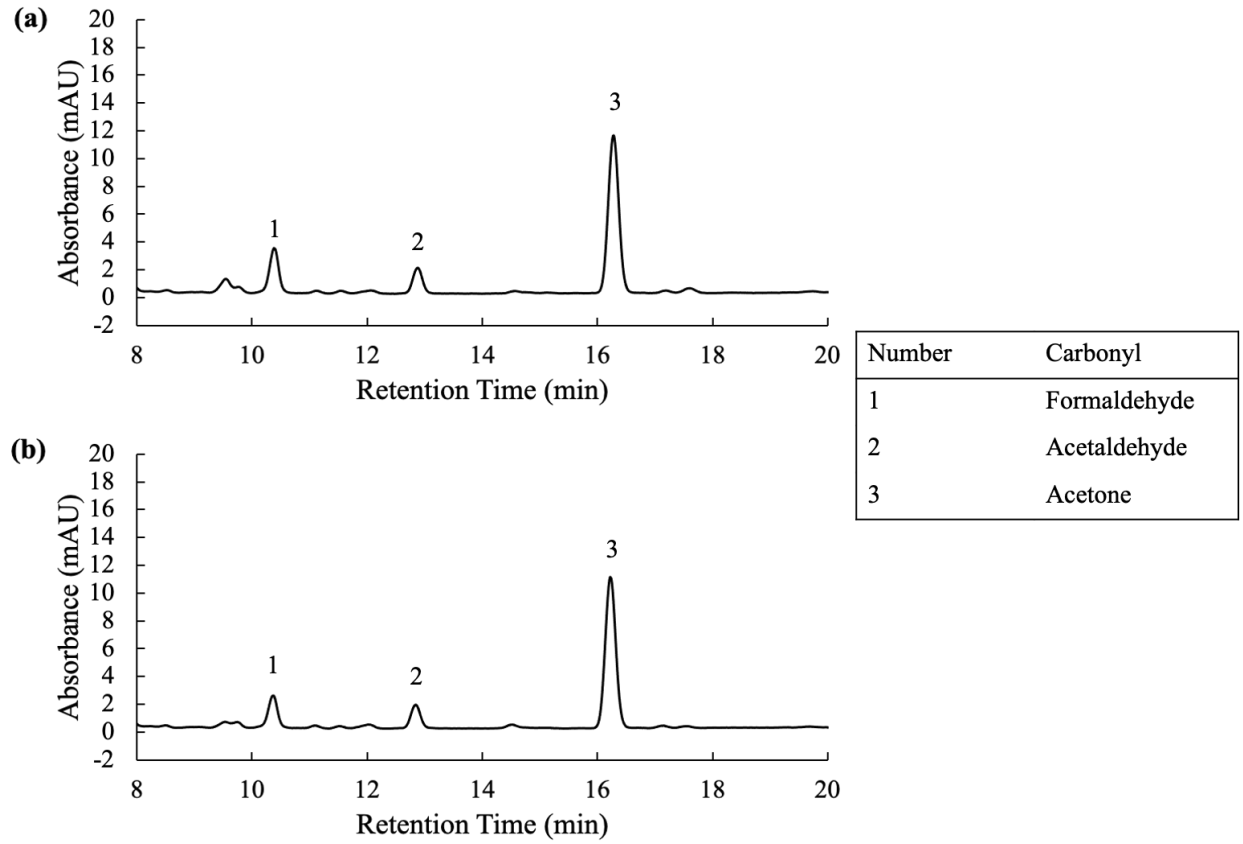

Number	Carbonyl
1	Formaldehyde
2	Acetaldehyde
3	Acetone

Figure 32 Absorbance (mAU) vs. retention time (min) HPLC graph of silica-DNPH cartridge from site 3 on August 27, 2021 (a), pump 1 (b), pump 2.

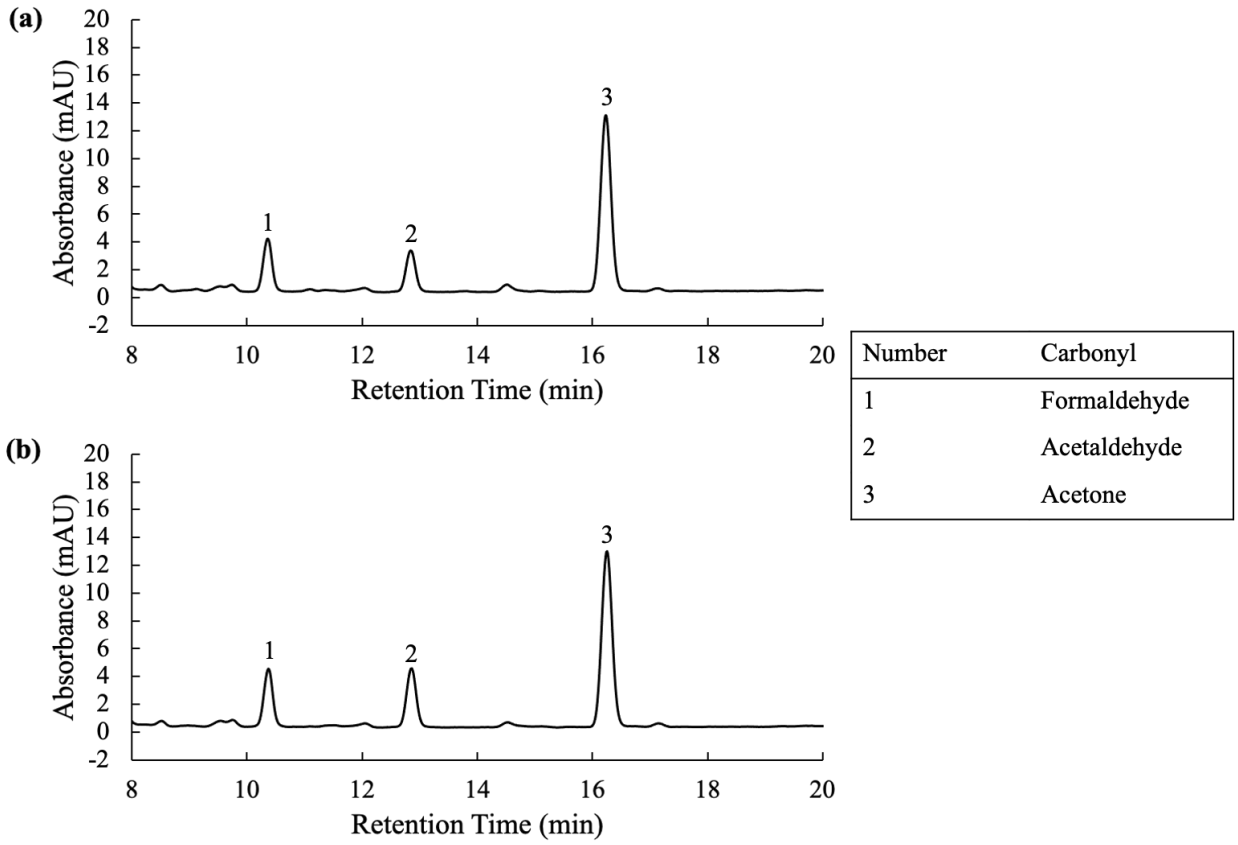

Number	Carbonyl
1	Formaldehyde
2	Acetaldehyde
3	Acetone

Figure 33 Absorbance (mAU) vs. retention time (min) HPLC graph of silica-DNPH cartridge from site 1 on September 1, 2021 (a), pump 1 (b), pump 2.

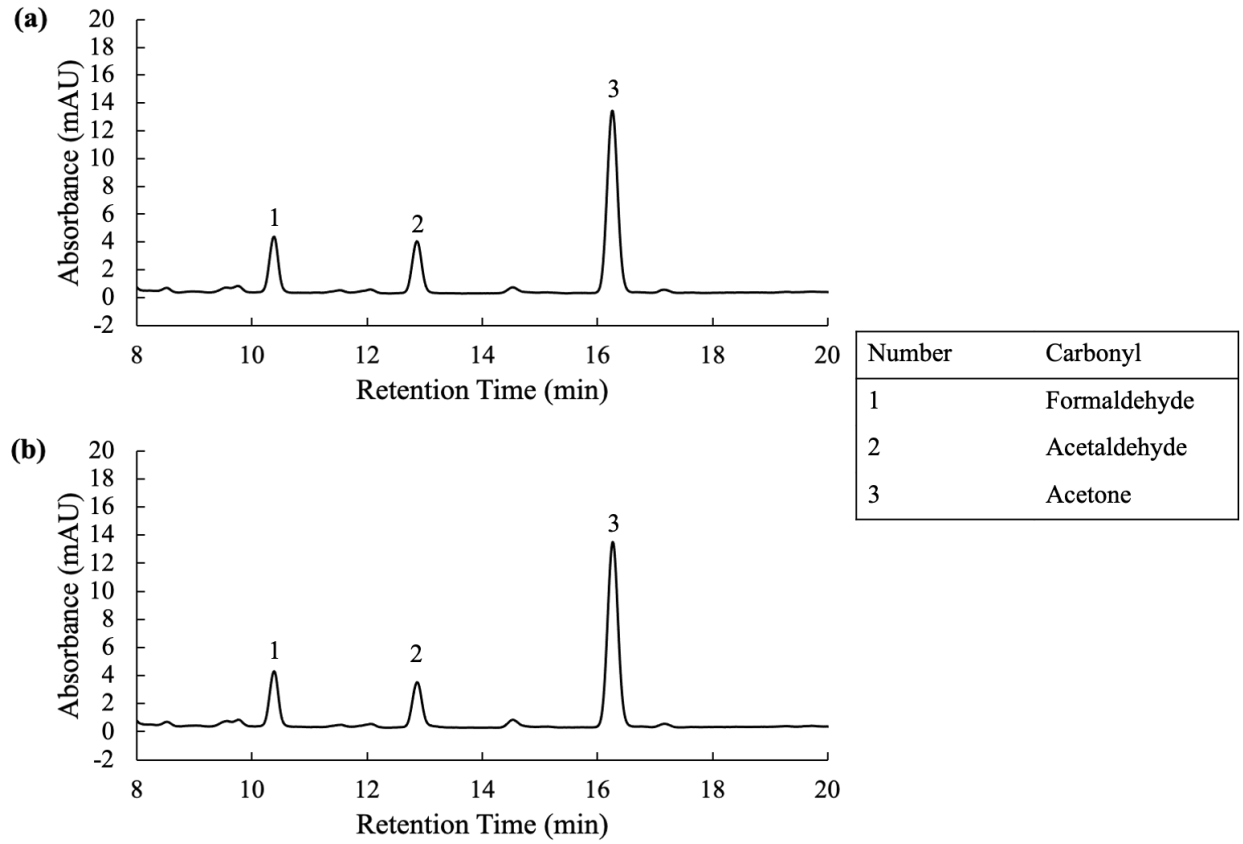

Number	Carbonyl
1	Formaldehyde
2	Acetaldehyde
3	Acetone

Figure 34 Absorbance (mAU) vs. retention time (min) HPLC graph of silica-DNPH cartridge from site 2 on September 1, 2021 (a), pump 1 (b), pump 2.

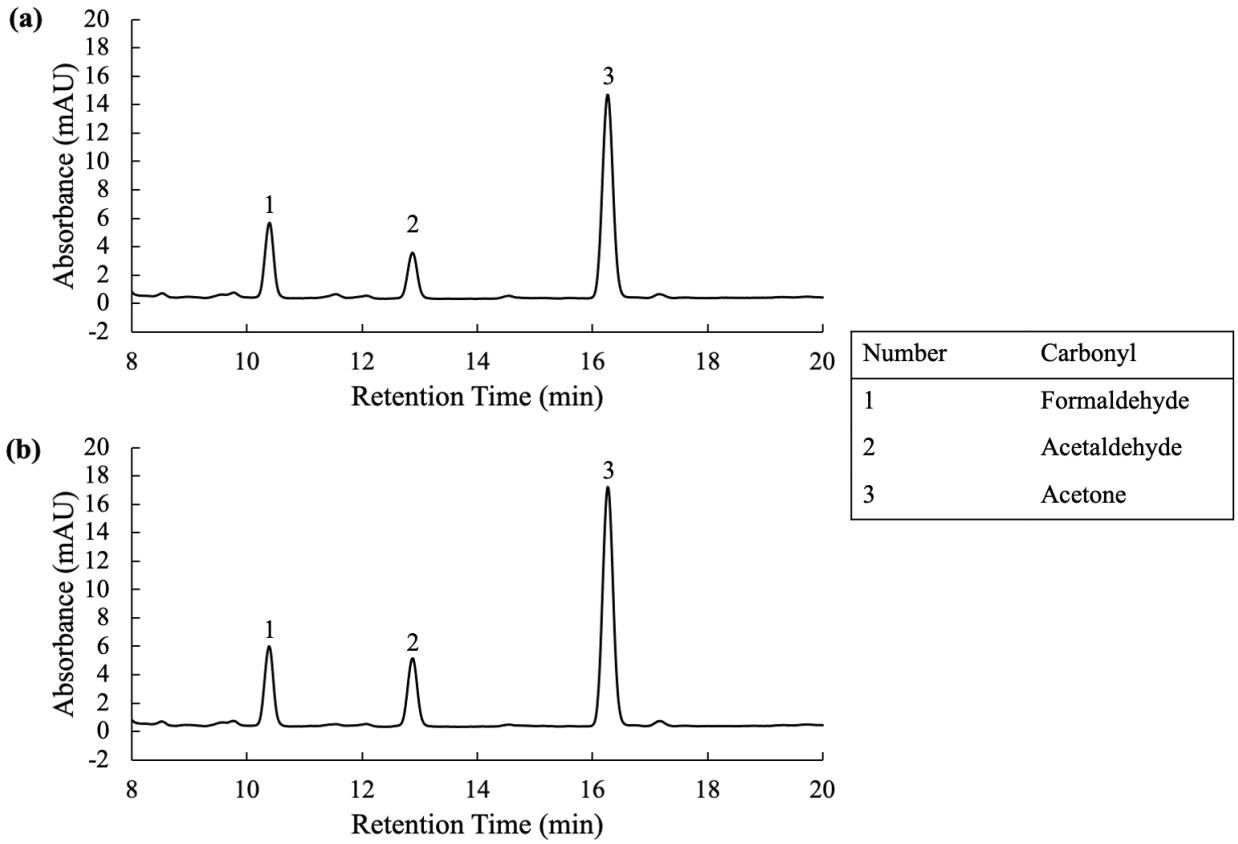

Figure 35 Absorbance (mAU) vs. retention time (min) HPLC graph of silica-DNPH cartridge from site 4 on September 8, 2021 (a), pump 1 (b), pump 2.

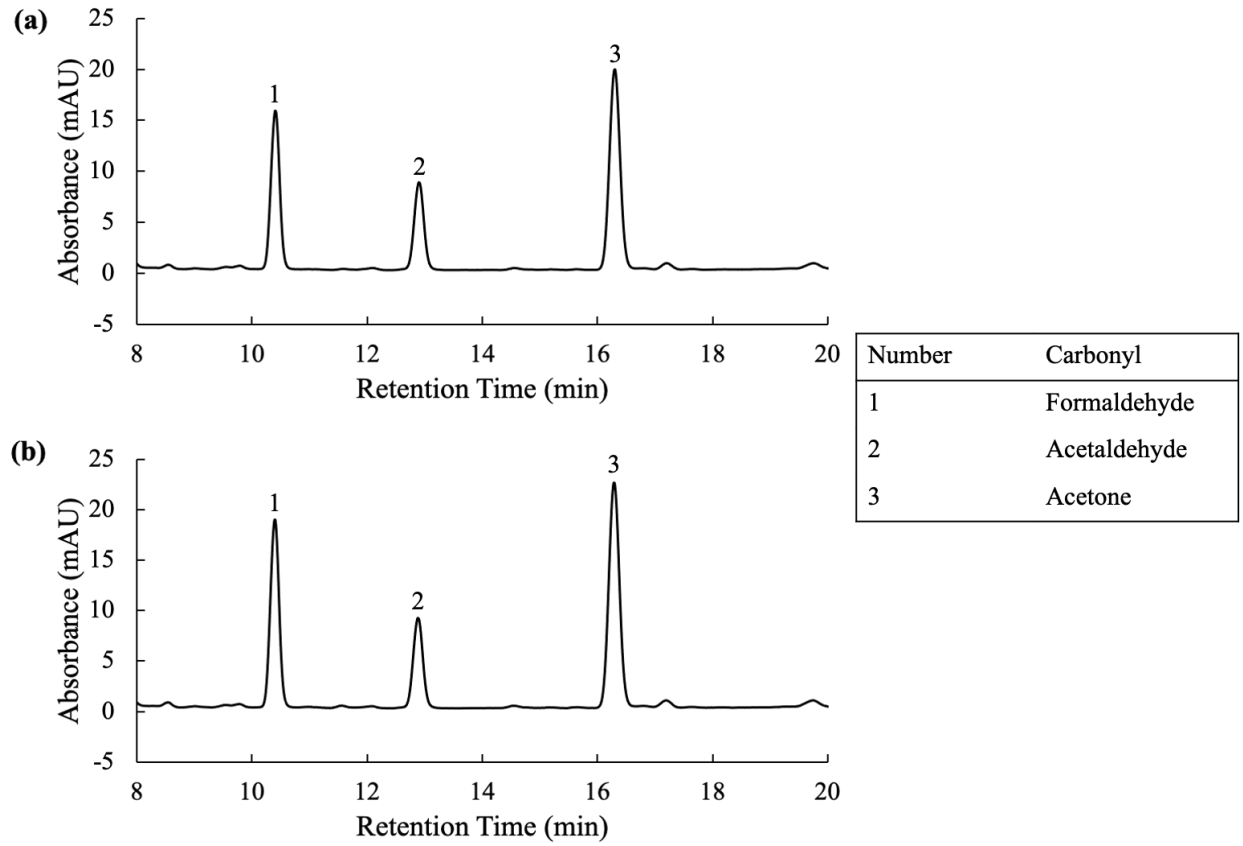

Number	Carbonyl
1	Formaldehyde
2	Acetaldehyde
3	Acetone

Figure 36 Absorbance (mAU) vs. retention time (min) HPLC graph of silica-DNPH cartridge from site 3 on September 9, 2021 (a), pump 1 (b), pump 2.

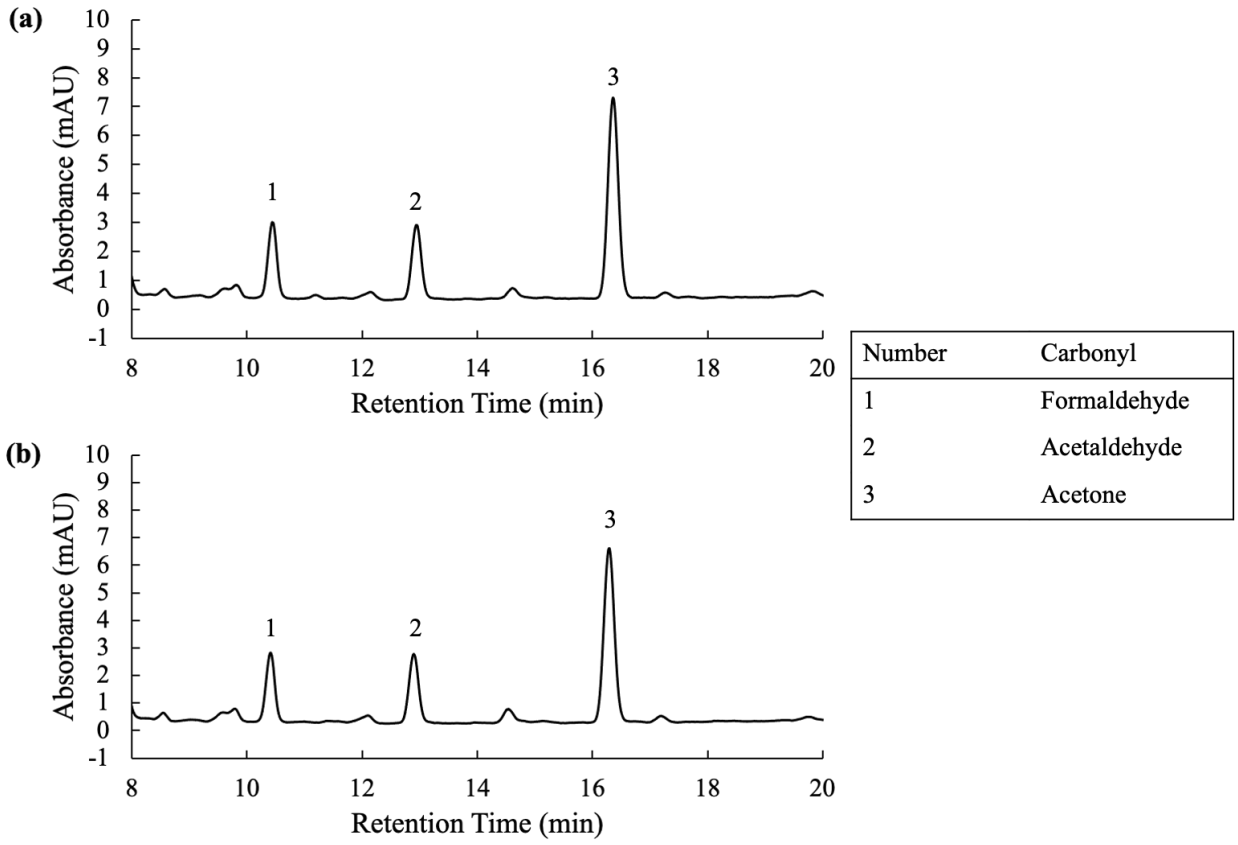

Number	Carbonyl
1	Formaldehyde
2	Acetaldehyde
3	Acetone

Figure 37 Absorbance (mAU) vs. retention time (min) HPLC graph of silica-DNPH cartridge from site 4 on September 23, 2021 (a), pump 1 (b), pump 2.

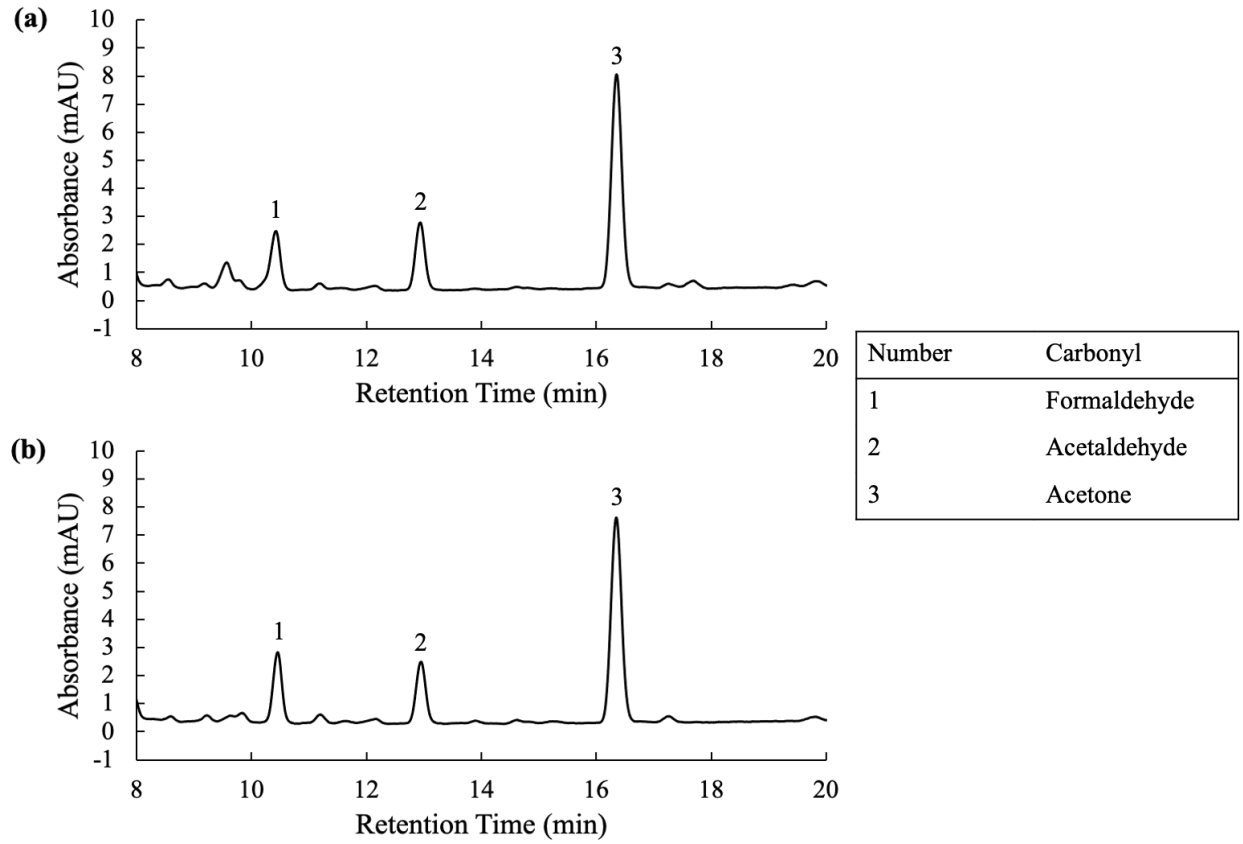

Number	Carbonyl
1	Formaldehyde
2	Acetaldehyde
3	Acetone

Figure 38 Absorbance (mAU) vs. retention time (min) HPLC graph of silica-DNPH cartridge from site 3 on September 28, 2021 (a), pump 1 (b), pump 2.

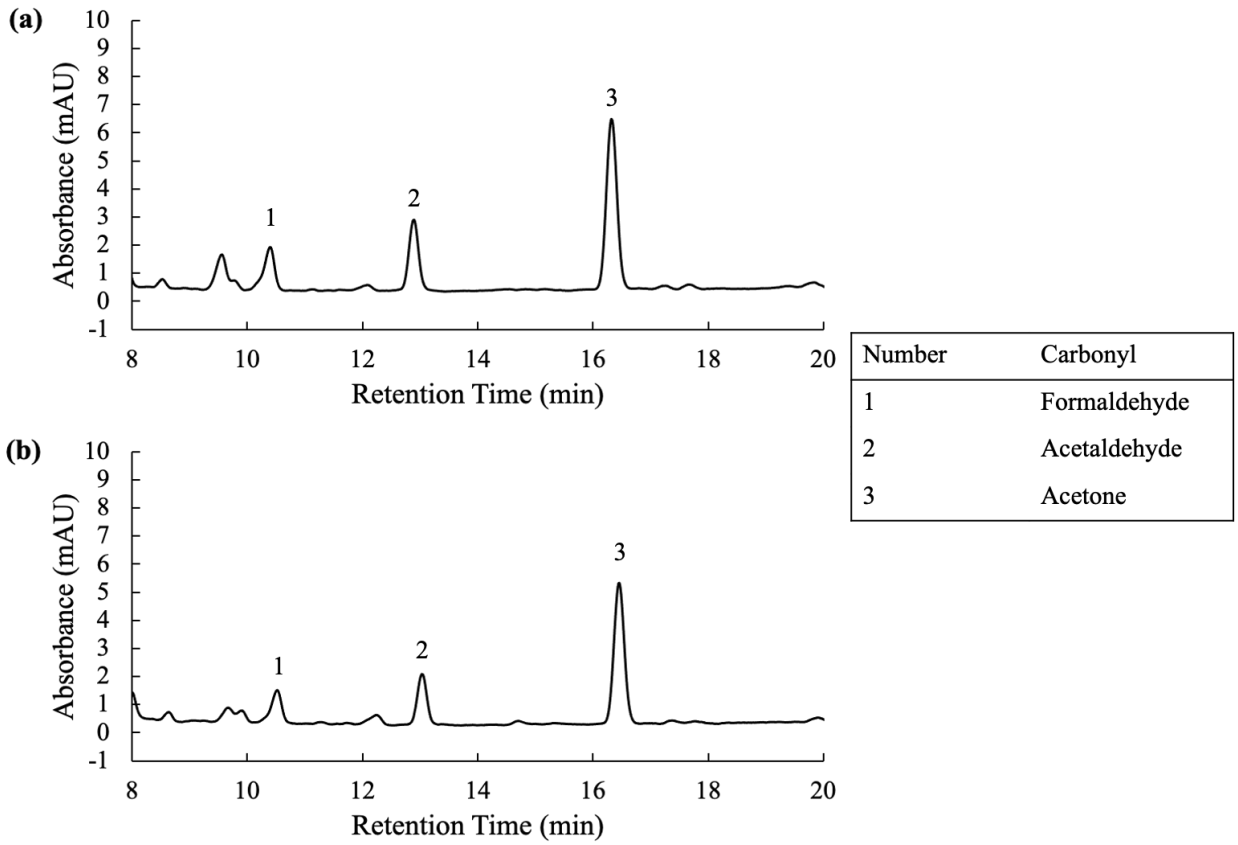

Figure 39 Absorbance (mAU) vs. retention time (min) HPLC graph of silica-DNPH cartridge from site 4 on October 27, 2021 (a), pump 1 (b), pump 2.

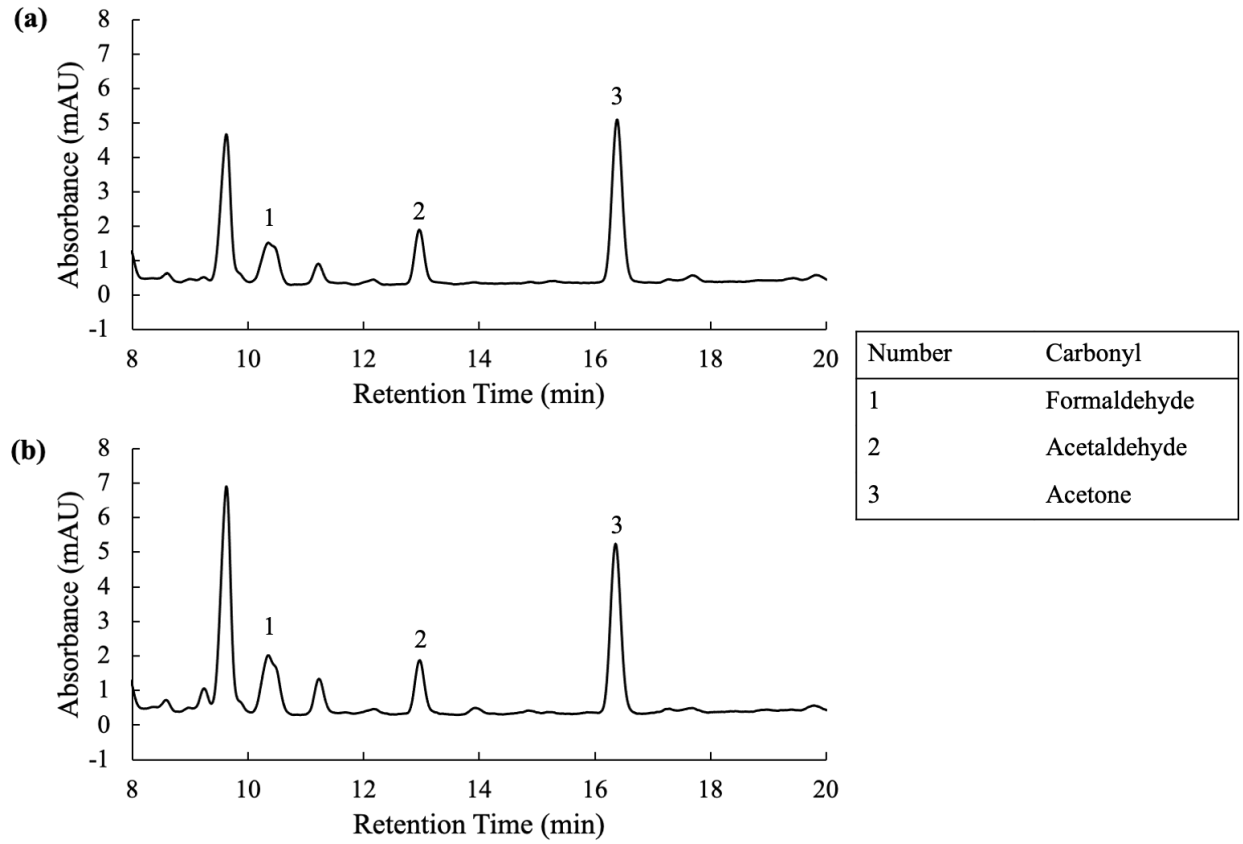

Number	Carbonyl
1	Formaldehyde
2	Acetaldehyde
3	Acetone

Figure 40 Absorbance (mAU) vs. retention time (min) HPLC graph of silica-DNPH cartridge from site 1 on November 1, 2021 (a), pump 1 (b), pump 2.

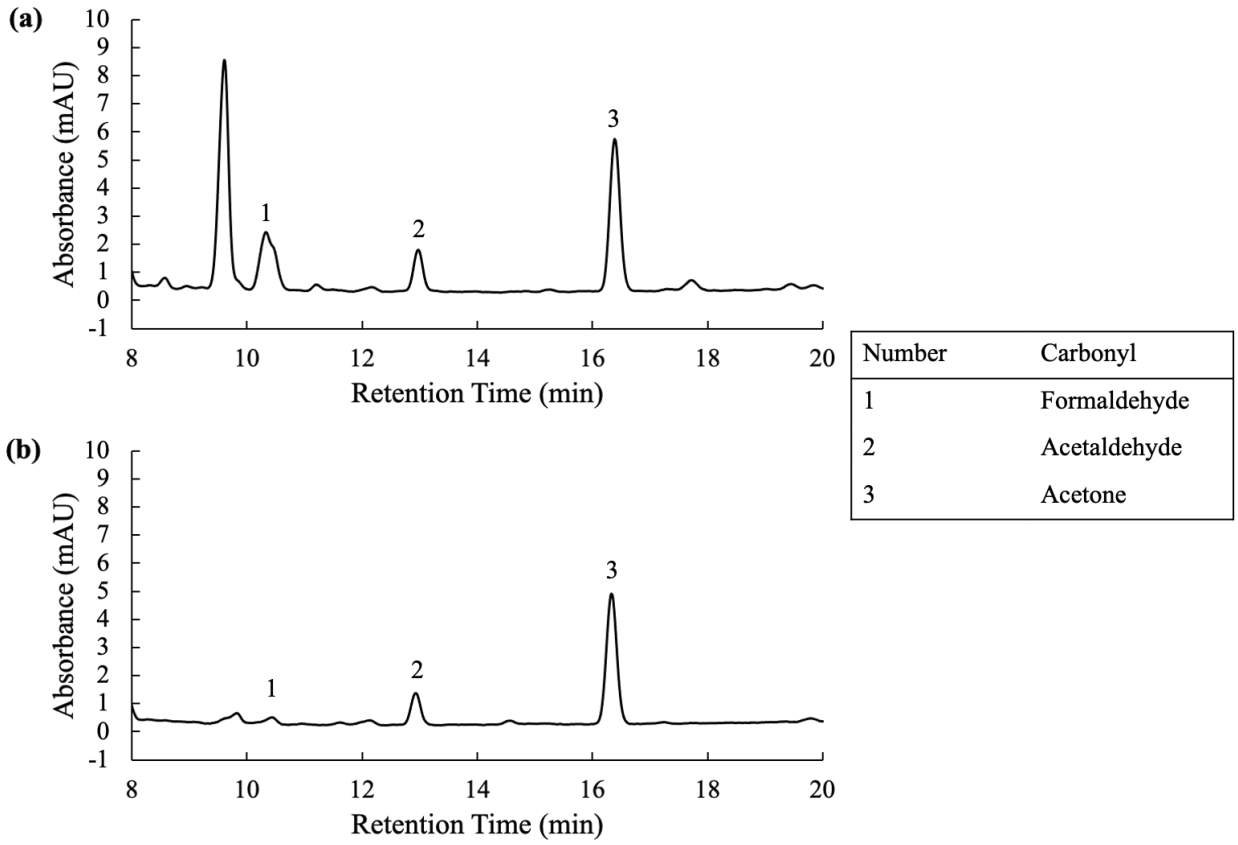

Number	Carbonyl
1	Formaldehyde
2	Acetaldehyde
3	Acetone

Figure 41 Absorbance (mAU) vs. retention time (min) HPLC graph of silica-DNPH cartridge from site 2 on November 1, 2021 (a), pump 1 (b), pump 2.